NONLINEAR EFFECTS IN GROUND MOTION SIMULATIONS: MODELING VARIABILITY, PARAMETRIC UNCERTAINTY AND IMPLICATIONS IN STRUCTURAL PERFORMANCE PREDICTIONS

A Dissertation
Presented to
The Academic Faculty

by

Wei Li

In Partial Fulfillment
of the Requirements for the Degree
Doctor of Philosophy in the
School of Civil and Environmental Engineering

Georgia Institute of Technology
August 2010

NONLINEAR EFFECTS IN GROUND MOTION SIMULATIONS: MODELING VARIABILITY, PARAMETRIC UNCERTAINTY AND IMPLICATIONS IN STRUCTURAL PERFORMANCE PREDICTIONS

Approved by:

Professor Dominic Assimaki,
Committee Chair
School of Civil and Environmental Engineering
Georgia Institute of Technology

Professor Zhigang Peng
School of Earth and Atmospheric Sciences
Georgia Institute of Technology

Professor Dominic Assimaki, Advisor
School of Civil and Environmental Engineering
Georgia Institute of Technology

Professor Glenn J. Rix
School of Civil and Environmental Engineering
Georgia Institute of Technology

Professor Bruce R. Ellingwood
School of Civil and Environmental Engineering
Georgia Institute of Technology

Professor Karim Sabra
School of Mechanical Engineering
Georgia Institute of Technology

Date Approved: 24 June 2010

To my family

ACKNOWLEDGEMENTS

First and foremost, I would like to express my sincere gratitude to my advisor, Professor Dominic Assimaki, for her patient guidance, enthusiastic advice and constant support throughout the period of the study.

I would like to extend my appreciation to other member of my thesis committee, Dr. Bruce R. Ellingwood, Dr. Zhigang Peng, Dr. Glenn J. Rix, and Dr. Karim Sabra for their interests and insightful advice in my research. I also want to acknowledge other faculty members of Geosystem Group at Georgia including Dr. Carlos Santamarina, Dr. Paul Mayne, Dr. Susan Burns, Dr. Haiying Huang for their contribution to my education.

I also want to thank Dr. Grigori Muravskii and Dr. Michalis Fragiadakis for their help in the study.

Special thanks are given to my fellow graduate students of the Geosystem Group, particularly to Varun and Seokho Jeong in our Geoquake group for their helpful discussion, to Bate, Qian Zhao, Fengshou Zhang and Sheng Dai for their friendship.

The financial support for this study provided by the Southern California Earthquake Center (SCEC) is greatly acknowledged.

Last but not least, I cannot adequately express how deeply indebted I am to my family. None of this would have been possible without their perpetual love and support.

TABLE OF CONTENTS

LIST OF TABLES

LIST OF FIGURES

LIST OF SYMBOLS OR ABBREVIATIONS

Amp	The first mode amplification amplitude of a soil site.
BSSC	Building Seismic Safety Council.
C	Inelastic deformation ratio.
COV	Coefficient of Variation.
CSIP	California Strong-Motion Instrumentation Program.
DSCTH	Design Spectrum Compatible Acceleration Time History.
EAF	Empirical Amplification Function Model.
EDP	Engineering Demand Parameter.
EPRI	Electric Power Research Institute.
EQL	Equivalent Linear Model.
FI	Frequency Index.
FOSM	First Order-Second Moment analysis.
g	Gravity acceleration.
G	Shear modulus.
γ	Shear Strain.
γ_a	Cyclic shear strain amplitude.
γ_r	Reference strain.
G/G_{max}	Ratio of Modulus Reduction.
IBC	International Building Code.
LA	Los Angeles.
λ	Rate of layer boundaries.
LIE	Linear Visco-elastic model.
$\mathrm{PGA_{RO}}$	Peak ground acceleration at rock outcrop.
MCS	Monte Carlo Simulation.
ME	Mississippi Embayment.
MKZ	Modified Kondner and Zelasko model.
μ	Ductility ratio; Operator of taking mean value.

M_w	Moment magnitude.
NEHRP	National Earthquake Hazards Reduction Program.
NGA	Next Generation Attenuation Models.
ν	Poisson's Ratio.
PEER	Pacific Earthquake Engineering Research.
PGA	Peak ground acceleration.
PHA	Peak horizontal acceleration.
PSHA	Probabilistic Seismic Hazard Analysis.
Q	Quality factor; Ratio between mean inelastic deformation ratio.
ρ	Mass density; Serial auto-correlation coefficient.
R_y	Strength Reduction Factor.
SA	Spectral Acceleration.
SCEC	Southern California Earthquake Center.
SDOF	Single-Degree-Of-Freedom.
SHAKE	A equivalent-linear seismic site response program developed by UC Berkeley.
σ	Standard deviation.
$\sigma_{\ln SA}$	Standard deviation of the logarithmic spectral acceleration.
$\sigma_{\ln V}$	Standard deviation of natural logrithm of V_S.
SMGA	Strong-Motion Geotechnical Array.
SNR	Signal-to-Noise Ratio.
SSA	Seismological Society of America.
T	Fundamental vibration period of SDOF system.
$\tau_{\max}$	Shear strength.
UHS	Uniform Hazard Spectrum.
V_S	Shear wave velocity.
V_{S30}	Averaged shear wave velocity of upper 30 meters of a site.
ξ	Damping ratio.

SUMMARY

While site effects are accounted for in most modern U.S. seismic design codes for building structures, there exist no standardized procedures for the computationally efficient integration of nonlinear ground response analyses in broadband ground motion simulations. In turn,the lack of a unified methodology affects the prediction accuracy of site-specific ground motion intensity measures, the evaluation of site amplification factors when broadband simulations are used for the development of hybrid attenuation relations, and the estimation of inelastic structural performance when strong motion records are used as input in aseismic structural design procedures.

In this study, a set of criteria is established, which quantifies how strong nonlinear effects are anticipated to manifest at a site by investigating the empirical relation between nonlinear soil response, soil properties, and ground motion characteristics. More specifically, the modeling variability and parametric uncertainty of nonlinear soil response predictions are studied, along with the uncertainty propagation of site response analyses to the estimation of inelastic structural performance. Due to the scarcity of design level ground motion recording, the geotechnical information at 24 downhole arrays is used and the profiles are subjected to broadband ground motion synthetics.

For the modeling variability study, the site response models are validated against available downhole array observations. The site and ground motion parameters that govern the intensity of nonlinear effects are next identified, and an empirical relationship is established, which may be used to estimate to a first approximation the error introduced in ground motion predictions if nonlinear effects are not accounted for.

The soil parameter uncertainty in site response predictions is next evaluated as a function of the same measures of soil properties and ground motion characteristics. It is shown that the effects of nonlinear soil property uncertainties on the ground-motion variability strongly depend on the seismic motion intensity, and this dependency is more pronounced for soft soil

profiles. By contrast, the effects of velocity profile uncertainties are less intensity dependent and more sensitive to the velocity impedance in the near surface that governs the maximum site amplification.

Finally, a series of bilinear single degree of freedom oscillators are subjected to the synthetic ground motions computed using the alternative soil models, and evaluate the consequent variability in structural response. Results show high bias and uncertainty of the inelastic structural displacement ratio predicted using the linear site response model for periods close to the fundamental period of the soil profile. The amount of bias and the period range where the structural performance uncertainty manifests are shown to be a function of both input motion and site parameters.

CHAPTER I

INTRODUCTION

1.1 Motivation of Research

The widespread implementation of performance-based seismic design procedures in current engineering practice has underlined the need for the fields of engineering and seismology to become more rationally linked. To that end, advancements in the representation of dynamic source rupture models such as detailed descriptions of heterogeneous friction-based slip functions on fault surfaces (Oglesby and Day, 2002; Guatteri et al., 2003), and efforts on the development of detailed 3D crustal velocity and fault system models for seismically active regions (Magistrale et al., 2000; Kohler et al., 2003) have enabled high spatio-temporal resolution of earthquake ground motion predictions. As a result, broadband ground motion models can nowadays predict realistic seismic waveforms over the engineering application range (<10 Hz), and their implementation in physics-based earthquake simulations from-rupture-to-rafters is currently transforming basic and applied earthquake science into an interdisciplinary, system-level research field where rupture models are integrated with discipline-based observations in seismology and engineering.

"Rupture-to-rafters" (end-to-end) ground motion predictions for engineering applications, however, require continuous representation of the physics. While the studies on source mechanism and seismic wave propagation in the lithosphere conventionally draw more attention in the history of seismological research, it is relatively recent there comes the agreement between seismological and engineering communities that site effects or the effects of surface geology play a very important role in characterizing seismic ground motion. For instance, the expansion of U.S. ground motion recording database during the 1989 Loma Prieta and the 1994 Northridge earthquake provided abundant data which illustrated the significance of sediment nonlinearity in the in-situ stress state by revealing the strain-dependent soil behavior (Chin and Aki, 1991; Darragh and Shakal, 1991; Field et al., 1997,

1998; Su et al., 1998; Beresnev et al., 1998). These effects of near-surface soil stratigraphy on the amplitude and frequency content of ground motion have been accounted for in most modern U.S. seismic design codes for building structures as a function of the soil conditions prevailing in the area of interest.

In the NEHRP provisions (BSSC, 2003), soil conditions are classified into six categories (Class A – F) based on the averaged shear wave velocity in the upper 30 meters of the site (V_{S30}), and site-specific analyses are required by the International Building Code (IBC, 2006) for category F site, namely "*soils vulnerable to potential failure or collapse under seismic loading* ", and frequently category E site. Intensity- and period-dependent site factors are assigned for each A to E category to account for the site amplification effects. Nonetheless, these site factors are derived from all sites within the same site class, and as a result, represent a blended average site amplification effect from that site category. Furthermore, while the NEHRP site classification system does provide a quantitative description of the stiffness of near surface soil layers, it does not reflect the susceptibility of these sites to nonlinear effects during strong seismic shaking: soil profiles that belong to the same site class will not necessarily experience similar strains and thus equally severe nonlinear effects when subjected to the same incident motion.

Improved nonlinear site amplification factors based on more detailed parameterization than the NEHRP site classification have been developed in the recent past as part of the Pacific Earthquake Engineering Research (PEER) Center Next Generation Attenuation Relations (NGA) project (Abrahamson and Silva, 2008; Abrahamson et al., 2008; Boore and Atkinson, 2008; Campbell and Bozorgnia, 2008; Chiou and Youngs, 2008; Walling et al., 2008). These factors are for the most part formulated as functions of the site conditions and the PHA (Peak Horizontal Acceleration) at rock outcrop (reference site) for a given period of SDOF (Single Degree Of Freedom) oscillator, while they are parameterized as a function of V_{S30} to describe the site conditions prevailing at the area of interest, instead of the A–E site categories in the NEHRP provisions.

At the interface of strong motion seismology and earthquake engineering, empirical amplification factors based on observation regression analyses have been compared to site

response simulations at soil sites (Baturay and Stewart, 2003). The results indicated that the ground response analyses are beneficial for soft clay sites but provide little benefit for other site conditions. Residuals relative to NEHRP employed factors were attributed to uncertainties in the profile depth, soil-to-rock impedance ratio and 3D geology effects. However, the simulation were conducted by means of simplified iterative visco-elastic procedures and nonlinear analyses also need to be evaluated by assessing the reductions in bias and uncertainty versus their additional computational cost and quantifying the modeling variability propagation of alternative nonlinear formulations.

The role of modeling variability and nonlinear parameter uncertainty in site-specific response predictions has been investigated in a series of recent studies. Among others, Stewart and co-workers developed a database of site and ground motion data form geotechnical arrays (PEER Project 2G01), benchmarked nonlinear models implemented in some of the currently available computer codes (Li et al., 1992; Pyke, 1992; Yang et al., 2003; Park and Hashash, 2004; Elgamal et al., 2006; Matasović and Ordonez, 2007; Hashash et al., 2008a) (PEER Project 2G02), and conducted a theoretical verification exercise, based on which, code-specific and generic material input guidelines were developed for the use of nonlinear analyses in engineering practice (Stewart et al., 2008). Protocols were tested against seismic records from vertical arrays (Stewart and Kwok, 2008).

A blind prediction experiment via multiple ground response models was also conducted using data from the Turkey Flat vertical array site during the 2004 Parkfield earthquake (Real et al., 2006; Shakal et al., 2006a,b; Cramer, 2008; Haddadi et al., 2008; Kwok et al., 2008; Real et al., 2008). Overall, the estimated bias in site-specific ground motions was attributed to overestimation of damping at large strains, nonlinear code-specific differences, inaccuracies in soil properties and 3D geology effects etc.

Nonlinear models have also been integrated into regional seismic hazard studies and their effects on PSHA's have quantified. Among others, Park and Hashash (2005a,b) developed a procedure that directly accounts for nonlinear site effects in PSHA by conducting wave propagation analyses (PSHA-NL). Cramer et al. (2004) generated a suite of seismic hazard maps for Memphis, TN, that account for site effects related to the sediments in

the Mississippi Embayment (ME). The site response was simulated by approximate or fully nonlinear analyses, and prediction scatter was also found to arise from uncertainties in soil properties and the selection of nonlinear code. Successively, Cramer (2006) combined the methodology by Cramer (2003) and the reference profile approach of Toro and Silva (2001) to better estimate seismic hazard in the ME. The added uncertainty in site amplification estimates due to the choice of site response model was on the order of 20–50% for PSHA. Recently, Hashash et al. (2008b) extended the PSHA-NL procedure an developed updated seismic hazard map for upper ME, which generally provides a lower hazard at short periods but a higher hazard at longer periods because of incorporation of the depth-dependent seismic site coefficient.

Considering the critical role soil response predictions, at the "interface" of the two disciplines, strong motion site response simulations are often required in the following procedures:

- design of earthquake-resistant structures on soft soils;
- development of synthetic-based attenuation relations for stable continental, low seismicity regions for implementation in probabilistic seismic hazard analyses (PSHA) in absence of observations;
- hybrid attenuation relations where ground motion recordings are integrated with predictions for regression analyses to be conducted on statistically significant datasets that include rare, damaging events (e.g. Hybrid attenuation relations NGA-H);
- development of time-history suites for input into nonlinear structural response analyses to design level motions, typically associated with permanent ground deformations at soft sites.

However, the use of synthetic ground motions for implementation in performance-based seismic design procedures raised the concerns as to whether these analyses are biased relative to real records. Among others, Bazzurro et al. (2004) studied the post-elastic response of structures to synthetic ground motions (Beresnev and Atkinson, 1997, 1998; Dreger and

Kaverina, 2000; Pavlov, 2002; Hutchings, 1994; Silva et al., 1990; Somerville et al., 1995, 1996; Zeng et al., 1994) generated for near-field stations, and compare the results to the median response computed using recorded motions in the 1994 Northridge earthquake. The comparison showed that the synthetic motions produce nonlinear structural responses that are less variable and less severe than those caused by real records in the short period range, namely the period range corresponding to wavelengths on the same length scales as those of near-surface soil layers, which are susceptible to nonlinear effects.

Realistic predictions of the dynamic response of soft soils to strong ground motion, in turn, may only be achieved via incremental nonlinear analyses, which require large computational cost and effort for development of the required input model parameters. Currently, subject to the limited number of strong motion records available at soft, free-field soil sites, the lack of quantitative guidelines for the efficient implementation of nonlinear models in large-scale simulations from source-to-structure hinders their integration in ground motion models. Considering these constraints, broadband ground motion synthetics are combined with downhole geotechnical observations to study the uncertainty propagation in the nonlinear site response and derive optimal guideline for efficient integration of nonlinear site response models into end-to-end ground motion simulations.

1.2 Objective and Research Outline

As concluded from the review of the state-of-art, the critical role of soil response predictions in physics-based earthquake simulations necessitates the development of a unified methodology to allow their interdisciplinary implementation. The role of nonlinear effects in ground motion simulations is in part a function of the soil stiffness in the near surface (as quantified by V_{s30}), but this is not the only parameter that governs the response of soil to strong ground motion. In order to identify the conditions under which nonlinear effects manifest, and establish quantitative criteria that will allow efficient integration of inelastic soil models in ground motion simulations, this work involves the following aspects:

1. Compilation of near-surface geotechnical information and strong motion recordings at geotechnical strong motion arrays installed in soft soil profiles;

2. Evaluation, improvement and validation of existing nonlinear constitutive models for site response analyses by comparison with field observations;

3. Study of the uncertainties associated with site response analyses in ground motion predictions by assessing the modeling variability and parametric uncertainty;

4. Identification of the conditions under which nonlinear effects manifest in the near-surface, and establishment of quantitative criteria to describe the susceptibility of soil profiles to nonlinear effects; and

5. Evaluation of the site response prediction uncertainty propagation to the inelastic structural performance estimation.

1.3 Organization of Study

This study is divided into four main chapters that fulfill in detail what was described in the research outline.

In chapter 2, the site response models used in this study are reviewed and the implementation of the nonlinear model is described. These models are validated using the downhole array observations at three sites in Los Angeles basin.

Chapter 3 shows the detailed site-response modeling variability study for 24 sites in Southern California using combined broadband synthetics and downhole observations. A set of criteria are proposed to quantify the nonlinearity susceptibility of the sites. A frequency index is developed to describe the frequency content of incident ground motion relative to the resonant frequencies of the soil profile. A empirical relation between the linear prediction error and site-ground motion parameters is established.

Chapter 4 investigates the parametric uncertainty in site-response analysis for the same sites in chapter 2 .

In chapter 5, the bias and uncertainty propagation in the site response model into nonlinear structure performance prediction are further explored. Preliminary correlations between the bias in prediction of inelastic deformation ratio and site-motion parameter are proposed.

Chapter 6 presents a summary and main conclusions of the study and recommendations for future work.

CHAPTER II

STRONG-MOTION SITE RESPONSE MODELS: OBSERVATIONS VERSUS SYNTHETICS

[1]

2.1 Introduction

The engineering community has long believed that sediment nonlinearity is significant, a perspective that has been widely confirmed based on laboratory studies (Seed and Idriss, 1970; Hardin and Drnevich, 1972b,a; Seed et al., 1984; Drnevich et al., 1966) where observed stress-strain loops implied a reduced effective shear modulus and an increased material energy absorption (damping) at higher levels of strain (Fig. 2.1). This relationship has been shown to describe the in-situ soil response to earthquake loading as well, and site-response calculations need to accommodate these strain dependencies through nonlinear constitutive relations. In this chapter, the commonly used strong motion site response models are reviewed and the implementation of a modified nonlinear model is elaborated. The models used in the study are validated using downhole array observations at three sites in Los Angeles basin.

2.2 Strong-Motion Site Response Analyses: Modeling and Numerical Implementation

Currently,two approaches are conventionally used to model cyclic soil-response, equivalent-linear, and nonlinear models. The models are briefly described in the ensuing sections and successively implemented for the prediction of nonlinear site response at the three SMGA in the LA basin.

[1]This chapter is extracted and modified from Assimaki et al. (2008b), and the permission from SSA to reprint the tables, figures and extracts is greatly acknowledged.

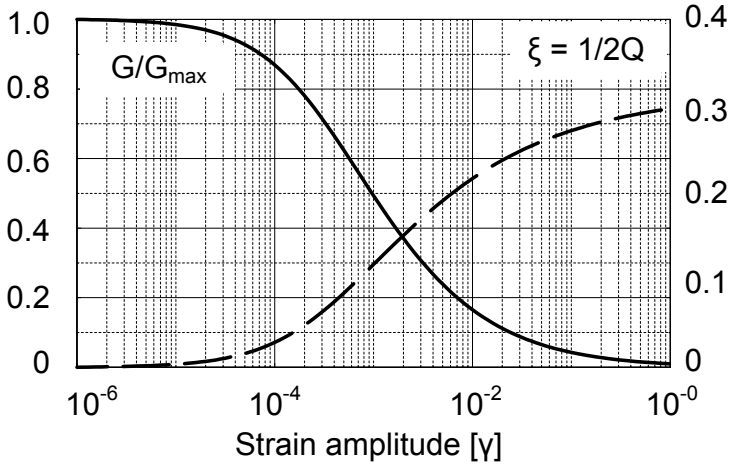

Figure 2.1: Typical modulus degradation (G/G_{max}) and damping (ξ) versus cyclic shear-strain amplitude (γ), characteristic of nonlinear soil response.

2.2.1 Equivalent-Linear Model

The equivalent-linear approach, introduced by Seed and Idriss (1970), approximates a second-order nonlinear equation by a linear operator by defining a characteristic strain that is assumed to be constant for the duration of the excitation. Moduli and damping curves (Fig. 2.1) are then used to define new parameters for each layer. The linear response calculation is repeated, new characteristic strains evaluated, and iterations are performed until convergence. This stepwise analysis procedure has been formalized into a computer code termed SHAKE (Schnabel et al., 1972), which currently is the most widely used analysis package for 1D site-specific response calculations. The advantages of the equivalent-linear approach are that the mathematical simplicity of linear analysis is preserved and the determination of nonlinear parameters is avoided.

Despite the effectiveness of the approach for the analysis of relatively stiff sites subjected to intermediate levels of strain ($< 10^{-3}$), however, the equivalent-linear method has been shown to overestimate the peak ground acceleration for large events and artificially suppress the high-frequency components when applied for the analysis of deep sites. An alternative methodology that accounts for the frequency dependence of strain amplitudes and associated dynamic soil properties has been proposed by Assimaki and Kausel (2002), and it has been

shown to yield more satisfactory results for deep sedimentary deposits; the applicability of the alternative formulation, however, is still limited to the medium strain levels (Hartzell et al., 2004). In addition, The linear stress-strain material behavior and total stress approach associated with equivalent-linear models entirely prohibit their use for problems that involve large levels of strain (e.g., near-fault motions), deep and/or soft, and very soft sedimentary sites.

2.2.2 Nonlinear Model: Monotonic Stress-Strain Response and Hysteretic Behavior

In the nonlinear formulations of transient soil behavior, the wave equation is directly integrated in the time domain, and the material properties are adjusted to the instantaneous levels of strain and loading path according to the mathematical description of nonlinear stress-strain model and hysteretic (loading and unloading) soil response. As a result, nonlinear constitutive models can simulate soil behavioral features unavailable in the equivalent-linear formulation such as updated stress-strain relationships and/or cyclic modulus degradation, which are critical for the prediction of large strain problems at soft sedimentary sites.

Nonlinear simulations were evaluated by means of the central difference method as described in Bardet et al. (2001). Figure 2.2 illustrates schematically the geometry and boundary conditions of the response simulations conducted for a horizontally stratified system of homogeneous layers extending horizontally to infinity and subjected to vertically propagating horizontally polarized shear waves.

The monotonic idealizations of the constitutive soil behavior used in this study is the modified hyperbolic model (referred to as MKZ), which is an extension of the hyperbolic model proposed by Matasović and Vucetic (1993), which uses the following modified hyperbolic formulation as initial (backbone) loading:

$$\tau = F_{bb}(\gamma) = \frac{G_{max}\gamma}{1 + \beta\left(\frac{\gamma}{\gamma_r}\right)^s} \tag{2.1}$$

The MKZ model has three independent fitting parameters (γ_r, β, and s) and is therefore much more flexible to be calibrated in fitting the experimental data both for the modulus

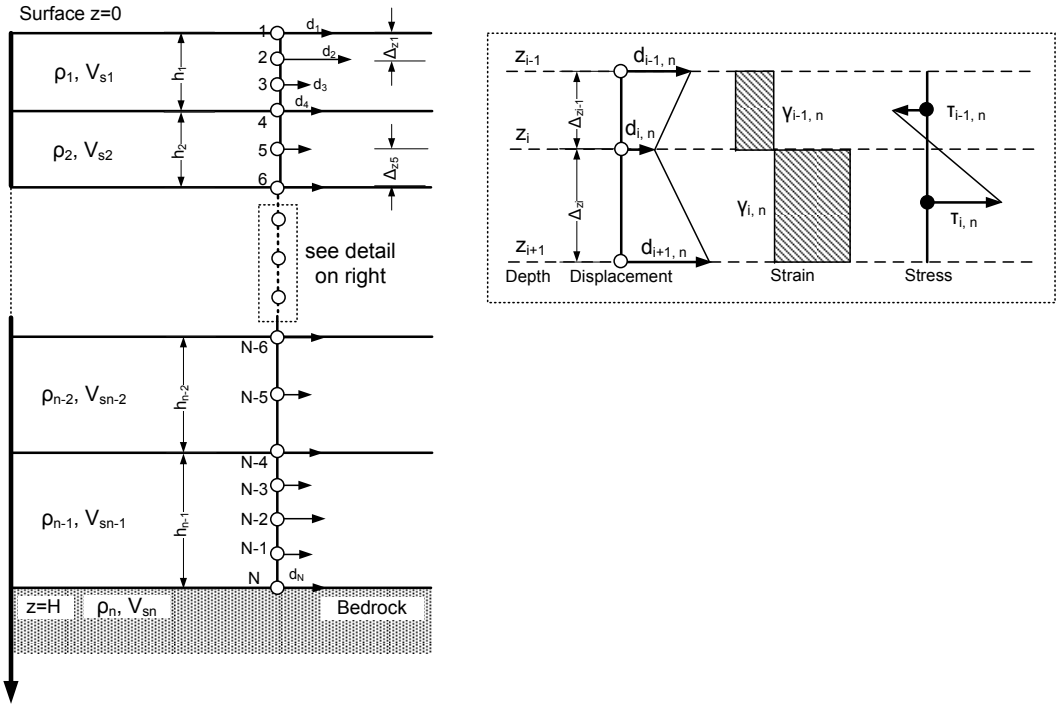

Figure 2.2: Schematic representation of spatial discretization for a one-dimensional soil deposit system, along with the detail illustrating the definition of displacement, strain, and stress in the finite-difference formulation. The displacement d and stress τ are evaluated at N grid nodes, which define sublayers within layers. The displacement of node i at time step t_n is denoted as $d(z_i, t_n) = d_{i,n}$ where z_i is the depth of node i. Similarly, the stress and strain at node i at time step t_n are denoted $\tau_{i,n}$ and $\gamma_{i,n}$ (modified from Bardet, 2001).

reduction and damping ratio curves. Despite the versatility of the model, the shear strain increases in proportion to the shear stress for large strains, a drawback that prohibits the use of the model for large levels of strain at which the soil is anticipated to reach the level of shear strength of the material.

For the representation of the hysteretic soil behavior in transient loading, the most often used in practice is the extended Masing criteria, (Kramer, 1996), which consists of the following rules:

1. For initial loading, the stress-strain curve follows the backbone curve $\tau = F_{bb}(\gamma)$.

2. If a stress reversal occurs at a point defined by $(\gamma_{rev}, \tau_{rev})$, the stress-strain curve follows a path given by

$$\frac{\tau - \tau_{rev}}{2} = F_{bb}\left(\frac{\gamma - \gamma_{rev}}{2}\right) \tag{2.2}$$

   or

$$\tau = \tau_{rev} + 2F_{bb}\left(\frac{\gamma - \gamma_{rev}}{2}\right) \tag{2.3}$$

3. If the unloading or reloading curve exceeds the maximum past strain and intersects the backbone curve, it follows the backbone curve until the next stress reversal.

4. If an unloading or reloading curve crosses an unloading or reloading curve from the previous cycle, the stress-strain curve follows that of the previous cycle.

One of the major limitations associated with the hysteretic behavior described by the extended Masing criteria is the damping ratios at high strain level are often over-estimated as a result of fixation of the shape of unloading-reloading curve, i.e. the second rule. To resolve this limitation, A new hysteretic scheme based on the model proposed by Muravskii (2005) is developed, which is capable of simultaneously matching the G/G_{max} and material damping (ξ) curves of soils in the intermediate to high strain range ($\gamma > 10^{-3}$).

The second term in the right hand side of Equation 2.3 is denoted as hysteretic function $\Phi(u)$ by Muravskii (2005). Apparently, the hysteretic function corresponding to the extended Masing criteria is the reversed and scaled version of backbone curve. Muravskii

(2005) generalized this hysteretic function and proposed a new formulation defined by

$$\Phi(u) = d_1 u + \frac{(d_0 - d_1)t}{1 + g\,|t|^R},\ t = u(1 - \beta\,|u|^q)\ (R, q, B > 0, g >= 0) \tag{2.4}$$

The parameters in this hysteretic function need to be reevaluated in order to modulate the damping ratio to match the observation. In the new hysteretic scheme proposed in this study, the backbone curve and hysteretic functions of the new model are described by the same constitutive law yet different sets of parameters. As a result, matching of the G/G_{max} curve is achieved by calibration of the monotonic curve parameters, while matching of the material damping (ξ) curves by calibration of the unload-reload parameters. The new hysteretic scheme requires calibration of the hysteretic function parameters once and scaling of the backbone curve at stress reversals thereafter. An additional feature of the new hysteretic model is that the stiffness upon unloading may be less than the initial modulus at large shear strains, which is consistent with the material degradation observed in the laboratory by Darendeli (2001). An example of the new hysteretic model response is shown in Figure 4.8, where a soil element with the nonlinear dynamic properties shown in Figure 4.7 is subjected to a transient excitation. The hysteretic loops predicted using the extended Masing rules (Kramer, 1996) are compared to the new hysteretic scheme: the narrower loops of the new model imply lower, more realistic material damping values at the corresponding shear strain amplitudes.

In order to numerically integrate the constitutive relation, both backbone curve and hysteretic function can be discretized by a series of mechanical models described by Iwan (1967), according to which the shear strain may be easily decomposed into elastic and plastic components as required by the formulation of incremental elasto-plasticity. The Iwan model implemented in this study for the incremental solution of the wave equation in nonlinear media consists of a group of N elastic perfectly plastic elements in parallel, each comprising a linear elastic spring and a rigid slip element connected as shown in Figure 2.4. The number of elasto-plastic elements and corresponding stiffness and Coulomb resistance values were in each case selected to fit the target material model behavior [$\tau = f(\gamma)$]. Based on this mathematical representation originally proposed by Iwan (1967), the multi-linear

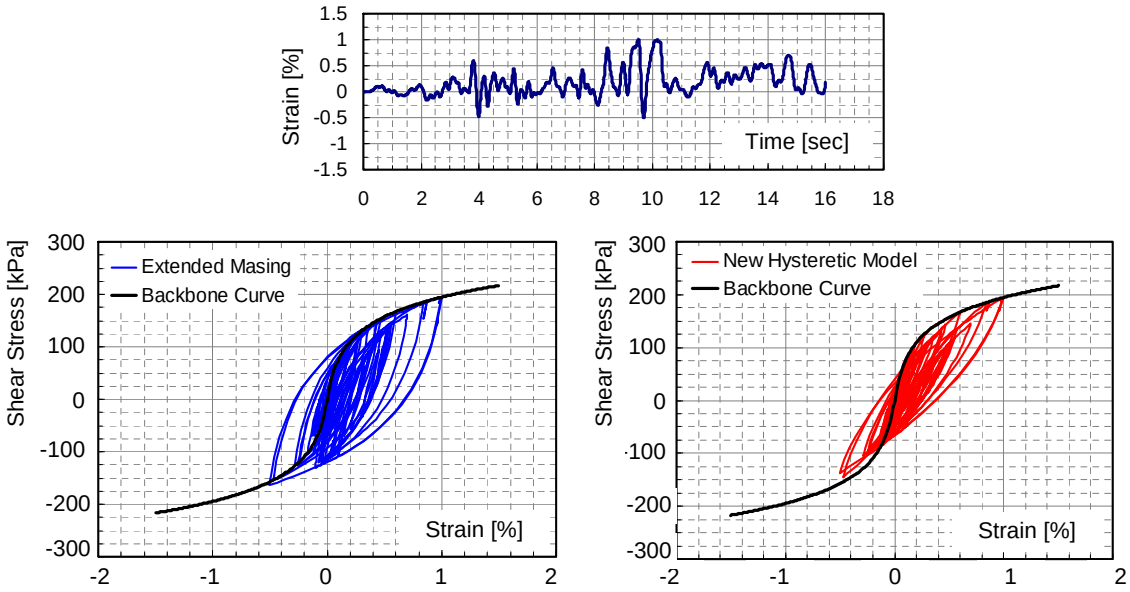

Figure 2.3: Nonlinear soil element subjected to transient strain time history (top). Comparison of backbone curve from MKZ model and hysteretic loops evaluated by means of the extended Masing rules (bottom, left) and backbone curve from MKZ model and hysteretic loops from the new hysteretic scheme developed based on Muravskii (2005) (bottom, right).

shear stress-strain behavior for N elastoplastic springs subjected to a strain amplitude γ is

$$\tau = \sum_{i=1}^{N} \frac{k_i}{N}\gamma + \sum_{i=n+1}^{N} \frac{\tau_{yi}}{N} \tag{2.5}$$

where k_i is the shear stiffness of the ith element, τ_{yi} is the critical slipping (Coulomb) stress of the ith element, n is the number of elastoplastic elements that remain elastic upon the application of a strain increment, and τ is the estimated level of shear stress at a given level of strain amplitude γ. The first and second terms of the right-hand side of equation (2.5) indicate the elastic and plastic components, respectively, of the total stress τ . Note that the form of the stress-strain relationship for subsequent unloading at any reversal point may be evaluated by means of the response of the three following groups of slip elements: (i) elements that did not yield upon previous loading remain elastic, (ii) elements under the state of yielding that have stopped slipping after reversal, and (iii) elements that have yielded during loading and now yield in the opposite direction. It has to be noted that the Iwan model can actually replicate the extended Masing behavior if the same set of k_i and τ_{yi} values are used for both backbone and unload-reload curve. Obviously, different set of

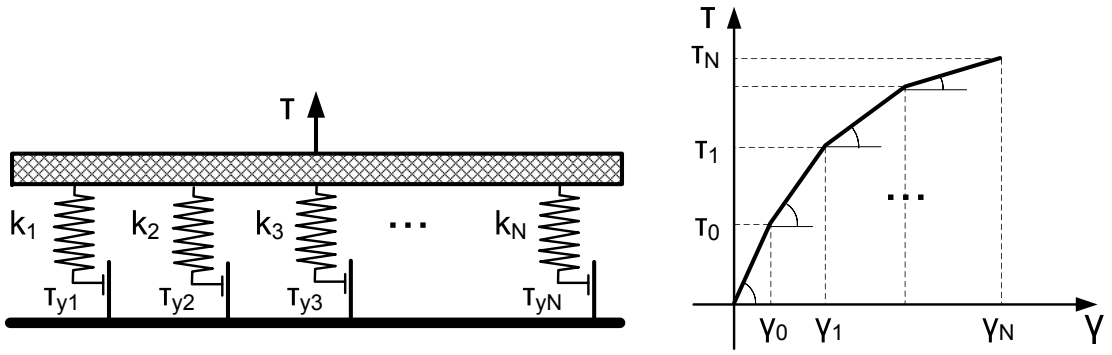

Figure 2.4: Iwan (1967) model of elastoplastic springs in parallel simulating the nonlinear stress-strain soil behavior and corresponding approximation of continuous backbone curve by a series of linear segments.

k_i and τ_{yi} values should be employed for the backbone and unload-reload curves in order to fulfill the new hysteretic rule.

2.2.3 Calibration of Nonlinear Soil Parameters

For the MKZ model with new hysteretic scheme, the input parameters were selected to optimally fit the available experimental data of soil modulus reduction and damping versus shear strain amplitude. For this purpose, a genetic algorithm was implemented, with objective function targeted to simultaneously minimize the square error between the measured and theoretically predicted modulus reduction and damping data as follows:

$$\sum_{i=1}^{N} w_i [O_G(\gamma_i) - G(P, \gamma_i)]^2 \tag{2.6}$$

or

$$\sum_{j=1}^{N} w_j [O_\xi(\gamma_j) - \xi(P, \gamma_j)]^2 \tag{2.7}$$

where w_i and w_j are the weight coefficients of the global search, $O_G(\gamma_i)$ and $O_\xi(\gamma_j)$ are the ith and jth experimental points for the modulus reduction and damping curves at γ_i and γ_j strain amplitudes correspondingly, and $G(P, \gamma_i)$ and $\xi(P, \gamma_j)$ are the corresponding predicted values as a function of the model parameters P.

Due to the specific form of the backbone curve of MKZ model, it is difficult to get the close form expression of the damping ratio as a function of cyclic strain level. As such,

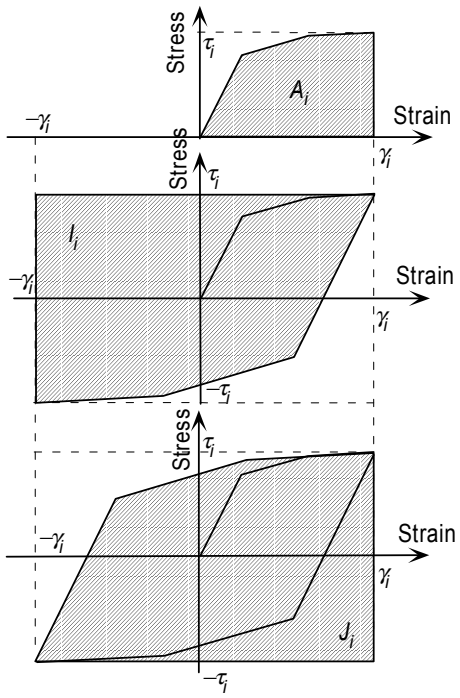

Figure 2.5: Geometric illustration of the numerical procedure used to derive discretized damping ratios. Areas A_i, I_i, and J_i are used for calculation of hysteretic loop of during loading-unloading cycle.

numerical integration are used to derive the discretized form of damping ratio as a function of modulus reduction and cyclic strain level. Figure 2.5 illustrate the geometry relation used to derive the discretized damping ratio (Bardet and Tobita, 2001) and the final formulation of damping ratio is shown as follows: $\xi(\gamma_1) = 0$ and $\xi(\gamma_i) = (2/\pi)(2A_i/G_i\gamma_i^2 - 1)$, i=2,...,n. in which A_i is shown in Figure 2.5 and G_i is the normalized modulus or G/G_{max} value at strain level γ_i. With the formulation of discretized damping ratio, it is possible to calibrate the unload-reload parameters by matching of material damping.

In particular for the representation of small-strain intrinsic attenuation, the experimentally measured value was subtracted from the damping curve prior to the stochastic search because the evaluation of anelastic intrinsic attenuation is only a function of the modulus reduction function. Successively, for each model investigated, the small-strain damping was implemented in the finite-difference formulation by means of the memory-variable technique described previously, a formulation yielding a frequency-independent intrinsic attenuation across the frequency and strain spectra of interest.

2.2.4 Simulation of Small-Strain Frequency-Independent Damping

Energy loss through nonelastic process is usually measured by intrinsic attenuation and parameterized with the quality factor Q. Incorporation of seismic Q in the ground motion modeling is important because it can strongly affect the amplitude and duration of the ground motion when waves travel within shallow soft materials. When the wave equation is solved in the time domain (e.g., finite differences) given a nonlinear stress-strain formulation, material absorption is replicated by the hysteretic unloading-reloading cycles when the material is subjected to strain amplitudes beyond the linear elastic range. Nonetheless, frequency-independent material absorption is also observed in the laboratory when the soil is subjected to very low-strain amplitudes, heretofore referred to as low-strain damping.

The most widely used implementation of low-strain damping in strong ground-motion modeling is Rayleigh damping, a formulation also used in finite element modeling of structural dynamics for the representation of energy loss mechanisms in structures (Bao et al., 1998). Also known as proportional damping, Rayleigh damping is formulated on the assumption that the damping matrix ($[C]$) of a system is a linear combination of the mass $[M]$ and stiffness $[K]$ matrices as follows:

$$[C] = \alpha[M] + \beta[K] \tag{2.8}$$

where the coefficients α and β are computed to give the required levels of attenuation at two different frequencies (Chopra, 2000). The Rayleigh damping formulation is very computationally efficient, yet may be only implemented in a narrow frequency band for frequency-independent target Q, as shown in Figure 2.6. An extended formulation of Rayleigh damping, referred to as Caughey damping, may be implemented to fit the target Q-values at more than two frequencies. Hashash and Park (2002) employed Caughey damping for the nonlinear site-response analysis in Mississippi embayment. In their formulation, the choice of significant frequencies/modes was optimized by comparison with the viscoelastic solution in the frequency domain (Park and Hashash, 2004). Recently, Kwok et al. (2007) used theoretical wave propagation solutions to provide guidelines for the definition of material attenuation in site-response analyses, and they concluded that the target frequencies should

be established through a process by which linear time-domain and frequency-domain solutions are matched; as a first approximation, the first-mode site frequency and five times that frequency was suggested.

Alternatively, the target low-strain material attenuation may be fitted via time-domain wave-field simulations by the memory-variable technique originally described by Day and Minster (1984) and successively implemented by both Emmerich and Korn (1987) and Carcione et al. (1988). This technique can be implemented to accurately model both a frequency-independent and frequency-dependent Q over a wide frequency range by using a linear combination of multiple relaxation mechanisms (Liu and Archuleta, 2006, e.g.). Each relaxation mechanism is represented by a set of memory variables that can be updated using first-order differential equations, while the accuracy of modeling Q depends on the number of relaxation mechanisms used, namely, more relaxation mechanisms will result in a more accurate modeling of Q.

The memory-variable representation of frequency independent Q was implemented in the simulations of nonlinear site response, and it was incorporated in the time-domain simulations based on the rheology formulation of a generalized Maxwell body, modified here as follows:

$$\tau(t) = G\left[\gamma(t) - \sum_{k=1}^{N} \zeta_k\right] \tag{2.9}$$

where ζ_k are memory variables that correspond to the solution of the following first-order set of differential equations, with τ_k being the relaxation times and w_k being the weight coefficients:

$$\tau_k \frac{\mathrm{d}\zeta_k(t)}{\mathrm{d}t} + \zeta_k(t) = w_k \gamma(t) \tag{2.10}$$

The accuracy of low-strain damping modeling depends on the accuracy of estimation of τ_k and w_k. The nonlinear simulations in this section were evaluated by means of the empirical interpolating algorithm proposed by Ma and Liu (2006). The suggested values for τ_k and w_k are show in Table 2.1. The weight coefficients w_k^{ξ} for a target value of damping ratio ξ are calculated using the interpolation formula,

$$w_k^{\xi} = \chi \cdot (\chi \alpha_k + \beta_k) \tag{2.11}$$

Table 2.1: Relaxation Coefficients for Modeling Frequency-Independent Small-Strain Damping (Q)

k	τ_k	α_k	β_k
1	1.72333×10^{-3}	1.66958×10^{-2}	8.98758×10^{-2}
2	1.80701×10^{-3}	3.81644×10^{-2}	6.84635×10^{-2}
3	5.38887×10^{-3}	9.84666×10^{-3}	9.67052×10^{-2}
4	1.99322×10^{-2}	-1.36803×10^{-2}	1.20172×10^{-1}
5	8.49833×10^{-2}	-2.85125×10^{-2}	1.30728×10^{-1}
6	4.09335×10^{-1}	-5.37309×10^{-2}	1.38746×10^{-1}
7	2.05951	-6.05035×10^{-2}	1.40705×10^{-1}
8	13.2629	-1.33696×10^{-1}	2.14647×10^{-1}

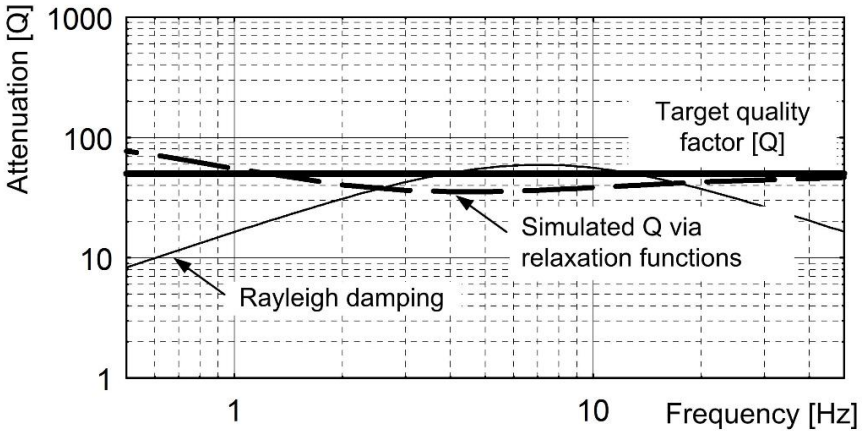

Figure 2.6: Typical example of target low-strain damping (intrinsic attenuation) simulation by means of the Rayleigh damping formulation, the Caughey damping, and the memory-variable technique (Liu and Archuleta, 2006) implemented in this study.

where the values of α_k and β_k are also listed in Table 2.1. Finally, the factor χ depends only on the target value of ξ and is estimated by the following expression:

$$\chi = [3.071 + 1.443(0.5/\xi)^{-1.158} \ln(0.1/\xi)]/[1 + 0.2075/\xi] \tag{2.12}$$

An example of implementation of equation (2.12) within the context of a time-domain direct integration of the wave equation is shown in Figure 2.6 for a target value of low-strain material damping $\xi = 0.01$ (or $Q = 50$), and the effectiveness of this formulation may be readily seen by comparison to the Rayleigh damping and higher-order Caughey damping formulations.

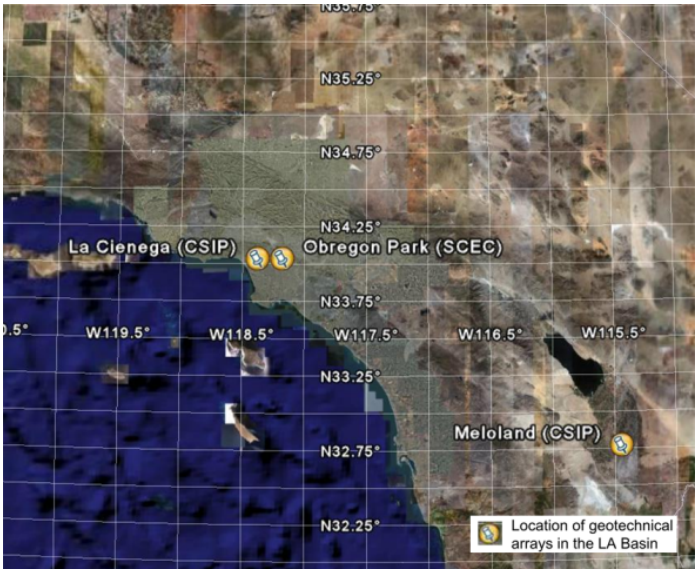

Figure 2.7: Satellite map depicting the location of strong-motion geotechnical arrays (SMGA) in the Los Angeles basin investigated in this study

2.3 Site Conditions at Three Strong-Motion Geotechnical Arrays in the Los Angeles Basin

Figure 2.7 depicts the locations of the three instrumented geotechnical downhole arrays in southern California used in this study to validate the previously described site-specific response models These downhole arrays are operated by the Southern California Earthquake Center (SCEC) and the California Strong-Motion Instrumentation Program (CSIP). Geotechnical data available at these stations comprise downhole and suspension logging shear-wave velocity profiles (V_S), as well as scarce laboratory resonant column modulus reduction (G/G_{max}) and damping (ξ) versus shear-strain amplitude curves from samples extracted at a few locations in the near surface.

A detailed description of the near-surface stratigraphy is achieved by employing the seismogram inversion algorithm developed by Assimaki et al. (2006) to weak ground motions recorded at the three arrays (Table 2.2). This optimization technique comprises a genetic algorithm in the wavelet domain coupled to a nonlinear least-squares fit in the frequency domain, and it has been shown to improve the computational efficiency of the former while avoiding the pitfalls of using local linearization techniques such as the latter (Houck et al., 1996). The parameters estimated are stepwise variations of the shear-wave

Table 2.2: Strong-Motion Geotechnical Array Stations in the Los Angeles Basin

Site Name	Latitude(◦)	Longitude(◦)	Agency	Station Depth (m)	Geology	Site Class
Obregon Park	34.037	-118.178	SCEC	0, 70	Q	C
La Cienega	34.036	-118.378	CSIP	0, 18, 100, 252	Deep alluvium	D
Meloland	32.773	-115.447	CSIP	0, 30, 100, 252	Deep alluvium	E

velocity, attenuation, and density with depth for horizontally layered media with predefined layer thickness. Deterministic lower and upper bounds were imposed on the vector of unknowns to constrain the search space, based on independent geological and geotechnical site characterization data.

For each array, the algorithm was repeated in a series for multiple borehole and surface waveform pairs, selected on the basis of their available signal-to-noise ratio (SNR). Averaging of the optimal solution for multiple events has been shown to minimize the error propagation of the measured process and the error translation of the forward idealized model limitations, leading to a robust estimate of the bestfit solution to the inverse problem. For more information, the reader is referred to Assimaki et al. (2006) and Assimaki and Steidl (2007).

The averaged inverted profiles of shear-wave velocity (V_S), attenuation (Q), and density (ρ) at the three arrays are illustrated in Figure 2.8, along with the available onsite suspension logging and cross-hole velocity data. Two points should be highlighted in reference to the inversion results:

1. Overall, the inverted Vs profiles compare well with the in-situ geotechnical data with the exception of a few layers, such as the 15-m layer at 60-m depth at Meloland Strong-Motion Geotechnical Array (SMGA). Nonetheless, seismogram inversion evaluated at the three sites using multiple low intensity events showed low scatter of depth-dependent soil properties, while the limited in-situ geotechnical data had no redundancy. As a result, the inverted profiles were implemented in the site-response simulations described in the ensuing. A typical example of implementation is shown in Figure 2.8b, where the ground surface response computed from the inverted soil

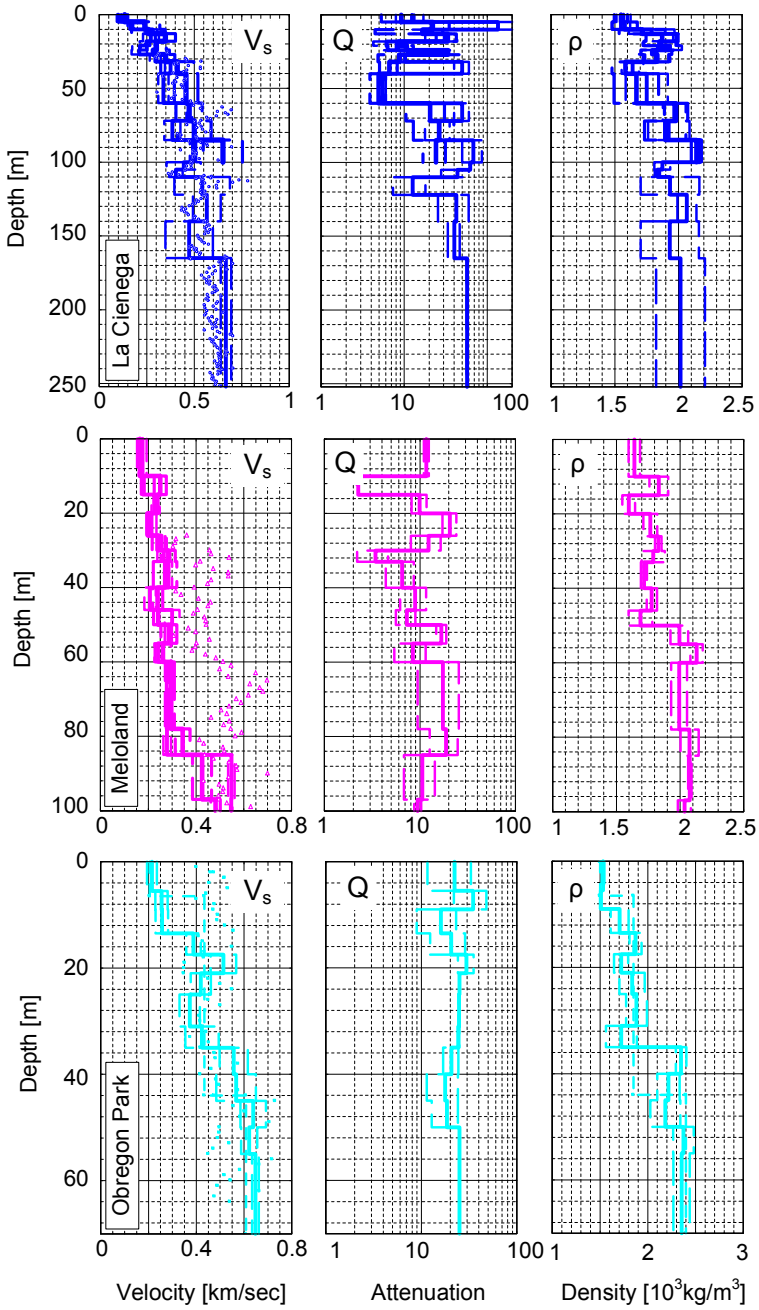

Figure 2.8: Velocity (V_S), attenuation (Q), and density (ρ) evaluated by means of down-hole array seismogram inversion at three SMGA stations in the LA basin (depicted in Fig. 2.7).

parameters and the response computed using the in-situ geotechnical data are compared to the recorded ground motion at Meloland SMGA during an M_w 5.1 event not used in the inversion process; as can be readily seen, the former predictions compare better with the observations.

2. The attenuation profiles (Q) in the near surface show a wide statistical distribution, attributed to the forward model operator where the physical configuration is idealized by a stack of horizontally stratified homogeneous layers subjected to vertically propagating anti-plane shear waves. This model cannot properly account for the strong scattering of high-frequency components in the naturally heterogeneous near-surface soil layers, and it attributes the late arrivals of noncoherent redistributed energy to energy loss. As a result, inverted Q-values in the near-surface are both lower than the material energy absorption measured in the laboratory and strongly motion dependent for wavelengths comparable to typical correlation lengths of the heterogeneous formations.

2.4 Validation of Nonlinear Site Response Models

The strong-motion site-response models described previously were initially bench marked for weak ground motions by comparison with downhole array recordings. Successively, the limited number of strong-motion recordings at the three sites was used to quantify the error introduced in the predictions by the alternative formulations and to identify a proxy for the observed site response to be used as the reference prediction in the synthetic ground motion simulations.

A typical example of a medium intensity event (M_w 4.2, peak ground acceleration PGA=0.22g) recorded at La Cienega SMGA is shown in Figure 2.9 and Figure 2.10, where predictions are compared to the time history and response spectrum of the recorded motion on ground surface. The comparisons show that the fit between observed and predicted ground motion becomes better as the site response model becomes more elaborate and the modified MKZ model gives the best prediction result. Therefore, it is identified as the proxy for the observed site response and will be used as the reference prediction in modeling

variability study and parametric uncertainty study.

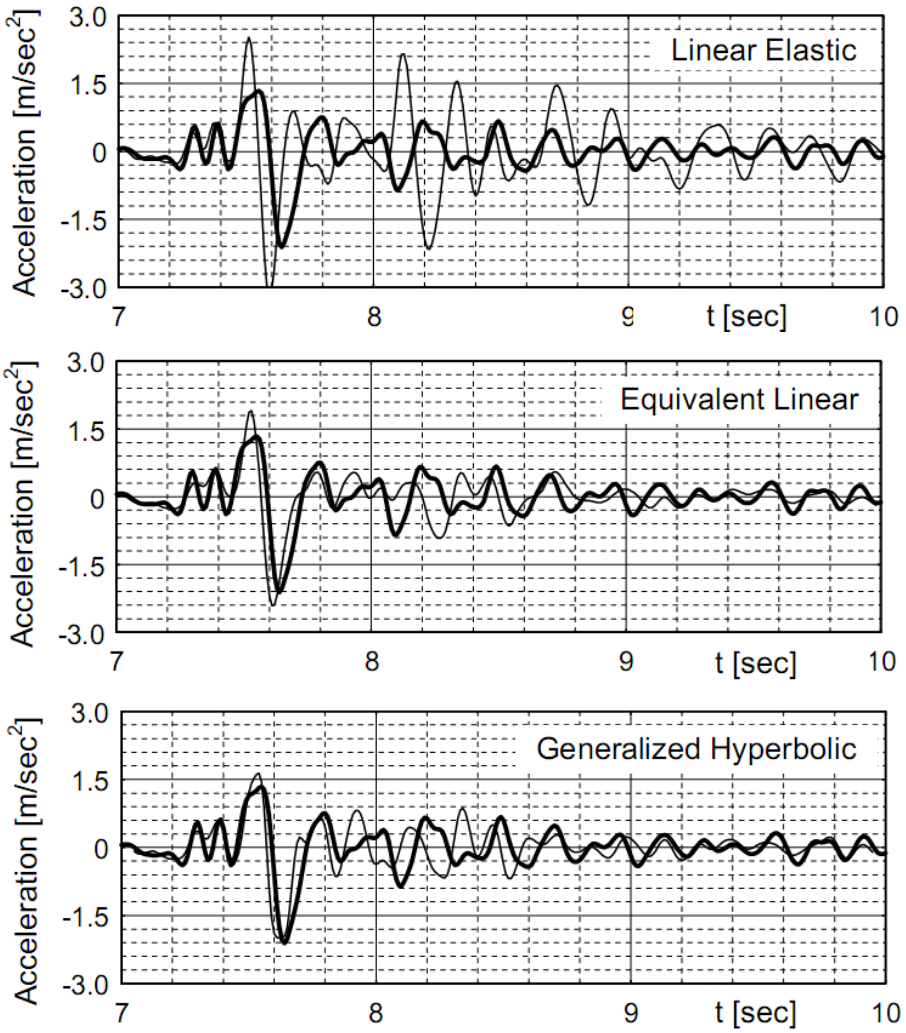

Figure 2.9: Comparison between observations and predictions of strong ground motion acceleration time history at the La Cienega SMGA during the 9 September 2001 M 4.2 event (Observations plotted as dark line, while predictions plotted as light line)

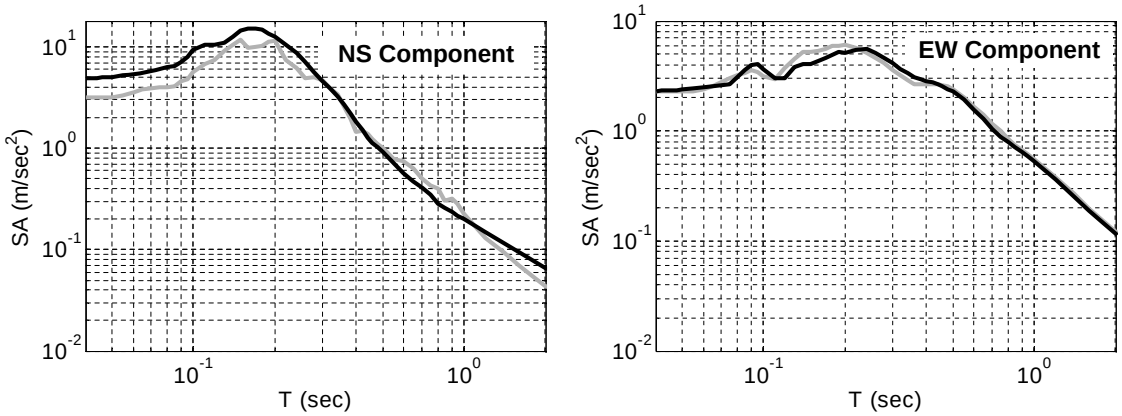

Figure 2.10: Comparison between observations and predictions of strong ground motion spectral acceleration at the La Cienega SMGA during the 9 September 2001 M 4.2 event (Observations plotted as dark line, while predictions plotted as light line)

CHAPTER III

MODELING VARIABILITY IN GROUND RESPONSE ANALYSIS

3.1 Introduction

The advancements in the representation of dynamic source rupture simulations and the development of detailed 3D crustal velocity and fault system models for seismically active regions have enabled the high spatio-temporal resolution of design-level ground motion predictions through physics-based simulations. As a result, broadband synthetic ground motions may nowadays be used by the engineering community in the aseismic design of civil infrastructure, either supplementing the existing database of recorded ground motions, or providing a more sophisticated method of developing artificial seismograms than alternative methodologies such as stochastic simulation and design spectrum compatible time histories.

Physics-based ground motion predictions for engineering applications require realistic predictions of the so-called high frequency components at the source, propagation of these frequencies through the lithosphere, and interaction of the incident seismic waves at the engineering bedrock with the near-surface soil layers. Specifically for the latter, the recent expansion of U.S. ground motion recording database during the 1989 Loma Prieta, 1994 Northridge and 2004 Parkfield earthquake provided abundance of data to the seismological and engineering communities alike that highlighted the significance of the near-surface sediment nonlinearity during strong ground motion (Chin and Aki, 1991; Darragh and Shakal, 1991; Field et al., 1997, 1998; Su et al., 1998; Beresnev et al., 1998; Cramer, 2008; Kwok et al., 2008), and perhaps the most reliable source of information came from downhole array recordings (Borcherdt, 1970; Seed and Idriss, 1970; Hartzell, 1992; Wen et al., 1994; Zeghal and Elgamal, 1994; Elgamal et al., 1995; Iai et al., 1995; Satoh et al., 1995; Sato et al., 1996; Steidl et al., 1996; Aguirre and Irikura, 1997; Boore and Joyner, 1997; Satoh et al., 2001, e.g.). Field and laboratory experiments have shown that nonlinear effects dominate the

propagation on seismic waves through the soft soil layers during strong ground motion, and therefore, when high frequency ground motion components (i.e. wavelengths comparable to the thickness of soft soil layers) are simulated as part of seismological model predictions, nonlinear site effects need to be accounted for to ensure accuracy of the ground surface motions. As a example of a recent study, Assimaki et al. (2008b) used downhole array recordings in the Los Angeles basin to show that insufficient consideration of nonlinear site effects may cause up to 60% relative error in spectral acceleration prediction.

The spatial and temporal resolution required for the simulation of soil nonlinearity in seismological models, however, implies excessively large computational time and effort. Therefore, efficient integration of nonlinear site response analyses in ground motion models may only be achieved by developing quantitative criteria that will indicate when nonlinear effects are anticipated to be important and need to be accounted for. Towards this goal, Assimaki et al. (2008b) used downhole array records and broadband ground motion synthetics, and showed that soil nonlinearity manifests when the incident wavelengths are comparable to the thickness of soil layers, and when the motion intensity is large enough to cause nonlinear deformation. Next, they developed a set of site and ground motion dependent indices to quantify the nonlinearity susceptibility of a site, comprising the peak ground acceleration (PGA) of the rock-outcrop motion, and the so-called frequency index (denoted as FI) which is the cross-correlation between the site transfer function and the motion frequency spectrum. They finally illustrated the concept for three downhole array sites in Southern California, by showing that the extent of soil nonlinearity increased with increasing PGA and increasing FI for all NEHRP site class profiles investigated.

In this study, the concept described above is used to derive an empirical correlation between site- and ground-motion parameters and the susceptibility of soil profiles to nonlinear effects. For this purpose, the work by Assimaki et al. (2008b) is extended by using a statistically significant number of site conditions and seismic input motions, namely the calibration sites compiled by Stewart and coworkers as part of the PEER 2G02 project

Calibration Sites for Validation of Nonlinear Geotechnical Models (http://cee.ea.ucla.edu/faculty/CalibrationSites/Webpage/main.htm), for which detailed velocity profiles, modulus reduction and material damping curves were available, and synthetic ground motions generated by the dynamic rupture model with random source parameters (Liu et al. (2006)). Multiple ways are investigated to quantify how strong nonlinear effects are anticipated at a given site, which include the spectral error between nonlinear site response predictions and each of the following: empirical amplification factors (EAF), linear visco-elastic (LIE) or equivalent linear (EQL) analyses. For the nonlinear site response predictions, a nonlinear model previously validated by comparison with downhole array recordings (Assimaki et al. (2008b)) is used. It is shown that the best measure is the divergence between linear and nonlinear analyses, and based on this result, an empirical correlation is developed, which can be used to estimate the intensity of soil nonlinearity at a given site during a given seismic event using simple measures of soil stiffness and motion characteristics.

3.2 Site conditions and broadband ground motion synthetics

Table 3.1 lists the sites used in this study and their corresponding NEHRP site classification based on the weighted average shear wave velocity of the top 30m of the profile (V_{S30}). With the exception of the Port Island site, all other sites are located in Southern California. As can be seen, the responses of 8 NEHRP class C sites, 11 class D sites and 5 class E sites with V_{S30} ranging from 142m/sec to 692 m/sec, are investigated in this study. The shear wave velocity profiles of the sites are shown in Fig. 3.1.

The crustal model used for the simulation of broadband ground motion synthetics was extracted from the SCEC CVM IV (http://www.data.scec.org/3Dvelocity/), and strong ground motion synthetics were computed for multiple rupture scenarios of a strike-slip fault rupture over a wide range of epicentral distances. More specifically, acceleration time histories were evaluated using a dynamic rupture source model (Liu et al., 2006) for medium and large magnitude events (M = 3.5, 4.0, 5.0, 6.0, 6.5 and 7.5) on a 100km by

Table 3.1: Site conditions for selected stations in this study

Location	**Station Name**	**Symbol**	**Site Class**	V_{s30} **(m/sec)**
Corralitos	Eureka Canyon Road	CLS	C	462.8
El Centro	El Centro Array # 7	E07	D	213.4
El Centro	Meloland Overcrossing	MEL	E	192.7
Emeryville	Pacific Park Plaza	EME	E	187.8
Gilroy	Gilroy Array # 2	G02	D	300.0
Halls Valley	Halls Valley	HAL	D	265.6
Los Angeles	Rinaldi Receiving Stn.	RIN	D	328.2
Los Angeles	Epiphany	EPI	D	281.8
Los Angeles	Obregon Park	OBR	C	457.4
Los Angeles	Sepulveda VA	SEP	C	370.0
Newhall	Fire Station	NEW	D	276.5
Oakland	Outer Harbor Wharf	OOH	D	245.1
Pacoima	Pacoima Kagel Canyon	PKC	C	509.0
Redwood City	Apeel # 2	A02	E	141.9
San Francisco	International Airport	SFO	E	213.9
Santa Clara	Santa Teresa Hill	STH	C	621.0
Santa Cruz	UCSC Lick Observatory	LOB	C	691.7
Simi Valley	Knolls School	KNO	C	555.1
Sylmar	Olive View Hospital	SYL	D	442.7
Sylmar	Jensen Generator Bldg.	JGB	C	526.2
El Centro	Meloland – Vertical Array	ELC	E	192.7
Eureka	Somoa Bridge – Vertical Array	EUR	D	187.1
Kobe	Port Island – Vertical Array	KPI	D	201.3
Los Angeles	La Cienega – Vertical Array	LAC	D	258.3

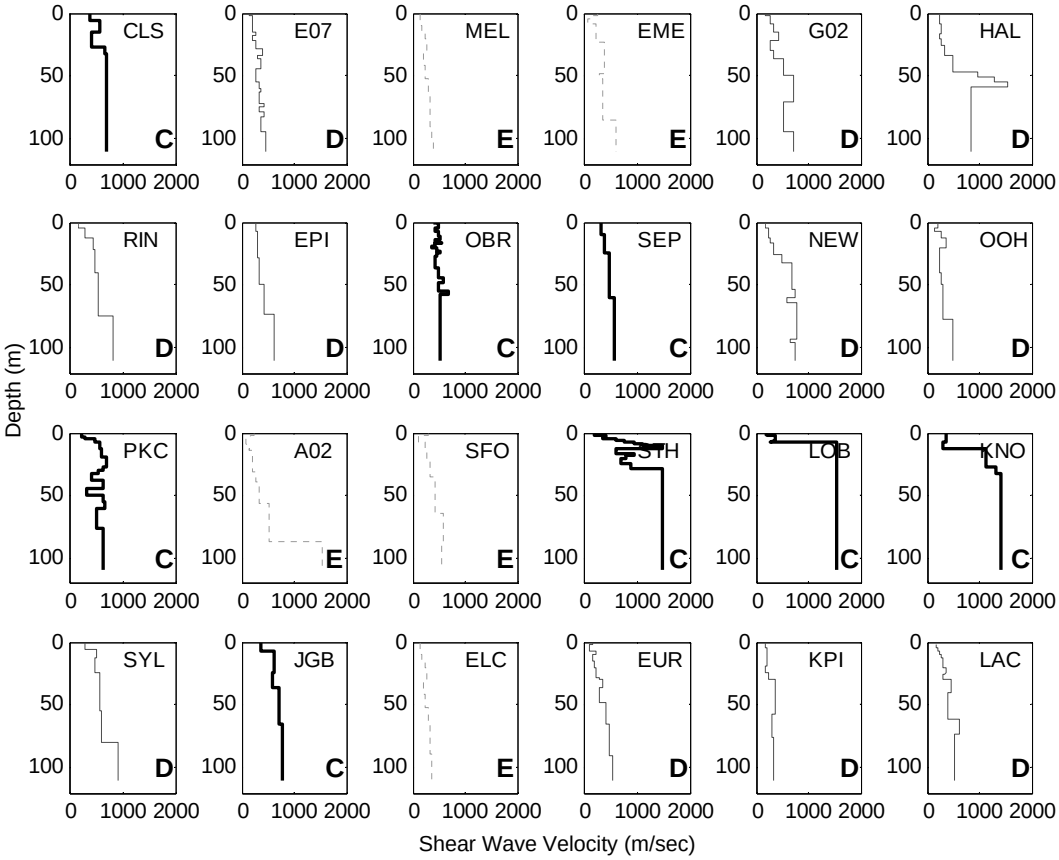

Figure 3.1: Shear wave velocity profiles at all the sites collected (The annotation in each figure denote the symbol of corresponding station; class C sites depicted by solid lines, class D sites by light lines and class E sites by dotted lines)

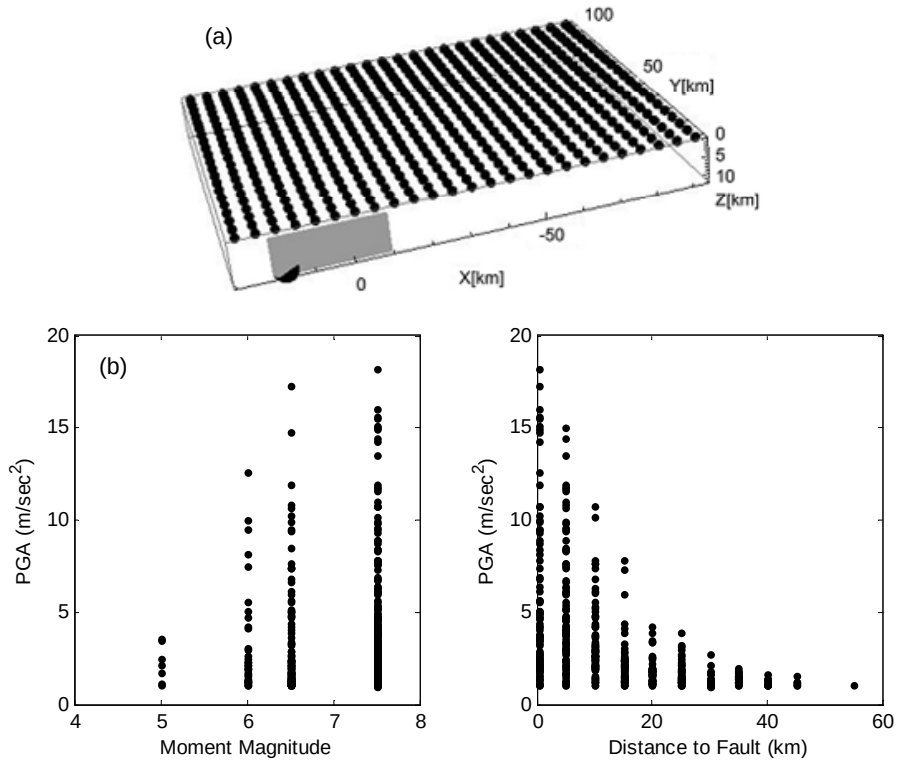

Figure 3.2: (a) Station layout over a $100 \times 120\text{km}^2$ grid where broadband ground-motion time histories were evaluated for a series of strike-slip rupture scenarios by means of the hybrid low-frequency/high-frequency approach with correlated source parameters (Liu et al., 2006). (b) Magnitude, Distance and PGA distributions of the synthetic rock outcrop motions used in the ground response and corresponding structure response analysis.

120 km square surface station grid (Fig. 3.2(a)) with spacing of 5km. Note that the low frequency synthetics (<1 Hz) were computed for a deterministic 3D crustal velocity structure using a finite-difference method, while the broadband components ($1< f <10$Hz) were computed for a 1D heterogeneous velocity model using a frequency-wave-number method. More details on the ground motion synthetics and the dynamic soil properties at the downhole array sites can be found in Assimaki et al. (2008b); Anderson (2003)

3.3 Empirical, Visco-Elastic and Nonlinear Site-Specific Analyses

Three widely employed site response models were used and compared in this study: the linear visco-elastic (LIE), the equivalent linear (EQL) and an incremental nonlinear model with a modified hyperbolic constitutive law (MKZ). Ground surface response results from

the site-specific analyses were also compared to the next generation attenuation relations (NGA) empirical amplification factors by Boore and Atkinson (2008).

The linear visco-elastic and equivalent linear models are based on the assumption of stationary motion and the site response analysis using these models is formulated in the frequency domain. The equivalent linear iterative analysis is perhaps the most widely employed approach for strong motion site response predictions in engineering practice, and details on the formulation and assumptions of the method can be found in multiple references such as Schnabel et al. (1972); Idriss and Sun (1992); Kramer (1996); Bardet et al. (2000).

The incremental nonlinear analyses were conducted using the modified Kondnor and Zelasko (MKZ) hyperbolic model (Matasović and Vucetic, 1993). Detailed description and validation of the MKZ model by comparison with downhole array recordings in the Los Angeles basin can be found in Assimaki et al. (2008b). Based on previous work by the authors, the nonlinear site response prediction by means of the MKZ model is used here as a benchmark, and the prediction error of the LIE, EQL site-specific response analyses is evaluated relative to it. Results of the nonlinear site-specific analyses were also compared to the NGA empirical amplification factors by Boore and Atkinson (2008) for each of the 24 profiles investigated, and the ensemble of synthetic ground motions. Attenuation relations account for site effects at soil profiles by scaling the frequency response of the BC-boundary reference site ($V_{S30} = 760$m/sec) outcrop motion as a function of the ground motion intensity level and the site conditions; here, the Peak Ground Acceleration (PGA) was used as ground motion intensity measure, while the NEHRP V_{S30} classification (BSSC, 2003) was used to describe the site conditions. Next, the amplification factors are estimated and the empirical model is employed to approximate the ground surface response as follows:

$$\mathrm{FAS_{GS}}(\omega) = \mathrm{EAF_{BA}}(\omega) \cdot \mathrm{FAS_{RO}}(\omega) \tag{3.1}$$

where FAS denotes the Fourier amplitude spectrum, GS and RO refer each to the Ground

Surface and Rock Outcrop motions, and $\mathrm{EAF_{BA}}$ is the amplification factor expressed as:

$$\mathrm{EAF_{BA}}(\omega) = \mathrm{SA_{V_{S30}}}(\omega)/\mathrm{SA_{BC}}(\omega) \tag{3.2}$$

where $\mathrm{SA_{V_{S30}}}$ and $\mathrm{SA_{BC}}$ are respectively the spectral acceleration ordinates evaluated for the soil site and the reference site.

The divergence of site-specific ground motion predictions from the empirically estimated site response, as well as the deviation between the site-specific analyses for the different soil models was next evaluated as a function of the site and ground motion characteristics.

3.4 Divergence of Site Response Spectral Predictions

Ground motion synthetics computed on rock-outcrop by the dynamic rupture seismological model were deconvolved to estimate the incident seismic motion at 100m depth, where nonlinear effects were unlikely to manifest during strong motion for the soil conditions studied here. Successively, the estimated incident motions were propagated through the 24 soil profiles to the surface by means of the three site response models investigated. Weak ground motions (rock-outcrop PGA $< 1\mathrm{m/sec^2}$), which are unlikely to cause yielding of medium soft to soft profiles and the overlying structures, were excluded from the ground and structural response analyses. Overall, 510 out of 6300 synthetic ground motions were selected for the simulations; Fig. 3.2(b) depicts the magnitude (M),PGA and distance (R)-to-fault distribution of these motions.

Next, the deviation between nonlinear (MKZ) and other (EAF, LIE, EQL) ground response predictions for all the profiles and all synthetic motions was evaluated. Note that the nonlinear MKZ model used here has been validated by comparison with downhole array recordings and was found to yield very satisfactory results for typical site conditions in Southern California. Differentiating the spectral acceleration (SA) at period T_i of each site response prediction by a superscript, the prediction error between each of the site response methods and the MKZ response can be defined; for example, for the case of the LIE response, the error was evaluated as:

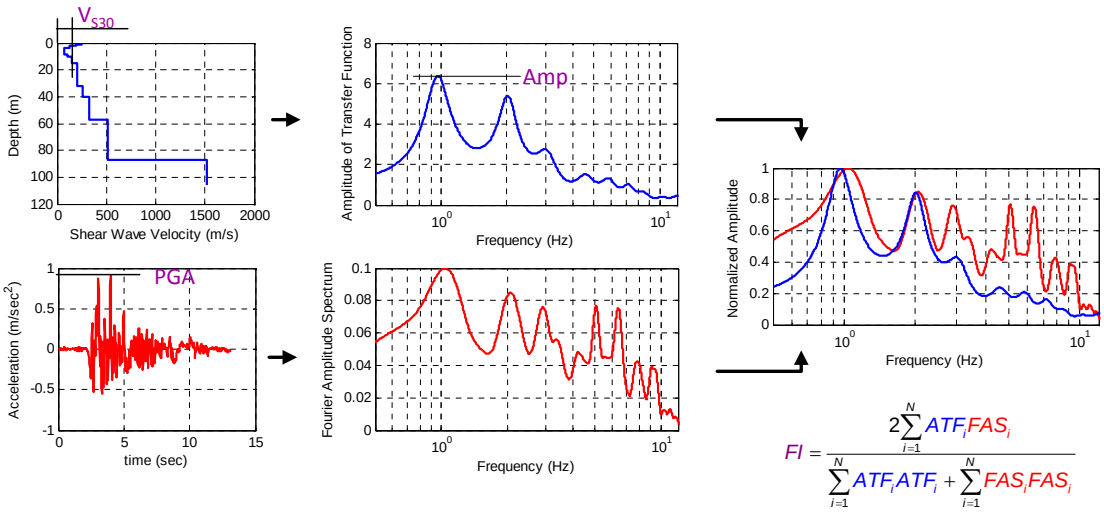

Figure 3.3: Graphic Illustration of frequency index (FI)

$$e_{SA}^{LIE} = \mu(e_{SA_i}) = \mu\left(\log\left(\frac{\mathrm{SA_i^{LIE}}}{\mathrm{SA_i^{MKZ}}}\right)\right) \tag{3.3}$$

where the operator μ corresponds to the non-weighted average, and the subscript i refers to period T_i. The averaged error is here evaluated for periods between 0.2 sec and 2.0 sec, a range that covers the dominant period of most common structures. In this case, the e_{SA}^{LIE} can be taken as a measure of misfit between the SA from LIE model and SA of MKZ model. In the ensuing, the site dependency of e_{SA}^{LIE} is first illustrated, and successively, the frequency-dependency of e_{SA}^{LIE} is highlighted by presenting results for different period bins.

The prediction error of the EAF, LIE, and EQL response relative to the MKZ response for selected sites was similarly evaluated and is shown in figure 3.4. The prediction error is presented in the form of a scattering plot as a function of the ground motion parameters PGA_{RO} (the peak ground acceleration at rock-outcrop) and FI (equation 3.4); fitting planes obtained by means of linear regression are also shown in the figure. The frequency index (FI), which is a measure of comparison between the seismic wavelengths and the thickness of the soil layers, is here defined as the normalized cross correlation between the amplitude of the linear transfer function of the site and the Fourier amplitude spectrum of the incident motion as follows:

$$\mathrm{FI} = \frac{2\sum_{\mathrm{i}=1}^{\mathrm{N}} \mathrm{ATF_i FAS_i}}{\sum_{\mathrm{i}=1}^{\mathrm{N}} \mathrm{ATF_i ATF_i} + \sum_{\mathrm{i}=1}^{\mathrm{N}} \mathrm{FAS_i FAS_i}} \tag{3.4}$$

where $\mathrm{ATF_i}$ and $\mathrm{FAS_i}$ are the amplitude of the elastic transfer function of the profile and the Fourier amplitude spectrum of incident motion at the i^{th} frequency point, normalized by their respective peak value, and N is the total number of frequency points in the range of interest, namely 0Hz to twice the fundamental frequency of the site. A graphic illustration of frequency index can be seen in figure 3.3. As mentioned above, FI is a quantitative measure of how well the incident motion can "see" the near-surface soil layers (Assimaki et al. (2008b)); the higher FI value, the greater similarity between the transfer function of the site and the Fourier amplitude spectrum of the incident motion that implies resonance phenomena, and when this FI value is combined with sufficiently high PGA, stronger nonlinear effects are anticipated to be triggered.

It can be seen in Figure 3.4 that the prediction error of LIE relative to MKZ shows clear linear dependency on both PGA_{RO} and FI, with the dependency onPGA_{RO} being stronger than that on FI. The LIE model lacks the ability to capture nonlinear site effects, and as a result, the divergence of LIE-predicted response relative to the MKZ response is clearly proportional to the ground motion intensity. By contrast, the prediction errors of EAF and EQL models are much more scattered, and no clear intensity and frequency content dependency is observed for most of the sites. The reason is that the EAF and EQL predictions, both approximately encapsulate the effects of soil nonlinearity; the former by averaging of soft soil response recordings, and the latter by strain-compatible approximation of soil response. For all of the sites, the overall prediction divergence between MKZ and EQL models is the least pronounced. The prediction divergence of EAF from the MKZ response is by contrast site-specific. Considering that the empirical amplification functions are a blended averaged strong motion recordings from past events at similar sites, the EAF prediction errors actually depend on how close the site-specific response is to the averaged amplification factors, given the ground motion.

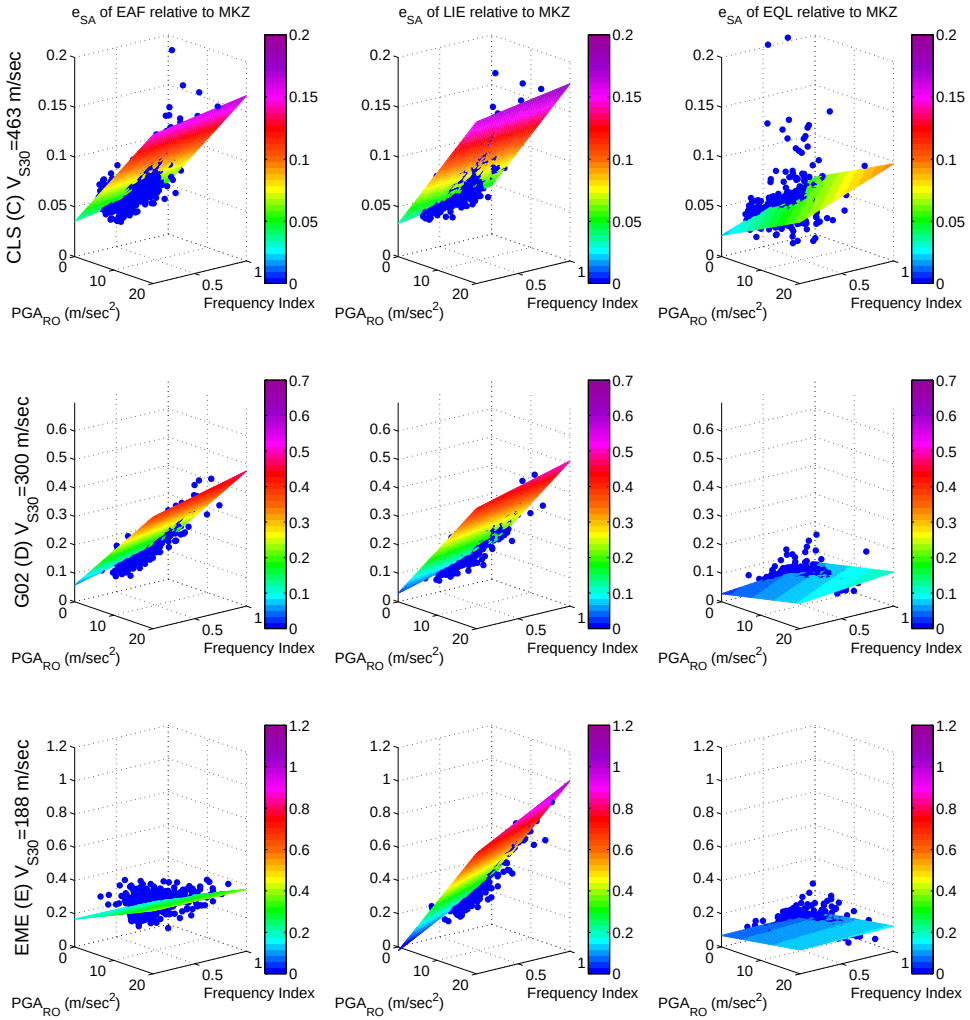

Figure 3.4: The spectral acceleration (SA) prediction errors of empirical amplification factor (EAF) model, visco-elastic (LIE) model, equivalent linear model relative to nonlinear (MKZ) model (averaged across the period interval [0.2sec - 2.0sec]) as functions of PGA_{RO} and frequency index (FI), and the regression planes are obtained based on the hypothesis that both PGA_{RO} and FI dependency of prediction errors are linear

By averaging all the prediction errors (relative to MKZ) across all ground motions estimated by a particular model for each site, an approximate assessment of the overall model performance can be obtained. Figure 3.5(a) shows the comparison of averaged prediction error of different models as a function of $760/V_{S30}$. As can be clearly seen, all the models (EAF, LIE, EQL) show increasing error with decreasing V_{S30}, while EQL model shows the weakest V_{S30} dependency and the LIE model shows strongest V_{S30} dependency. This observation is consistent with the abilities of models to capture nonlinear site effects. It should be noted that for stiffer sites ($760/V_{S30} < 2.5$), the performance of LIE model is very close to that of the EQL model and both show lower prediction error than that of EAF model, which is justified by the fact that the two former are site-specific. Also, comparison of the averaged prediction error of different models as a function of the first mode amplification of the linear transfer function is shown in figure 3.5(b). As can be seen, the prediction errors of the different models deviate from one another strongly when the first mode amplification is greater than 3. This deviation also reflects the capabilities of the different models to capture nonlinearity, since larger amplification at the first (resonant) mode tends to cause stronger nonlinear effects at the site.

Considering the clear PGA_{RO} and FI dependency of LIE prediction error (e_{SA}^{LIE}), this quantity is next used as a quantitative measure of the extent of soil nonlinearity at a given site, which, as revealed by figure 3.4, can expressed as the linear function of PGA_{RO} and FI, i.e.

$$e_{SA}^{LIE} = a \cdot PGA_{RO} + b \cdot FI \tag{3.5}$$

where a and b are regression coefficients. It should be noted that in figure 3.4, the intercepts of the regression plane for some sites slightly deviate from zero as a result of imperfect regression. Nonetheless, this deviation from zero will vanish in the final formulation of e_{SA}^{LIE}, in which both site and motion dependency are simultaneously considered.

As discussed previously, a and b are clearly site property dependent, and the two site

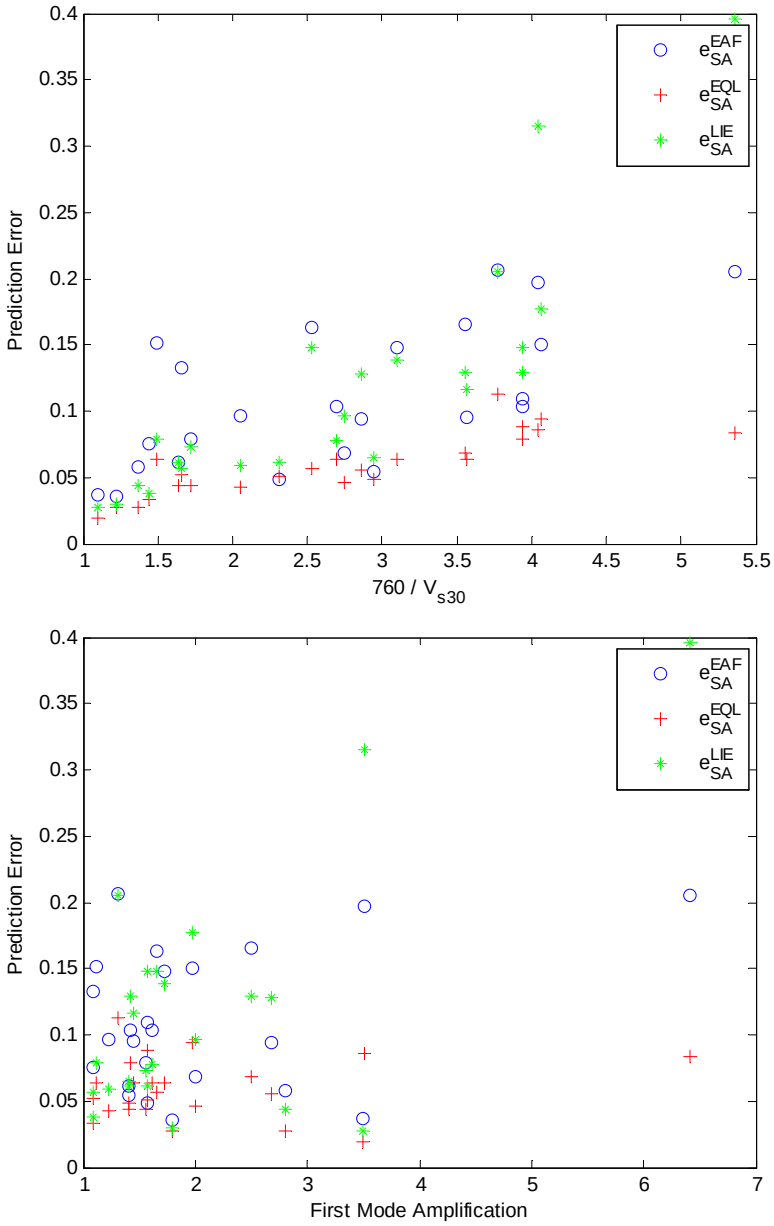

Figure 3.5: (a) SA prediction error of EAF, EQL, and LIE model relative to MKZ model as a function of site parameter V_{S30}; (b)SA prediction error of EAF, EQL, and LIE model relative to MKZ model as a function of site parameter Amp. For both (a) and (b), note that the prediction error is the averaged value for the motions

parameters selected here to express this dependency are V_{S30} and first mode amplification (Amp). The correlation analysis between coefficient a and site parameters shows that the V_{S30} dependency of a is much stronger than its Amp dependency. This relation can also be observed in figure 3.6(a). Therefore, a can be expressed as only function of V_{S30}. Correlation analysis between coefficient b and site parameters shows that the Amp dependency of b is slightly higher that its V_{S30}. However, to keep the final formulation of e_{SA}^{LIE} as simplified as possible, b is still expressed as only function of Amp. The consequence of this hypothesis can be seen in the residual-predictors plot. Based on the previous discussion, the final formulation of e_{SA}^{LIE} can be expressed as:

$$e_{SA}^{LIE} = \alpha \cdot \frac{760}{V_{S30}} \cdot \frac{\mathrm{PGA_{RO}}}{20} + \beta \cdot Amp \cdot FI + \varepsilon \tag{3.6}$$

where α and β are regression coefficients and ε is the residual, assumed to be normally distributed. It has to be noted that the unit of V_{S30} is m/sec and the unit of PGA_{RO} is m/sec^2 when applying this equation. The relation between e_{SA}^{LIE} and site-motion parameters can also be visualized in figure 3.7. It can be clearly seen that the intercept of the regression plane is indeed zero.

Figure 3.8 shows the residuals as function of first and second terms (predictor variables) in equation 3.6. It can be seen that the residual shows no dependency on both terms. The mean of residual is zero and the variance is assumed to be constant along both abscissas. It should be noted here that the linear response divergence from the nonlinear prediction, e_{SA}^{LIE}, was defined above as the averaged error within the period interval [0.2 - 2.0sec]. Since this quantity is clearly period dependent, the dependency of the error for a particular period is also investigated. For this purpose, the same procedure is repeated to establish the relation between $e_{SA_i}^{LIE}$ for period T_i and the site and ground motion parameters. Table 3.2 summarizes the values of the regression coefficients α, β and the standard deviation of residual (denoted as σ) for representative periods of interest in earthquake engineering.

In summary, the e_{SA}^{LIE} combined with the threshold error and corresponding confidence

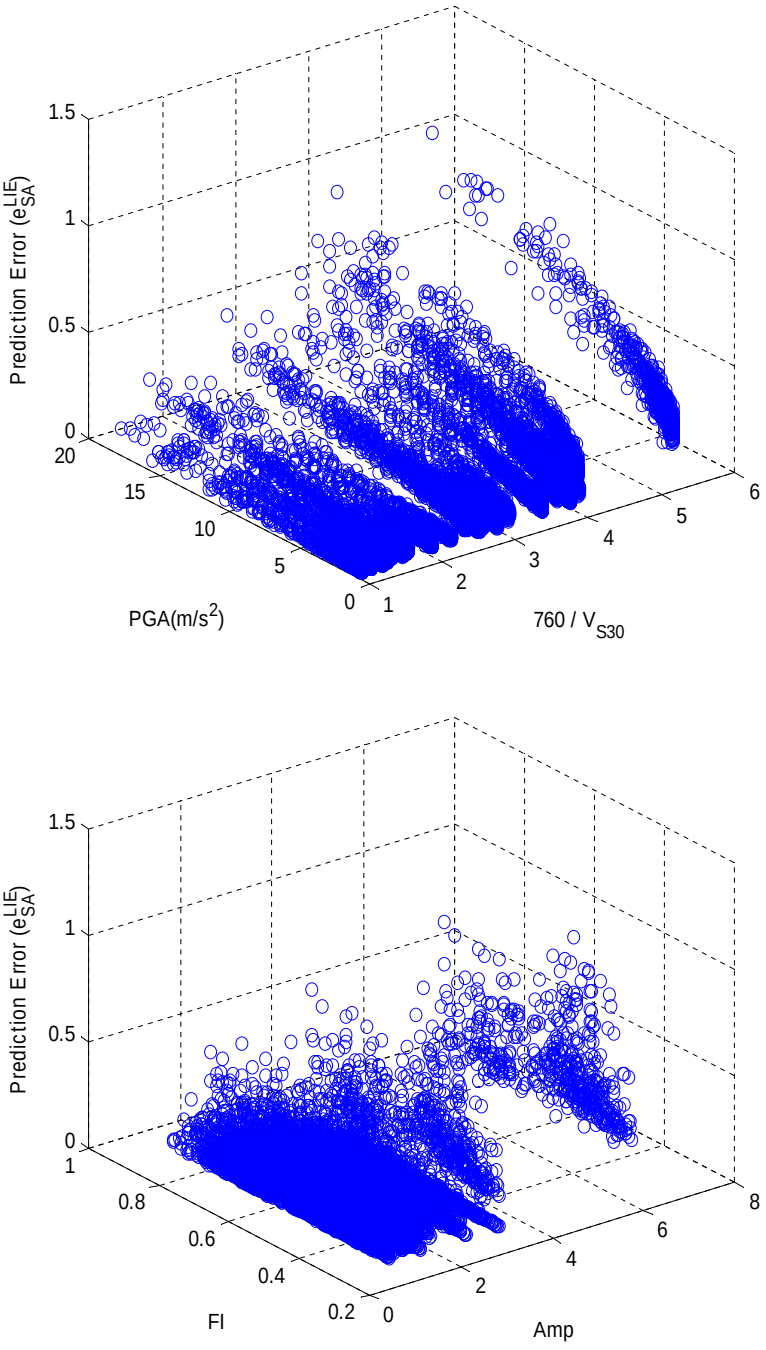

Figure 3.6: (a) The degree of PGA dependency as a function of V_{S30}, note that the softer of the site, the higher gradient along PGA direction; (b) the degree of FI dependency as a function of Amp, note that the higher Amp, the higher gradient along FI direction

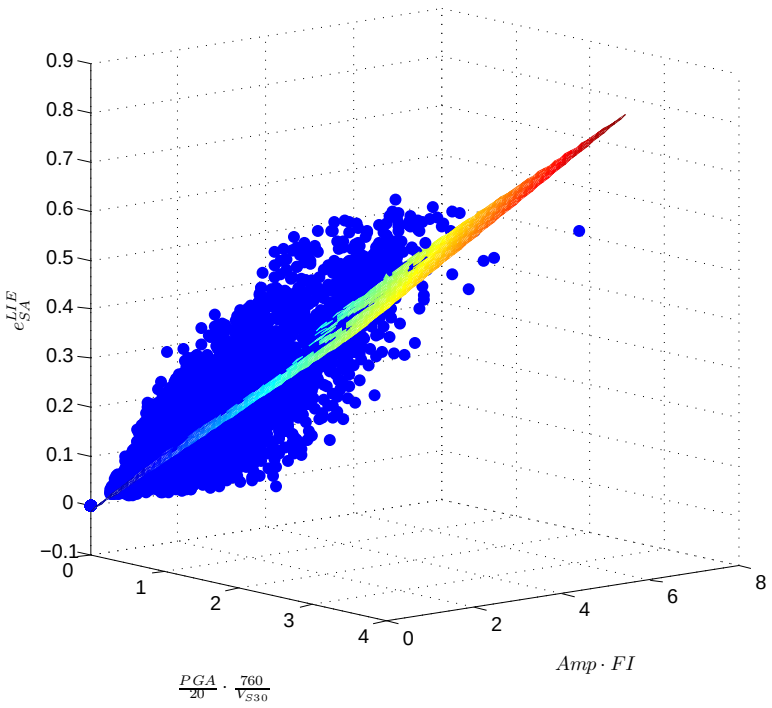

Figure 3.7: e_{SA}^{LIE} as a function of combined site and motion parameters

Table 3.2: Regression coefficients in equation 3.6 for different periods

T	α	β	σ
[0.2 - 2.0]	0.1342	0.0587	0.0442
0.0	0.1878	0.0517	0.0689
0.2	0.1517	0.0591	0.0712
0.5	0.1505	0.0752	0.0777
1.0	0.0817	0.0406	0.0534

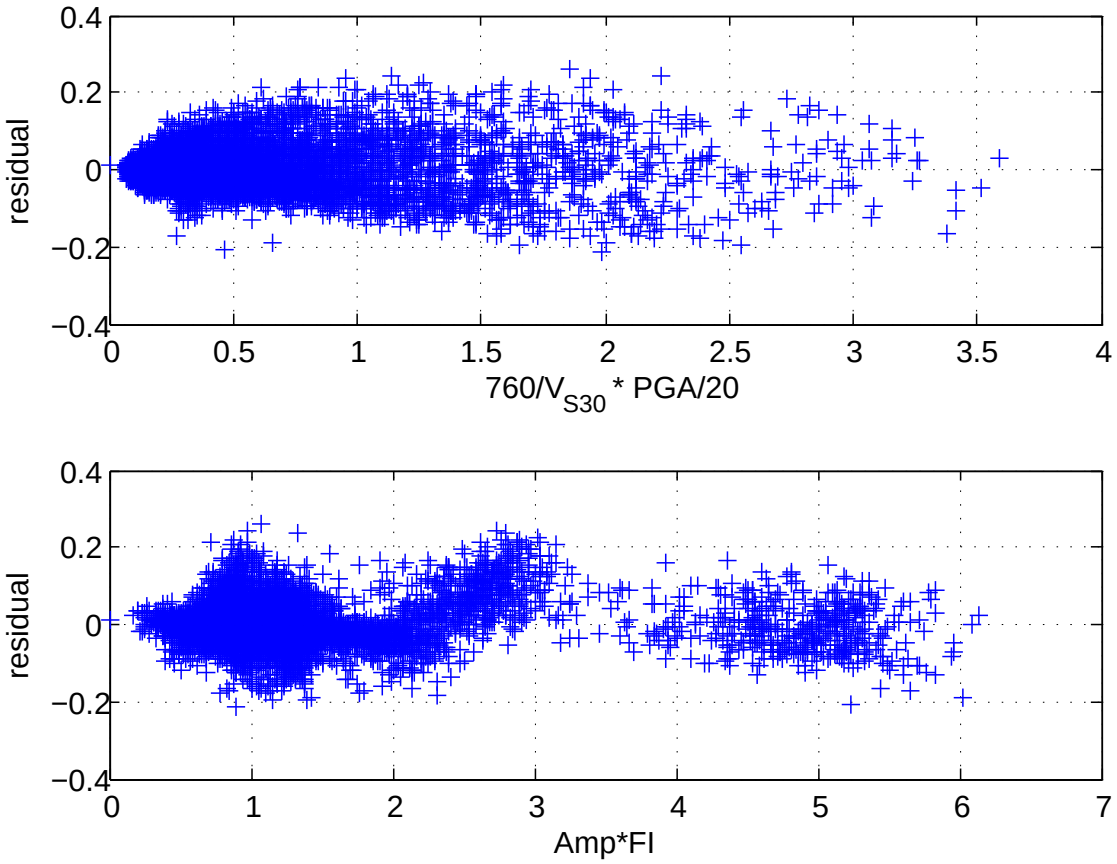

Figure 3.8: Residual in equation 3.6 against predictor variables

level, can be used to determine whether nonlinear site response should be employed for given motion and site conditions in a large-scale ground motion prediction.

3.5 Simplified Estimation of Site and Ground Motion Parameters for Large-Scale Seismological Models

While the parameters described above are shown to correlate well with the intensity of nonlinear effects at the sites investigated, the estimation of frequency index FI and first mode site amplification Amp requires detailed velocity and damping profiles, which may not be available for large scale seismological models or for implementation in engineering practice. As a result, a simplified procedure is necessary to estimate these parameters using the minimal available information at the site. Dobry et al. (2000) introduced the following empirical equation for the estimation of the first mode amplification (Amp):

$$Amp = \frac{1}{(1/I) + (\pi/2)\beta_s} \tag{3.7}$$

where I is rock/soil impedance ratio and β_s is the soil damping ratio. Assuming $I = V_{S100}/V_{S30}$ (V_{S100} corresponds to the shear wave velocity at depth of 100 m) and $\beta_s = 0.05$, Amp can be estimated using the above empirical relation. The comparison between the value of Amp extracted from the transfer function and Amp from the empirical relationship by Dobry et al. (2000) is shown in figure 3.9. It can be seen that the empirical equation yields a very good approximation of Amp for a wide range of impedance ratios.

For the approximate estimation of the frequency index, given the estimate of Amp above, the fundamental frequency of the site could be estimated using the H/V spectral ratio technique (Theodulidis et al., 1996; Rodriguez and Midorikawa, 2002; Parolai et al., 2004; Zhao et al., 2006, e.g.); admittedly, three-component ground motion records or ambient noise measurements are more widely available than detailed geotechnical information at soft sites. Successively, combining Amp with the H/V estimated fundamental frequency, one can obtain an approximation of the transfer function at first mode, that can be next used to calculate the frequency index FI at the site for a given motion.

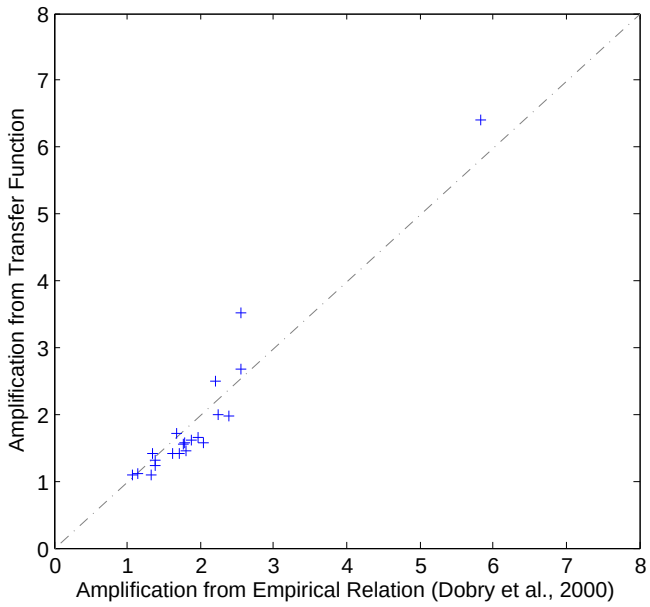

Figure 3.9: Comparison between the Amp from empirical relation and Amp from transfer function

3.6 Conclusion

The empirical relationship between site response nonlinearity, soil properties, and ground motion characteristics is investigated as a first step to enable efficient integration of nonlinear analyses in broadband ground motion simulations. Considering the impediment of limited number of design-level strong motion records on soft sites with detailed geotechnical information, ground motion synthetics at downhole array sites are employed, and the divergence between nonlinear analyses and more simplified models (e_{SA}) is estimated and used as a quantitative measure of how strong nonlinear effects are anticipated at a site during a seismic event.

Two site parameters are identified as the governing factors of the susceptibility of a site to nonlinear effects: V_{S30} (the weighted averaged shear wave velocity in the top 30 meters of the soil profile) and Amp (the site amplification at the fundamental period of the site); Two ground motion parameters are also identified: the peak ground acceleration (PGA_{RO}) at rock outcrop, and the so-called frequency index (denoted as FI, a quantitative measure of

how well the wavelengths of incident motion compare to the thickness of the soft soil layers). It is next shown that the e_{SA} increases proportionally to increasing PGA and Frequency Index (FI) for an individual site, and that the degree of PGA and FI dependency of each site is a function of V_{S30} and Amp, namely is site dependent.

Based on these observations, an empirical relation between e_{SA} and the site and ground motion parameters is established. This quantitative relationship allows an approximate estimate of the error introduced in ground response analyses when nonlinear effects are not accounted for, which may be used to identify the conditions when nonlinear analyses should be employed, and lead to efficient integration of nonlinear site response models in large-scale ground motion simulations.

It has to be noted that this study is specific to site conditions and ground motion synthetics in southern California. Nonetheless, the observations and interpretations are in line with the fundamentals of wave propagation theory, and therefore the proposed methodology may potentially be extended to a wider range of site and ground motion conditions.

CHAPTER IV

PARAMETRIC UNCERTAINTY OF NONLINEAR SITE RESPONSE ANALYSES

[1]

4.1 Introduction

Nonlinear site effects play a very important role in the development of successful seismic hazard assessment and mitigation strategies. The limited number of in-situ geotechnical investigation data, however, the effects of sample disturbance and scaling associated with laboratory tests, and the natural heterogeneity of soil profiles, are significant sources of uncertainty in nonlinear site response predictions. In addition, simulations of nonlinear effects are strongly affected by uncertainties in the intensity and frequency content of incident ground motion, the constitutive soil model used for the prediction, and the surface and subsurface geometry at the site (2D and 3D effects). The uncertainties associated with the description of soil parameters and the spatial variability of near-surface profiles have been long acknowledged, and their effects on the ground system response have been studied via stochastic finite elements, Monte Carlo simulations etc. Typical examples include the work of Ohtomo and Shinozuka (1990); Fenton (1990); Ural (1995); Popescu (1995) and Popescu et al. (1997) on the effects of spatial variability on soil liquefaction, Griffiths and Fenton (1993); Dham and Ghanem (1995) and Fenton and Griffiths (1996) on seepage through spatially random soils, Paice et al. (1996) on settlements, and the work of Nobahar and Popescu (2000) and Fenton and Griffiths (2001) on shallow foundations.

In this chapter, The effects of soil parameter uncertainty on the prediction of strong ground motion are examined. Several studies have been published on this topic in the past: Hwang and Lee (1991) studied the response of two hypothetical profiles of sand and

[1]This chapter is extracted and modified from Li and Assimaki (2010), and the permission from SSA to reprint the tables, figures and extracts is greatly acknowledged.

clay subjected to an M_w7.5 scenario earthquake in the New Madrid Seismic Zone. Tian and Jie (1992); Wu and Han (1992) and Suzuki and Asano (1992) investigated the effects of 1D spatial variability of shear wave velocity (V_S), density (ρ), damping (ξ) and soil layer thickness (h) using each randomized realizations of one base layered structure, and Field and Jacob (1993) evaluated the weak motion response of two base profiles in the Turkey Flat strong motion array. Roblee et al. (1996) used a stochastic finite-fault model to study the ground response variability due to uncertainties in the source, path, and site conditions, and showed that the controlling parameters in ground-motion predictions are the soil profile, ground motion amplitude, and frequency range of interest. They showed that for soil sites subjected to moderate-to-strong ground motion, site effects dominated the response variability for periods up to several seconds, and estimated the effects of soil parameter uncertainty on the response of a stiff site subjected to an M_w7 event at distance R=10km using nonlinear soil response analysis; for this site and ground motion, the maximum response variability was observed at T=0.2sec.

Additional work includes the published results by Rahman and Yeh (1999) for one base profile with the ground motion simulated as stationary random process with constant frequency content, Wang and Hao (2002) who included the effects of ground water level on the ground surface response variability, Nour et al. (2003) who investigated the effects of correlation distance of the soil V_S, ξ and Poisson's ratio (ν) for a 2D configuration, Assimaki et al. (2003) and Bazzurro and Cornell (2004) who investigated the effective stress transient nonlinear response of a cohesive and a cohesionless sites subjected to multiple recorded ground motions, Andrade and Borja (2006) who compared the ground response variability due to soil parameter uncertainty predicted at two sites by means of the equivalent linear (Idriss and Sun, 1992) and a time-domain nonlinear (Borja et al., 2000) models, and Stewart and Kwok (2008) and Kwok et al. (2008) who evaluated the effects of soil parameter uncertainty on the response of La Cienega SMGA and the Turkey flat vertical array profiles to strong ground motion events using the nonlinear site response computer code DEEPSOIL (Hashash et al., 2008a).

The most common limitations of these studies are associated with:

1. the statistical models used to describe the spatial variability of soils;

2. the small number of ground motions used in the analyses;

3. the shapes of simplified pulses compared to broadband seismograms;

4. the lack of design level records that illustrate the effects of soil parameter uncertainty for very large strains; and

5. the use of realistic nonlinear soil models in the analyses.

More specifically, Hwang and Lee (1991); Tian and Jie (1992); Assimaki et al. (2003); Andrade and Borja (2006) and Stewart and Kwok (2008) used a very limited number of ground motions, Wu and Han (1992); Rahman and Yeh (1999) and Nour et al. (2003) studied simplified pulses instead of true seismic excitations, Suzuki and Asano (1992) and Field and Jacob (1993) limited their study to weak ground motion recordings, and for the most part, results illustrated the effects of uncertainty in the low strain (visco-elastic) soil properties (Wu and Han, 1992; Suzuki and Asano, 1992; Tian and Jie, 1992; Field and Jacob, 1993; Rahman and Yeh, 1999; Nour et al., 2003; Assimaki et al., 2003). Finally, the spatial variability statistics of soil parameters (both visco-elastic and nonlinear) included in these studies correspond by enlarge to simplified probability distribution functions and correlation structures, while typical near-surface geologic formations tend to exert more complex spatial variability characteristics.

In this section, a comprehensive study on the effects of soil parameter uncertainty on site response analyses is conducted by addressing several of the issues described above. More specifically:

1. extensive geotechnical data on the spatial variability statistics of soils at three down-whole array sites in the LA Basin (Anderson, 2003; Toro, 1993; Darendeli, 2001) are used, and realistic stochastic fields of elastic and nonlinear dynamic soil properties are developed;

2. synthetic ground motions are generated by means of a finite source dynamic rupture

model (Liu et al., 2006) over a wide range of magnitudes and distances, and this statistically significant number of ground motions are used in the analysis;

3. realistic near-field broadband ground motions are used and the large-strain response of soils are simulated by means of a realistic hysteretic soil model (Assimaki et al., 2008b).

For each of the three sites, the effects of soil parameter uncertainty are evaluated as a function of the seismic input intensity and frequency content. It is shown that the frequency range where site response variability due to soil parameter uncertainty is maximized, is a function of both the site and the ground motion. The results are compared with previously published data, and show that differences in the estimated site response scatter might be significant for different soil models, spatial variability statistics or ground motion scenarios.

4.2 Site Conditions and Ground Motion Synthetics

This work is based on a previous study by the authors (Assimaki et al., 2008a), who evaluated the soil modeling variability in site response predictions at three downhole array sites in Southern California, using approximate and rigorous nonlinear site response models and synthetic ground motions. The position coordinates, operating agencies, depth of downhole instruments and geological description of the sites are given in Table 2.2. Downhole and suspension logging measurements, and laboratory resonant column modulus degradation and damping curves (Anderson, 2003) were available at these locations. Attenuation (Q) and density (ρ) profiles were estimated using low-amplitude seismogram recordings and the waveform inversion algorithm by Assimaki et al. (2006). The compiled shear wave velocity (V_S), attenuation ($Q = 1/(2\xi)$, where ξ is the material damping) and density profiles (ρ) are shown in Figure 2.8, and are used as base-profiles of the random soil property fields in this study.

Since strong ground motion recordings at these stations were scarce, Assimaki et al. (2008b) developed a statistically significant dataset of seismic input motions using synthetic records. For this purpose, they used 1D crustal compressional velocity (V_p), shear velocity (V_S) and density (ρ) models from the 3D Southern California Community Velocity Model

IV (SCEC CVM IV: http://www.data.scec.org/3Dvelocity/) and the hybrid low-/high-frequency dynamic rupture source model by Liu et al. (2006). They simulated multiple strike-slip fault rupture scenarios over a square grid of surface stations for medium to large magnitude events ($M_w = 3.5 - 7.5$) at distances $R = 2.0$ –75km. These ground motions are also used in the following analyses.

Finally, Assimaki et al. (2008b) conducted site response simulations at the three sites for the limited number of recorded ground motions, and the ensemble of synthetic seismograms using multiple soil models. They evaluated the deviation of ground surface predictions from the observed time histories, and selected the soil hysteretic model that yielded the minimum error on average. This corresponded to the monotonic constitutive law by Matasović and Vucetic (1993) coupled with a modified hysteretic formulation of the model proposed by Muravskii (2005), and is also implemented in the nonlinear analyses conducted here.

4.3 Statistical Description of Soil Parameter Uncertainty

Next, the sources of soil parameter uncertainty considered in this study are described, along with the idealized probability distribution functions selected to approximate the available empirical data. Among the three classes of methods widely used for studies of uncertainty propagation problems, namely the expansion-based, the point estimation and the simulation-based methods, Monte Carlo simulations (MCS) are implemented to evaluate the effects of parameter uncertainty on the ground surface response of soil profiles. Despite the computational effort associated with MCS:

1. the number of simulations to get a stable variance estimation is independent of the complexity of the propagation function, namely the strong nonlinearity of this system would only affect the computational time of each analysis;

2. the correlation between soil parameters adopted in this work requires a relatively small number of simulations to get a stable variance estimation; and

3. MCS is the most robust uncertainty analysis technique that could be used here given the high soil parameter variability of the problem (COV $\simeq 0.5$ as shown below)

For the MCS conducted in this work, the free soil parameters of the hysteretic soil model (see Assimaki et al., 2009) are first identified, idealized probability distributions are estimated based on available geotechnical information at the three arrays, and randomized nonlinear soil profiles are developed. Next, deterministic ground response analyses are conducted for the ensemble of recorded and synthetic ground motions by simultaneously varying all free parameters, and the total variability introduced in ground response predictions due to the soil property randomness are estimated. Successively, each of the free soil parameters is fixed, random profiles are re-generated, and site response simulations are repeated for the same incident ground motions to estimate the corresponding reduction in ground motion variability. Finally, the scatter in site response due to soil parameter uncertainty is expressed as a function of the ground motion intensity and frequency. The free parameters, available data and idealized probability distribution functions used in the MCS are next described.

The shear wave velocity (V_S), and the shear modulus reduction (G/G_{max}) and material damping (ξ) as a function of cyclic shear strain amplitude (γ_a) are selected as free soil model parameters. The soil shear strength ($\tau_{\max}$) is not considered since the database of synthetic records contained very few input motions that may cause failure in the soil, and for the medium to high strain region studied in this paper, the effects of max variability can be safely neglected. According to Phoon and Kulhawy (1999), typical sources of uncertainty in the description of these parameters are:

1. the inherent heterogeneity of soils,
2. the scarcity of geotechnical information on the soil nonlinear response, and
3. laboratory measurement errors related to sample disturbance, sample size, and implementation of empirical formulae to transform index to design soil properties.

Separation of the sources of uncertainty is rarely feasible, and a single probability distribution function is typically used for each parameter, without explicit consideration of the individual contributing factors (Toro, 1993; Darendeli, 2001). The variability statistics of the soil parameters investigated in this study are next described.

4.3.1 Low-Strain Shear Wave Velocity V_S

The statistical model by Toro (1993) is adopted to describe the uncertainties of low strain soil shear wave velocity (V_S). This probabilistic model was developed using data from generic soil profiles in the EPRI (1993) database, and describes the intra-layer (i.e. the probability distribution) and the inter-layer (i.e. the spatial variability statistics) shear wave velocity (V_S) statistical properties, as well as the layer thickness randomness in typical soils. Layered profiles tend to be more variable in the near-surface (i.e. require a finer discretization), and Toro's model (Toro, 1993) account for this characteristic by implementing a non-homogeneous Poisson process with depth-dependent rate to describe soil layering. A modified power-law model is selected to characterize the depth-dependent rate of layer boundaries, whose coefficients need to be estimated from the available geotechnical data by means of the method of maximum likelihood (Benjamin and Cornell, 1970). Based on the ensemble of data in the EPRI (1993) database, the rate (λ) was estimated as

$$\lambda(h) = 1.98(h + 10.86)^{0.89} \tag{4.1}$$

where λ is the rate of layer boundaries (foot[1]), and h denotes depth in feet.

In addition to the probabilistic description of the soil layer thicknesses, Toro's (1993) velocity model is used to idealize the variability of V_S within each layer and its correlation with adjacent layers. More specifically, Toro (1993) studied the probability distribution of $ln(V_S)$ using the cumulative distribution of standardized variables shown in equation 4.2 for generic soil profiles (Figure 4.1):

$$Z_i = \frac{\ln(V_i) - \ln(V_{median,i})}{\sigma_{\ln V}} \tag{4.2}$$

where V_i is the velocity at the midpoint of layer i, $V_{median,i}$ is the median velocity of the same layer and $\sigma_{\ln V}$ is the standard deviation of $\ln(V_S)$. Note that the thin solid lines in Figure 4.1 represent the 10% Kolmogorov-Smirnov bounds (Benjamin and Cornell, 1970), and the observed $\ln(V_S)$ values plot on a nearly straight line within the bounds, which indicates that variability of shear wave velocities for typical soil formations can be

described by a log-normal distribution. Following Toro (1993), the log-normal distribution of velocities and the velocity correlation among layers at the three sites are characterized using a first-order auto-regressive model, i.e.

$$\begin{aligned} z_1 &= \epsilon_1 \\ Z_i &= \rho Z_{i-1} + \sqrt{1-\rho^2}\epsilon_i, i > 1 \end{aligned} \tag{4.3}$$

where ρ is the serial auto-correlation coefficient of Z_i, and ϵ_i are independent normal random variables with zero mean and unit standard deviation. Equation 4.3, the parameters ρ and σ_{lnV} , and the median shear wave velocity (V_S) profile define completely the probabilistic velocity model. Toro (1993) estimated the parameters ρ and $\sigma_{\ln V}$ using data from generic soil profiles via linear regression as $\rho = 0.557$ and $\sigma_{lnV} = 0.39$ (corresponding to a velocity COV of 41%), and these values were also adopted in this study in absence of site-specific data on the V_S spatial variability statistics. Note that if more detailed geotechnical data were available at the site, the parameters ρ , $\sigma_{\ln V}$ of the log-normal distribution would have been calibrated based on the site-specific information, and the V_S stochastic model would have been characterized by a lower COV. As a result, the generic site probabilistic model adopted here yielded a wider range of ground surface response that may be interpreted as an upper bound ground motion variability due to soil parameter uncertainty.

The autocorrelation function used in this work is plotted in Figure 4.2, and the strong correlation between V_S values of adjacent layers described by $\rho = 0.577$ will be shown below to be favorable the in the Monte Carlo simulations. Using Toro's (1993) probabilistic velocity model, random realizations of the V_S stochastic fields were next generated using a two standard deviation truncation of the log-normal distribution to eliminate potential outliers. Realizations of the V_S profile at one of the downhole array sites are shown in Figure 4.3, where the thick black line corresponds to the median profile at the site (Assimaki et al., 2008b) and the thin gray lines to fifty randomized V_S profiles.

4.3.2 Modulus Reduction (G/G_{max})and Material Damping (ξ)

To describe the nonlinear soil parameter uncertainty, the probabilistic model proposed by Darendeli (2001) is used, in which who studied the covariance structure of modulus reduction

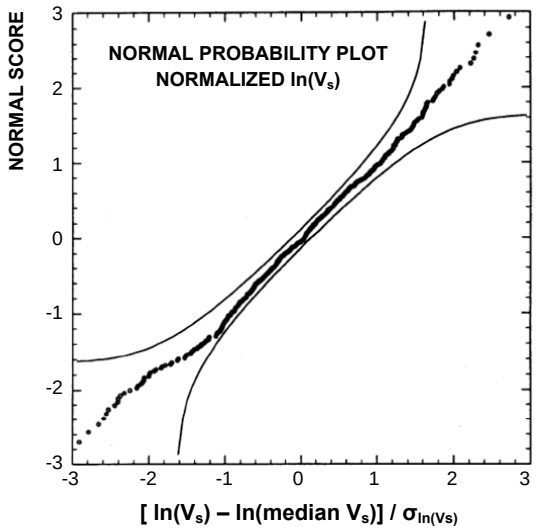

Figure 4.1: Lognormal probability plot evaluated using the ensemble of data from the EPRI shear-wave velocity (V_S) database. Smooth curves correspond to the 10% Kolmogorov-Smirnov bounds of the probability distribution. A lognormal distribution was implemented in this study as well to describe the VS distribution in each layer of the profiles studied (modified from Toro, 1993).

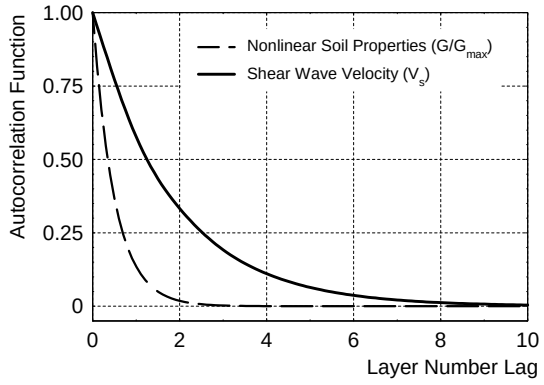

Figure 4.2: Autocorrelation function describing the layer-to-layer correlation of shear-wave velocity (V_S) and nonlinear dynamic soil properties in this study. Note that the latter was evaluated for the spatial distribution of G/G_{max} at 0.03% strain, while perfect correlation was assumed for the remaining of the G=Gmax data points and associated material damping (ξ) values.

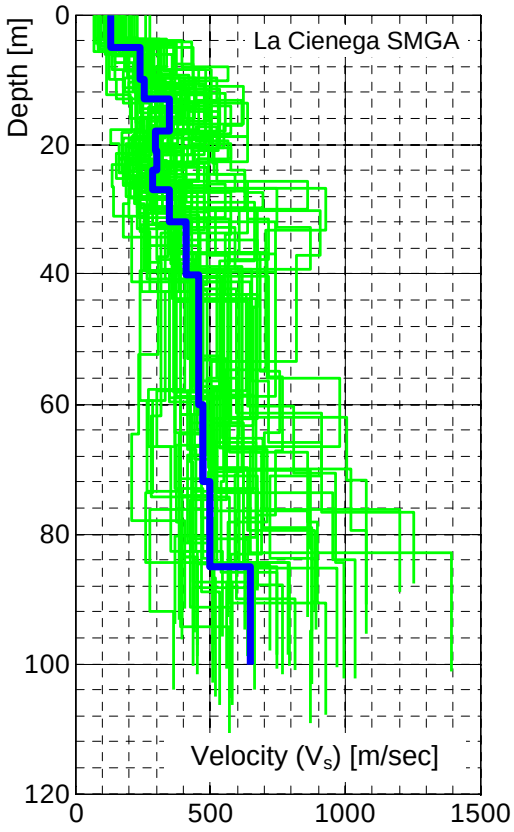

Figure 4.3: Sample realizations of shear-wave velocity (V_S) profile at the La Cienega SMGA (black line corresponds to the base profile, and gray lines to 50 realizations of the random field)

(G/G_{max}) and material damping (ξ) curves of soils using a First-Order Second-Moment Bayesian method on 110 soil samples from Northern California, Southern California, South Carolina and Taiwan (see also Kottke and Rathje (2009), who implemented Darendeli's statistical data to site response analyses using Random Vibration Theory). According to Darendeli (2001), the strain-dependent standard deviation of modulus reduction curves (G/G_{max}) for generic soil conditions can be represented by the following expression:

$$\sigma_{G/G_{max}} = \exp(\phi_{13}) + \sqrt{\frac{0.25}{\exp(\phi_{14})} - \frac{(G/G_{max} - 0.5)^2}{\exp(\phi_{14})}} \tag{4.4}$$

where $\sigma_{G/G_{max}}$ is the data standard deviation at a given strain level; G/G_{max} is the corresponding median value of modulus reduction; and ϕ_{13}, ϕ_{14} are model parameters which depend on the soil type. Darendeli (2001) also evaluated the strain-dependent standard deviation of material damping (ξ) curves for generic soils as follows:

$$\sigma_{\xi} = exp(\phi_{15}) + exp(\phi_{16}) \cdot \sqrt{\xi} \tag{4.5}$$

where σ_{ξ} is the data standard deviation at a given strain level; ξ is the corresponding median material damping ratio; and ϕ_{15}, ϕ_{16} are model parameters which also depend on the soil type. The mean values of the model parameters ϕ_{13}, ϕ_{14}, ϕ_{15} and ϕ_{16} for generic clays were estimated by Darendeli (2001) as 4.0, -5.0, -0.725 and 7.67 correspondingly, and these values were also adopted here. The resulting strain-dependent standard deviation of dynamic soil properties for generic sedimentary sites is shown in Figure 4.4.

To complete the statistical description of nonlinear soil parameters in this study, three additional assumptions are introduced to allow realistic realizations of G/G_{max} and ξ curves for layered soil profiles. These assumptions are based on the statistical analysis of dynamic soil properties for generic soil profiles conducted by Toro (1993) and the limited site-specific data collected at the downhole array site La Cienega in the LA Basin by Anderson (2003), and are briefly described below:

1. Perfect correlation between G/G_{max} values is assumed.

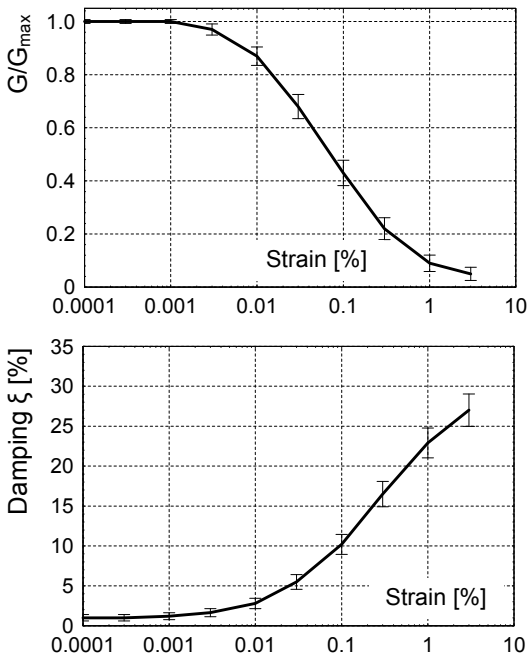

Figure 4.4: Strain-dependent standard deviation of normalized modulus (G/G_{max}) and material damping (ξ) (modified from Darendeli, 2001).

2. Perfect correlation between G/G_{max} and material damping (ξ) at each strain level is assumed. Figure 4.5 shows the regression analysis conducted on data from the EPRI (1993) generic soil database at multiple strain levels, which shows very strong correlation between G/G_{max} and material damping (ξ). The linear regression analyses are repeated for the ensemble of geotechnical data available, both site-specific and generic, and the regression slopes (referred to as coefficient of proportionality) are plotted in Figure 4.6. Consistency between the statistical properties of the various datasets is observed, with the coefficients evaluated for sands using data by Darendeli (2001) and Toro (1993) nearly coinciding at strain amplitudes above 0.05%. In this study, the proportionality coefficients derived for generic clay sites by Darendeli (2001), which is the most comprehensive soil property dataset available, is adopted.

3. The value of G/G_{max} at 0.03% strain is considered as a representative property of the nonlinear soil response for each layer. Successively, the perfect correlation between G/G_{max} values at different strains assumed in assumption 1 is used to estimate the

remaining G/G_{max} curve, and the perfect correlation between G/G_{max} and material damping (ξ) described by assumption 2 is used to generate the damping (ξ) curve.

The autocorrelation function used in Section 4.3.1 to describe the V_S spatial variability was also implemented to describe the spatial variability of nonlinear properties. Based on available geotechnical data at the La Cienega downhole array site and assuming G/G_{max} at γ=0.03% to be a representative value of the soil response, a site-specific autocorrelation coefficient is estimated to be 0.15 for the dynamic soil properties. Note that the corresponding coefficient for low-strain properties is estimated equal to 0.577.

The two autocorrelation functions are compared in Figure 4.2, and it can be readily seen that the nonlinear dynamic soil properties between adjacent layers are much more weakly correlated than the Vs values. This weak correlation between nonlinear soil properties of adjacent soil layers implies that the Monte Carlo simulations of nonlinear parameters will require a larger number of profile realizations than the corresponding V_S profiles as shown in the following section. Finally, due to lack of additional geotechnical information, an autocorrelation coefficient equal to 0.15 is implemented for all three arrays studied. An example of G/G_{max} and material damping (ξ) realizations at depth 7.5m of the La Cienega downhole array are shown in Figure 4.7. In accordance to the V_S stochastic model described in Section 4.3.1, a 2-σ truncation to the probability distribution function is implemented prior to generating random fields to avoid unrealistic soil profiles. It can also be shown in Figure 4.7 that the realizations of both G/G_{max} and material damping (ξ) curves are well bounded by the physical bounds extracted from EPRI data.

4.3.3 Random Field Realizations of Nonlinear Soil Parameters

To evaluate random realizations of the correlated G/G_{max} and material damping (ξ) stochastic fields, a new hysteretic scheme based on the model proposed by Muravskii (2005) is developed, which is capable of simultaneously matching the G/G_{max} and material damping (ξ) curves of soils in the intermediate to high strain range ($\gamma > 10^{-3}$). By contrast to the widely employed extended Masing rules (Pyke, 1979; Kramer, 1996) where the unload-reload branches of the hysteretic loop are scaled and reversed replicas of the monotonic

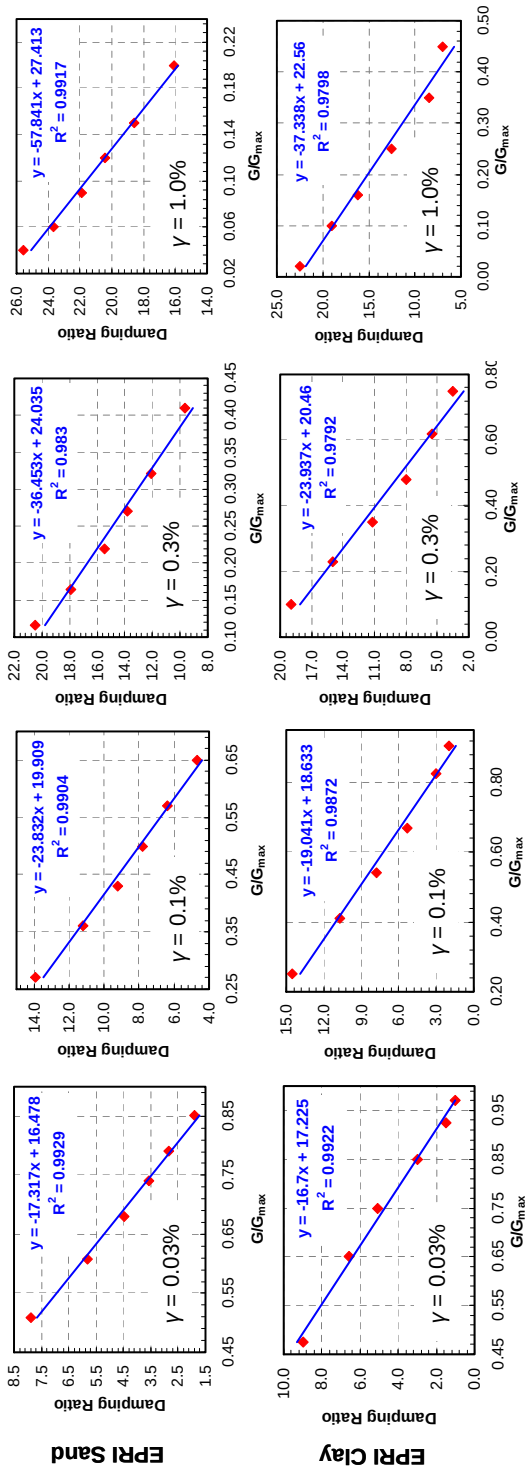

Figure 4.5: Correlation between normalized modulus (G/G_{max}) and material damping (ξ) at multiple levels of strain amplitude (γ) for the EPRI sand and EPRI clay database (Toro, 1993).

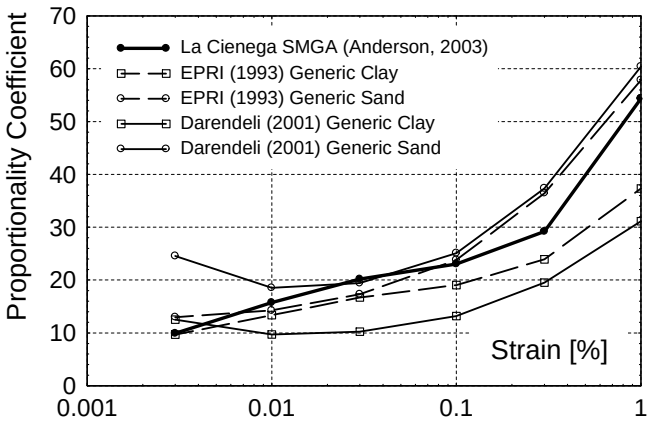

Figure 4.6: Proportionality coefficients between normalized modulus (G/G_{max}) and material damping (ξ) as a function of strain, evaluated using generic soil properties from the EPRI (1993) and the Darendeli (2001) databases and site-specific geotechnical information at La Cienega SMGA .

(backbone) loading curve, the backbone curve and hysteretic functions of the new model are described by the same constitutive law yet different sets of parameters. As a result, matching of the G/G_{max} curve is achieved by calibration of the monotonic curve parameters, while matching of the material damping (ξ) curves by calibration of the unload-reload parameters.

The new hysteretic scheme requires calibration of the hysteretic function parameters once and scaling of the backbone curve at stress reversals thereafter, by contrast to the original formulation by Muravskii (2005) that involves reevaluation of the unload-reload model parameters at every stress reversal point. An additional feature of the new hysteretic model is that the stiffness upon unloading may be less than the initial modulus at large shear strains, which is consistent with the material degradation observed in the laboratory by Darendeli (2001). An example of the new hysteretic model response is shown in Figure 4.8, where a soil element with the nonlinear dynamic properties shown in Figure 4.7 is subjected to a transient excitation. The hysteretic loops predicted using the extended Masing rules (Kramer, 1996) are compared to the new hysteretic scheme: the narrower loops of the new model imply lower, more realistic material damping values at the corresponding shear strain amplitudes.

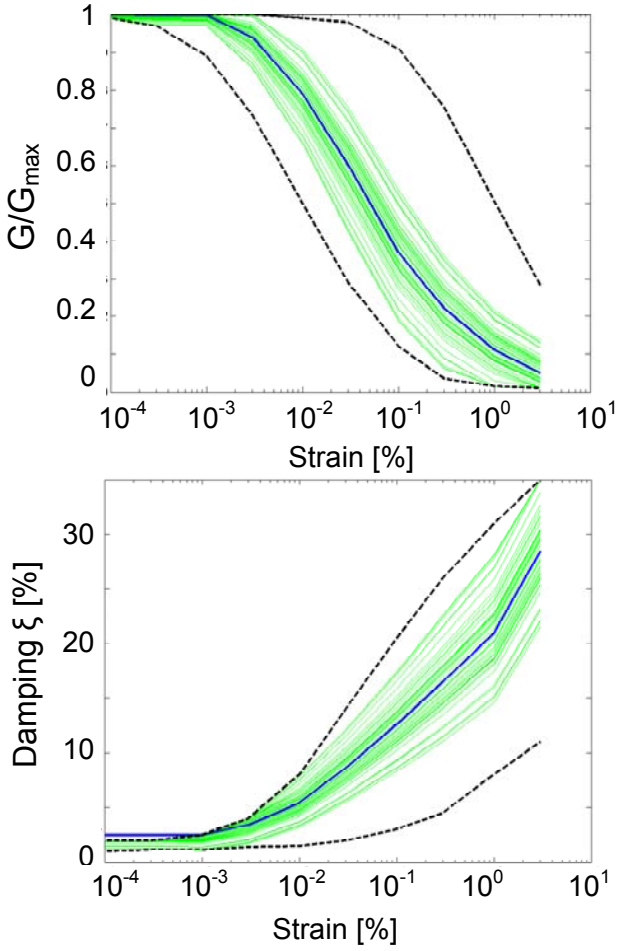

Figure 4.7: Sample realizations of normalized modulus (G/G_{max}) and material damping (ξ) curves. The solid black lines correspond to the dynamic soil properties evaluated at the La Cienega SMGA at depth 7.5 m by Anderson (2003); the gray lines correspond to sample realizations of the probability model, and the dashed black lines correspond to the physical upper and lower bounds of dynamic soil behavior as estimated by Toro (1993) for the ensemble of soil samples in the EPRI database

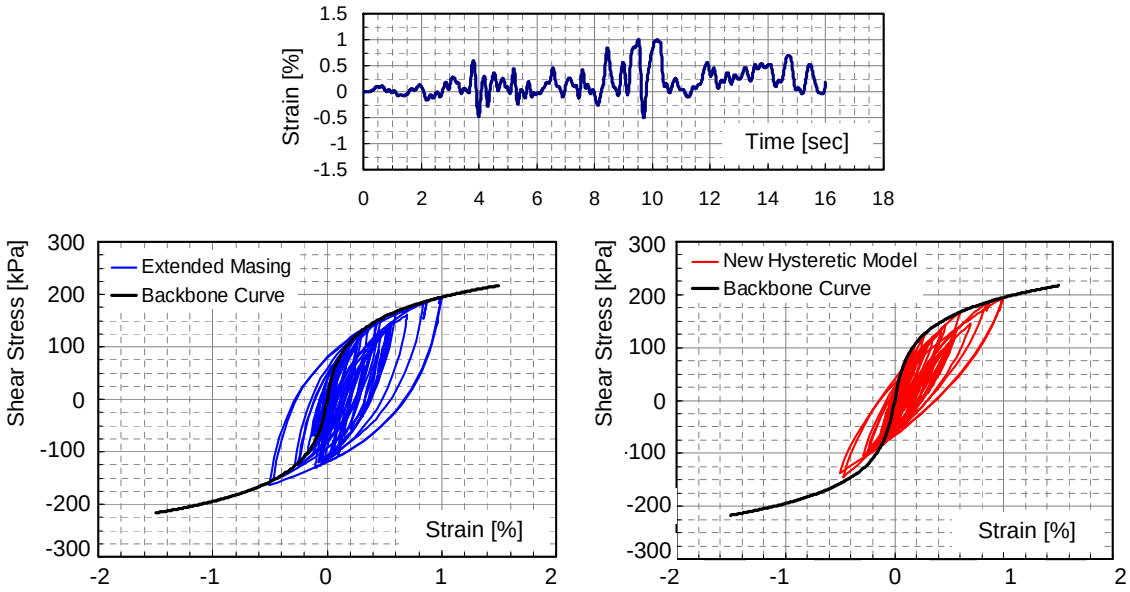

Figure 4.8: Nonlinear soil element subjected to transient strain time history (top). Comparison of backbone curve from MKZ model and 23 hysteretic loops evaluated by means of the extended Masing rules (bottom, left) and backbone curve from MKZ model and hysteretic loops from the new hysteretic scheme developed based on Muravskii (2005) (bottom, right).

4.4 Monte Carlo Simulations for Uncertainty Propagation

Using the statistical description of the V_S, G/G_{max} and material damping (ξ) described above, Monte Carlo simulations are conducted for each profile and ground motion scenario. For each case, the ground motion variability is expressed in terms of the standard deviation of the logarithmic spectral acceleration (SA) on ground surface ($\sigma_{\ln SA}$). The estimation of stable variance in Monte Carlo simulations is here discussed for two examples, a near-field strong motion anticipated to trigger significant nonlinear effects in the near surface, and a far-field weak motion expected to yield almost linear elastic site response.

First, Figure 4.9 depicts the ground response variability for the first case, a near-field motion with peak ground acceleration PGA=1.142g. The spectral accelerations evaluated from simultaneously randomizing the V_S, G/G_{max} and material damping (ξ) profiles are shown in Figure 4.9b, while the spectral accelerations computed for random realizations of the V_S and G/G_{max} stochastic models separately are shown in Figure 4.9c and Figure 4.9d respectively. As expected, the ground motion SA variability is very large and is attributed

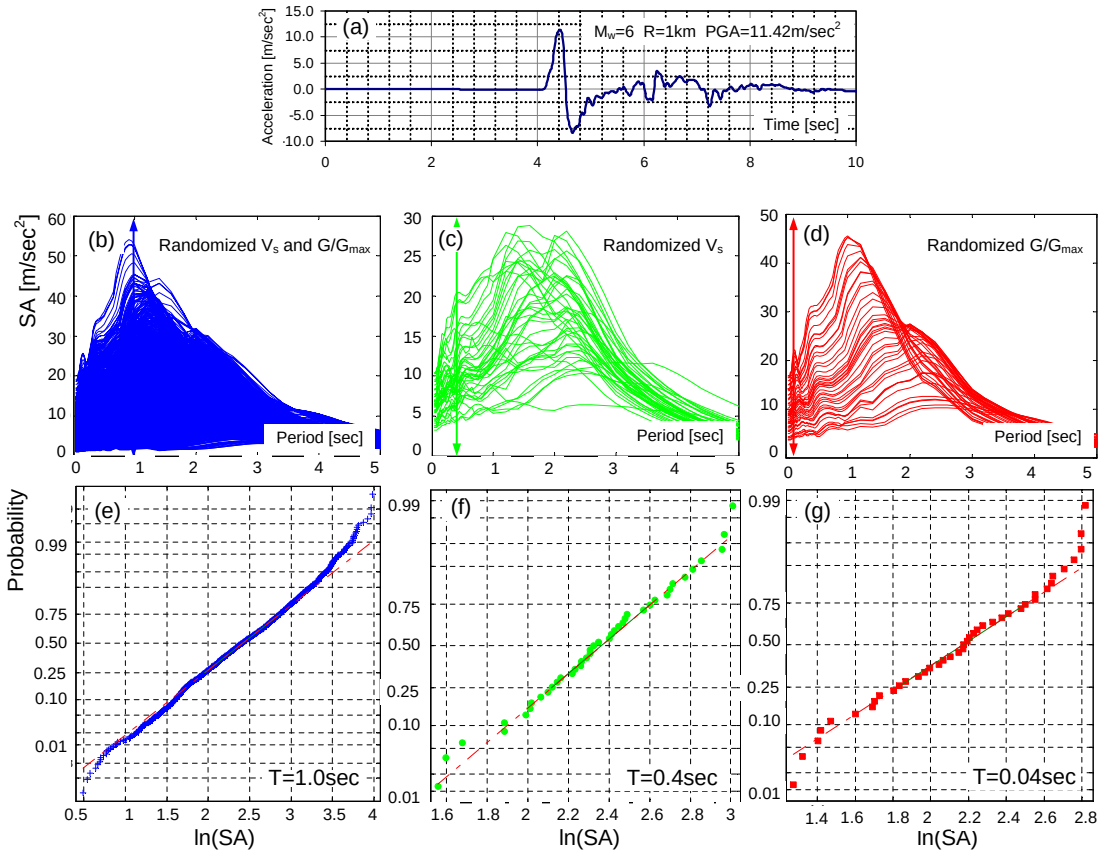

Figure 4.9: Variability in spectral acceleration (SA) caused by uncertainties in soil parameters for a strong seismic excitation. (a) Rockoutcrop acceleration time history; (b) SA variability caused by V_S and G/G_{max} randomness; (c) SA variability caused by V_S randomness; (d) SA variability caused G/G_{max} randomness; (e) normal plot of SA in (b) at period $T = 1.0$ sec; (f) normal plot of SA in (c) at period $T = 0.4$ sec; (g) normal plot of SA in (d) at period $T = 0.04$ sec.

both to the low-strain and the nonlinear soil parameter randomness.

Next, Figures 4.9e-g depicts the normal distribution of SA values at three different periods for the simulations shown in Figures 4.9b-d. As can be seen in all cases, the $ln(SA)$ distribution at arbitrary periods is approximately normal, with the exception of a small deviation at both ends of the distribution. This result verifies that the strong motion ground response variability may be successfully evaluated by means of $\sigma_{\ln SA}$.

The evolution of $\sigma_{\ln SA}$ with number of realizations for this example is shown in Figures 4.10a-c. As expected, the strong correlation between V_S values in adjacent layers (4.3.1) yields fast estimation of stable variance in (i.e. less than 30 realizations) the Monte Carlo

simulations. By contrast, more than 50 realizations are required for the estimation of stable variance of the randomized G/G_{max} profile due to the very weak correlation of dynamic soil properties between adjacent layers (see Section 4.3.1). The resulted $\sigma_{\ln SA}$ values of Figures 4.10a-c are compared in Figure 4.10d, where it can be seen that:

1. the ground motion variability for $T > 3.5$sec is relatively low ($\sigma_{\ln SA} \simeq 0.2$) and independent of which random fields are randomized,

2. for $T < 1.5$sec, uncertainties in the dynamic soil response (G/G_{max}) are the primary source in the total system variability, and

3. for 1.5sec $< T <$ 3.5sec, the low strain and nonlinear soil properties contribute equally to the total ground motion variability.

The Monte Carlo simulation for the weak motion event (PGA=0.083g) is illustrated in Figures 4.11 and 4.12, and as can be seen in Figures 4.11e-g, the ground response variability at any period may also be described by a log-normal distribution. The total ground response variability is almost exclusively attributed to uncertainties in V_S due to the low intensity ground motion that does not trigger nonlinear effects(Figure 4.12).

4.4.1 Comparison with Previous Studies

Stewart et al. (2008) evaluated the ground motion variability at the La Cienega downhole array for an M_w4.2 event that occurred on 09/09/2001 at distance 2.7km from the site and was recorded by the downhole and surface instruments. Using the nonlinear model and statistical description of soil properties described above, and the downhole recorded ground motion from Stewart et al. (2008), the surface ground motion are first computed and compared to the recorded motions; as can be seen in Figure 4.13, results are found to be in excellent agreement with the observations.

Next, the ground motion variability for this event (expressed in terms of $\sigma_{\ln SA}$) is estimated and compared to the results by Stewart et al. (2008). Figure 4.14 shows that results in the $T < 0.1$ sec period range deviate substantially, which is attributed to differences in the statistical description of soil properties and in the uncertainty propagation methodology

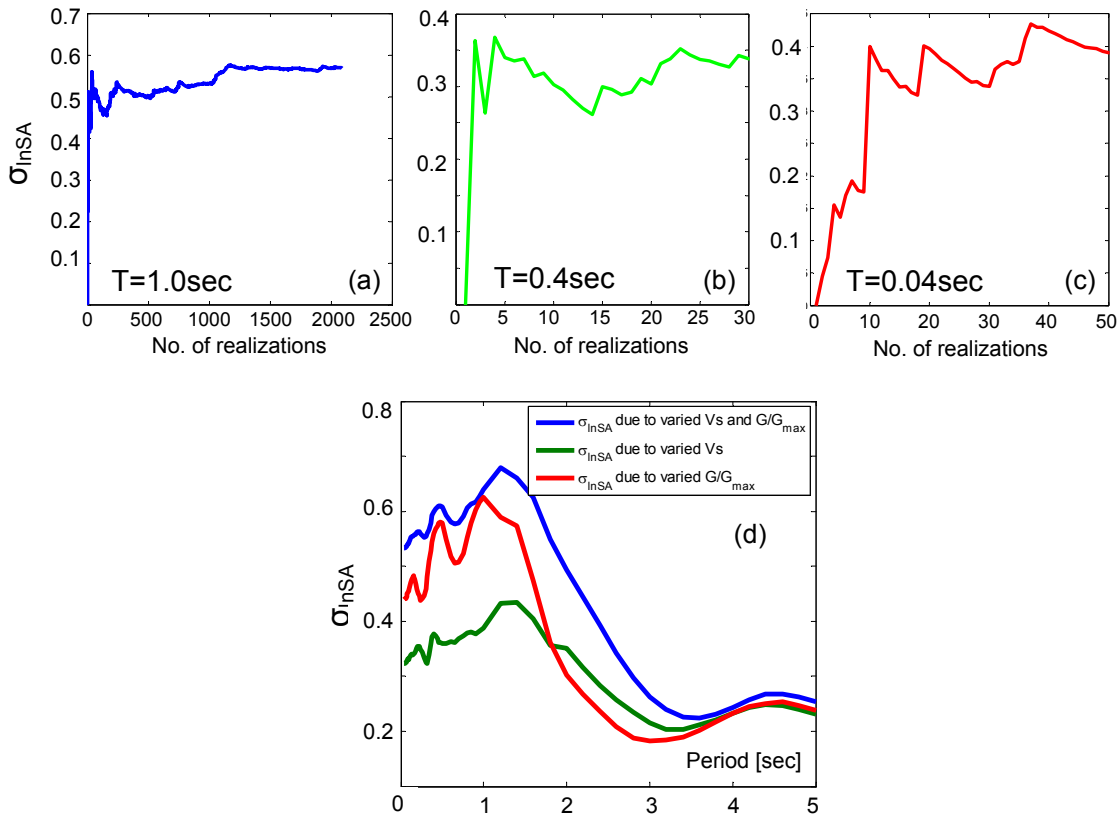

Figure 4.10: $\ln(SA)$ with increasing number of realizations of soil properties for strong ground motion excitation: (a) SA variability caused V_S and G/G_{max} randomness; (b) SA variability caused by V_S randomness; and (c) SA variability caused G/G_{max} randomness. (d) Comparison of $\sigma_{\ln SA}$ caused by different combinations of randomized soil properties for strong-motion excitation: the blue line corresponds to combined uncertainties in V_S and G/G_{max}, and the green and red lines correspond to uncertainties in V_S or G/G_{max}, correspondingly.

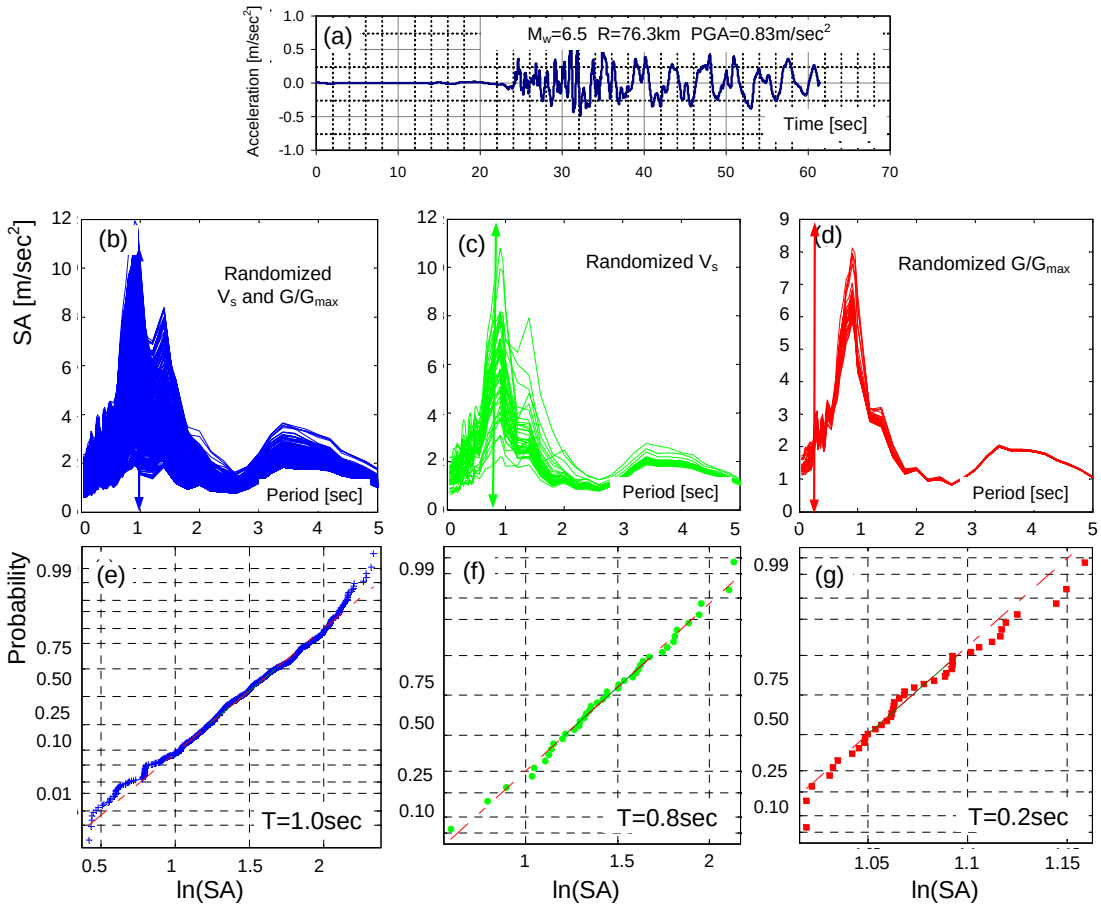

Figure 4.11: Variability in spectral acceleration (SA) caused by uncertainties in soil parameters for a weak seismic excitation. (a) Rockoutcrop acceleration time history; (b) SA variability caused by V_S and G/G_{max} randomness; (c) SA variability caused by V_S randomness; (d) SA variability caused G/G_{max} randomness; (e) normal plot of SA in (b) at period $T = 1.0$ sec; (f) normal plot of SA in (c) at period $T = 0.8$ sec; (g) normal plot of SA in (d) at period $T = 0.2$ sec.

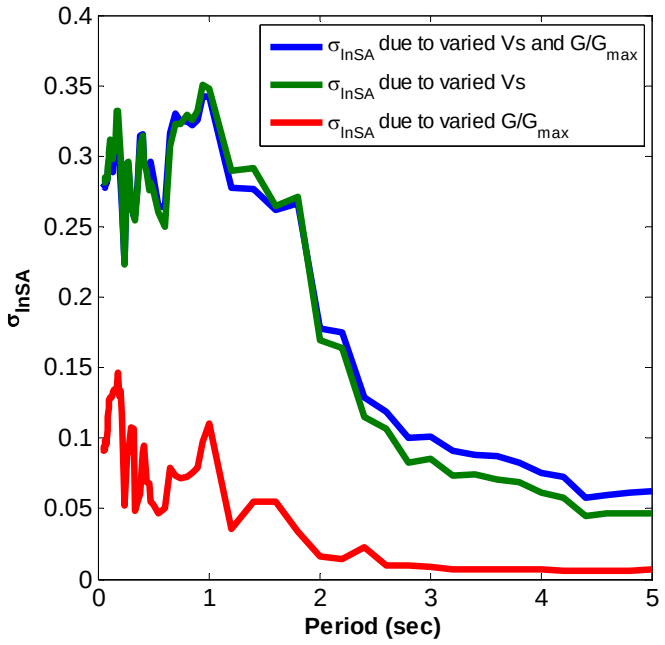

Figure 4.12: Comparison of $\sigma_{\ln SA}$ caused by different combinations of randomized soil properties for a weak-motion excitation: the blue line corresponds to combined uncertainties in V_S and G/G_{max}, and the green and red lines correspond to uncertainties in V_S or G/G_{max}, correspondingly

employed. More specifically, Stewart et al. (2008) did not implement a correlation structure between the soil layers of the profile as opposed to the autocorrelation function used here for both low-strain and nonlinear properties. Also, Stewart et al. (2008) evaluated the uncertainty propagation using a FOSM method instead of a Monte Carlo simulation, i.e. a method not suitable for problems with high coefficient of variation such as the soil parameter uncertainty studied here. This comparison highlights the role of statistical model selection and uncertainty propagation methodology in estimating the ground response variability due to soil parameter uncertainty. Nonetheless, both studies identify the same trend of variability as a function of period, i.e. the G/G_{max} variability dominates the low period uncertainty, while the effects of Vs uncertainty manifest in the long period region of ground response.

Finally, Figure 4.15 compares the ground motion variability estimated in this study at La Cienega downhole array for the strong motion example described in Section 4.3.2, to results from Roblee et al. (1996), Bazzurro and Cornell (2004), and the ground motion variability

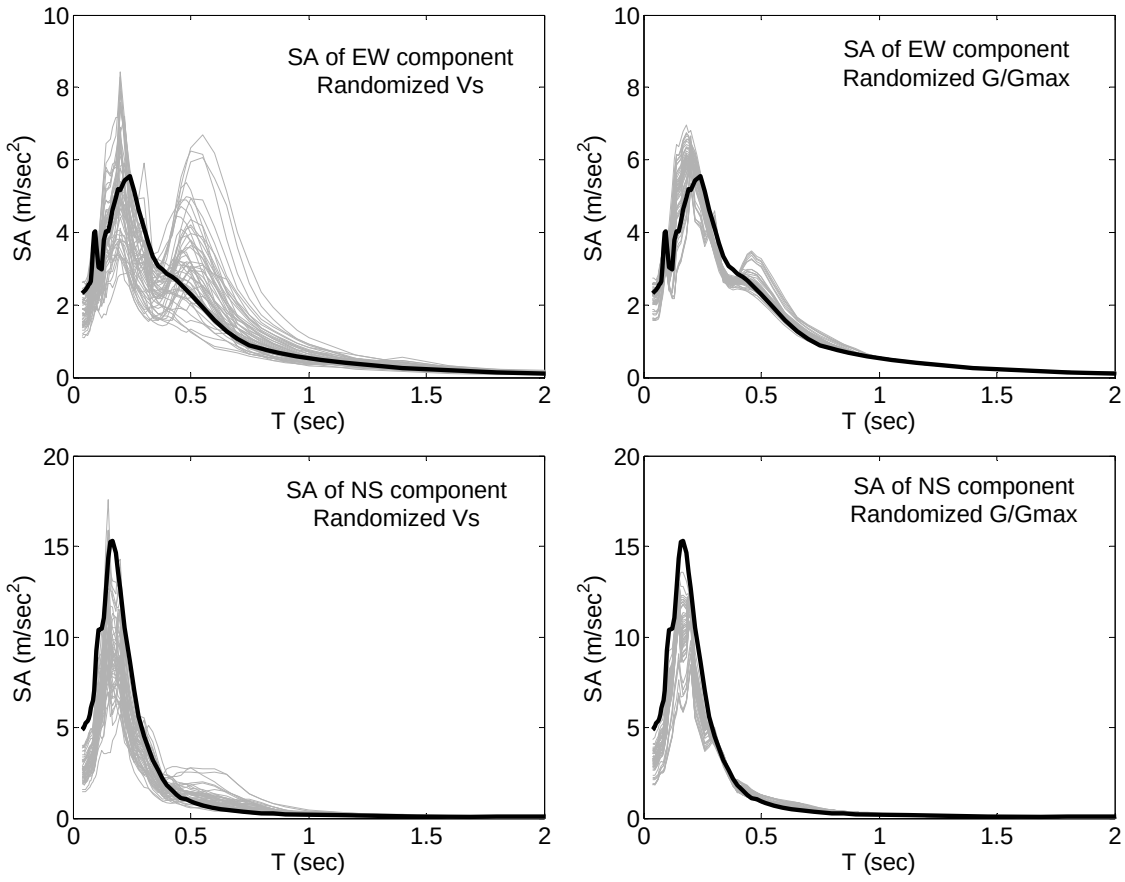

Figure 4.13: Comparison between ground surface predictions using randomized soil properties, and observations La Cienega downhole array site during a M_w4.2 event at distance $R = 2.7$km; the thick dark line corresponds to the spectral acceleration (SA) of ground motion observations, and the gray lines are SA predictions using the statistical model for soil properties in this work.

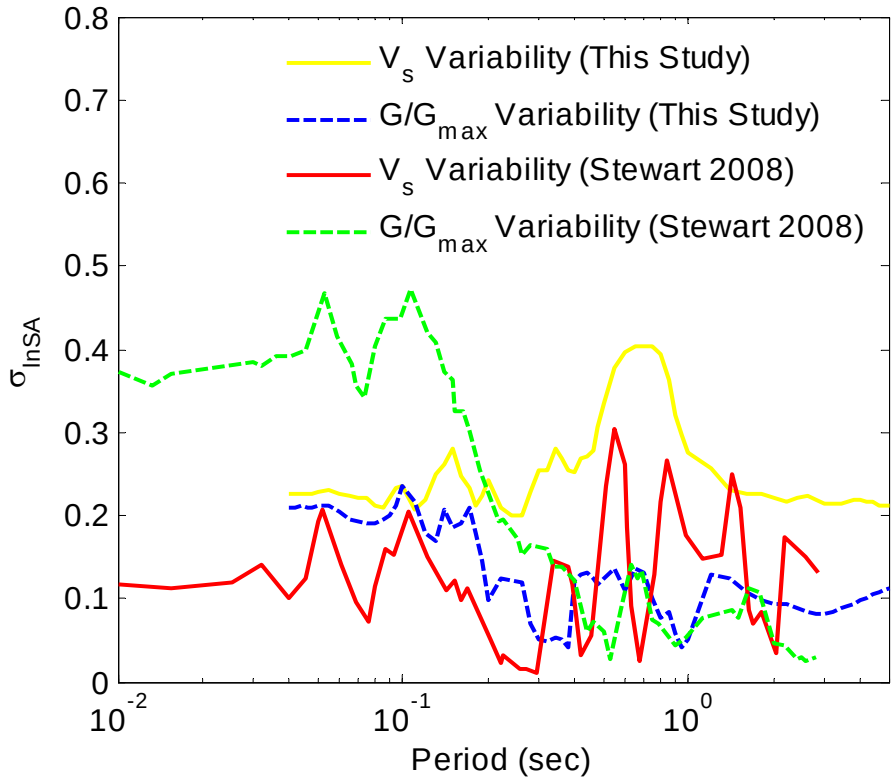

Figure 4.14: Comparison of the effects of soil parameter variability evaluated for the La Cienega downhole array site during an M_w4.2 event at distance R = 2.7km, and results obtained by Stewart et al. (2008)

for the attenuation relation by Boore and Atkinson (2008) for a similar site and event as the one used in this study (i.e. V_{S30}=270m/sec; M_w=6.5; R=10km). While the ground motion variability estimates in Figure 4.15 are evaluated for different scenario earthquakes (real or synthetic), some general conclusions can be drawn. First, the ground motion variability due to soil parameter uncertainty decreases for $T > 1.0$sec since the seismic wavelengths in the long period range are longer than the thickness of soft soil layers in the near surface; for $T > 1.0$sec, the primary source of total ground motion variability as estimated by Roblee et al. (1996) and Boore and Atkinson (2008) is the uncertainty in the description of source and path. Nonetheless, the effects of parametric variability are shown to be sensitive to the nonlinear model used in site response, the statistical description of soil properties, the methodology used for uncertainty propagation, as well as the ground motion characteristics (intensity and frequency content). As an example, the variability associated with parameter uncertainty decreases for $T > 0.15$sec in Roblee et al. (1996), for $T > 0.5$sec in Bazzurro and Cornell (2004), and for $T > 1.0$sec in this study.

Overall, results in Figures 4.10d, 4.12, 4.14 and 4.15 show that the role of soil parameter uncertainty in the total ground motion variability is a function of the ground motion intensity, both in terms of the amount of scatter (max =0.6 for the strong motion example and max =0.3 for the weak motion example) and in terms of relative contribution of low-strain and nonlinear soil property uncertainties in the total variability at different period ranges. The period range of parametric uncertainty influence is also strongly related to the site-specific conditions: softer sites exert nonlinearities at lower intensity incident motions, and their response variability is anticipated to manifest at longer periods due to their resonant characteristics. In summary, the period range and extent to which the various soil parameter uncertainties dominate the total ground motion variability are site and ground motion specific. This outcome will be used in the following section where the results of the Monte Carlo simulations are presented for the ensemble of ground motions and sites studied here.

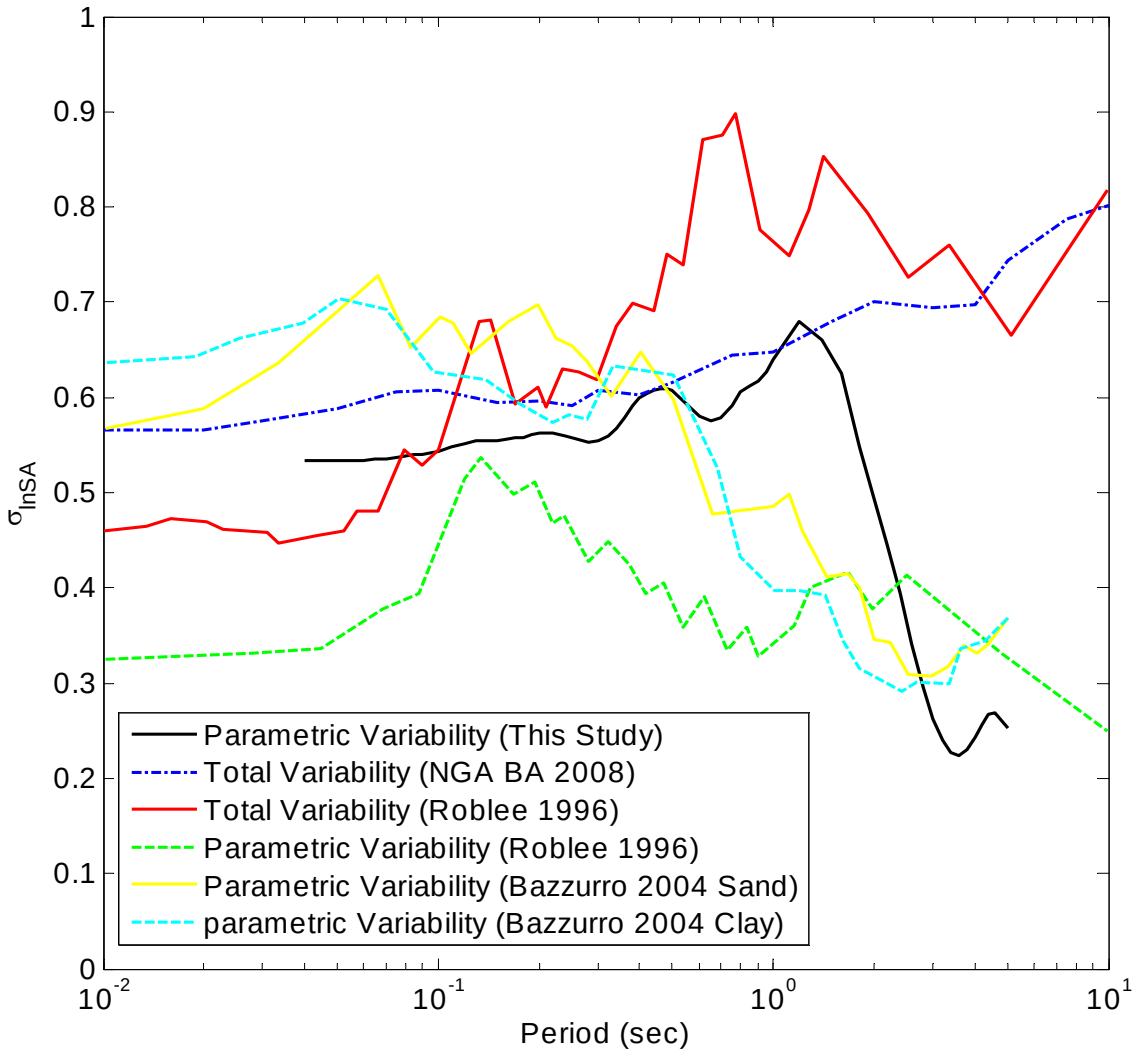

Figure 4.15: Comparison of ground motion variability from site, path and source-related uncertainties estimated by various studies: (a) the soil parameter variability in this study is estimated for La Cienega during an M6 event at distance 1km; (b) the total variability by Boore and Atkinson (2008), corresponds to a site with V_{S30} = 270 m/s, and an M6.5 event at distance R^{jb} = 10km; (c) the parametric variability by Roblee et al. (1996) is for a stiff site and an M7 event at distance 10km; and (d) the parameter uncertainty by Bazzurro and Cornell (2004) is for generic sand and clay sites, and the variability shown is for site amplification instead of ground motion.

4.4.2 Site- and Ground Motion-Dependent Ground Response Variability

Finally, the effects of soil parameter uncertainty on ground motion variability for each site and the ensemble of synthetic ground motions are illustrated, and the dependencies of ground motion scatter on the site conditions, and ground motion intensity and frequency content are depicted. $\sigma_{\ln SA}$ is used as measure of ground motion variability, and more specifically :

1. $(\sigma_{\ln SA})_{V_S}$ that corresponds to $\sigma_{\ln SA}$ evaluated for realizations of the V_S probability model described in Section 4.3.1, and

2. $(\sigma_{\ln SA})_{G/G_{max}}$ that corresponds to $\sigma_{\ln SA}$ evaluated for realizations of the G/G_{max} and damping (ξ) probability model described in Section 4.3.2.

Figure 4.16 shows contours of $(\sigma_{\ln SA})_{V_S}$ and $(\sigma_{\ln SA})_{G/G_{max}}$ as a function of period (T) and ground motion PGA for each site, and illustrates the intensity-frequency dependency of the effects of linear and nonlinear soil parameter uncertainty on ground motion variability. For the stiffer sites (Obregon Park and La Cienega), the period range of maximum variability increases with increasing PGA, reaching an overall maximum at approximately $T = 1.5$sec. This is attributed to characteristics of typical seismograms, where higher intensity motions are usually recorded in the near-field and are thus rich in long period components. This trend is not as clear for the softer site (Meloland), most likely due to the particularities of the velocity profile that varies smoothly with depth, and does not provide distinct resonance potential at any frequency range. As expected, the effects of nonlinear soil property variability are more pronounced for soft sites (Figures 4.16e and 4.16f), with the maximum being clearly a function of the site stiffness; on the other hand, the frequency-dependency of is similar for all three sites. By contrast, the effects of V_S randomness described by $(\sigma_{\ln SA})_{V_S}$ are much more pronounced for Obregon Park, namely the stiffer site studied (Figure 4.16a). This is most probably due to the strong impedance contrast of the site velocity profile at 20m, which controls the amount of seismic energy trapped and amplified in the near-surface. Therefore, fluctuations of the velocity model for this site are expected to directly reflect on changes in the surface ground motion.

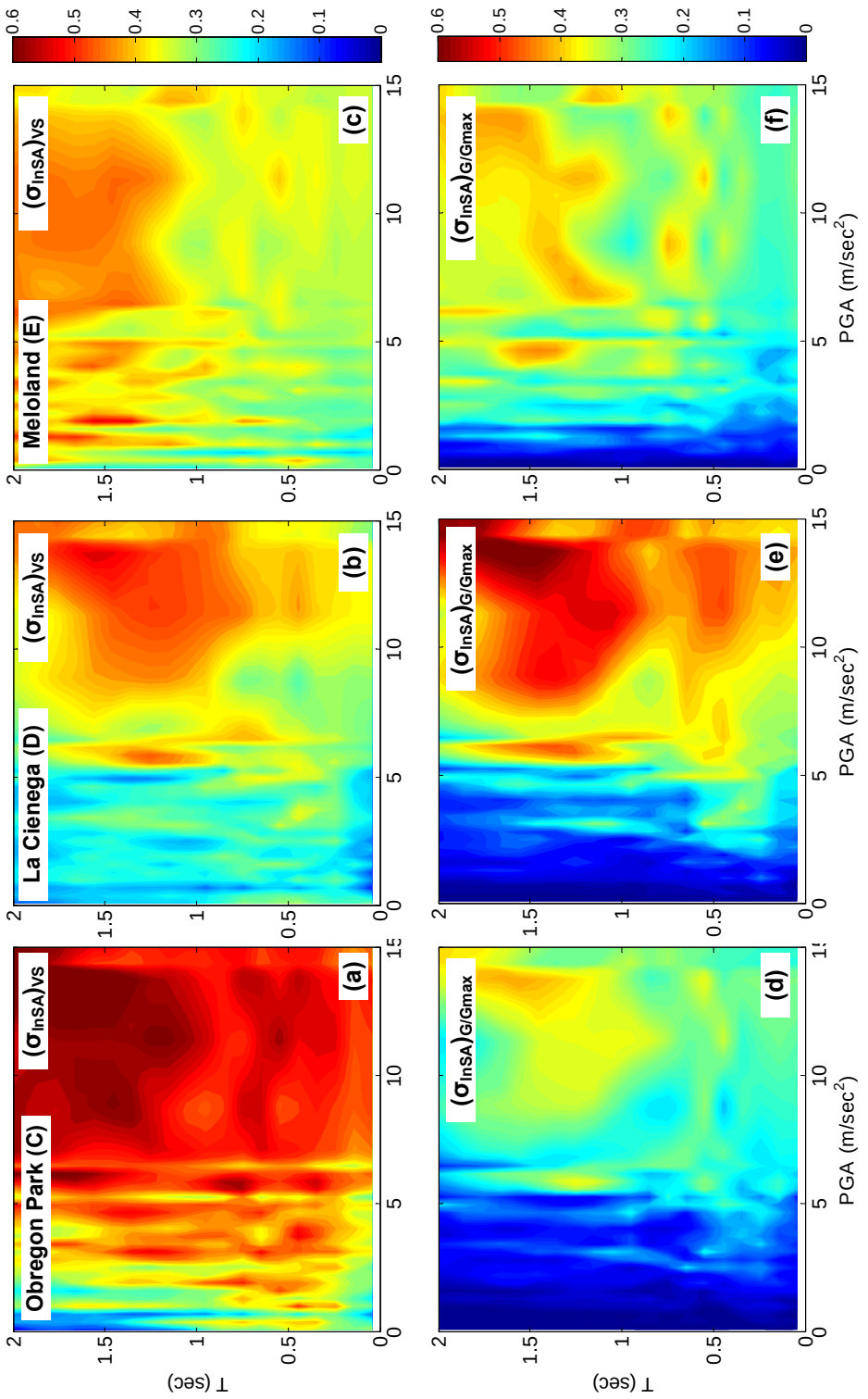

Figure 4.16: Contour map of spectral acceleration (SA) variability due to V_S randomness (evaluated via $(\sigma_{\ln SA})_{V_S}$) and spectral acceleration (SA) variability due to G/G_{max} randomness (evaluated via $(\sigma_{\ln SA})_{G/G_{\max}}$) as a function of the reference site peak ground acceleration ($\mathrm{PGA_{RO}}$) an period (T) for the three sites investigated

4.5 Conclusions

A systematic investigation of the ground motion variability in site response predictions arising from uncertainties in the soil parameters is presented in this chapter. More specifically, three soil profiles corresponding to downhole array sites in the Los Angeles basin are studied, for which realistic probability models for the linear elastic and nonlinear soil properties are developed based on site-specific and generic geotechnical investigation data. Based on these models, randomized realizations of the soil property stochastic fields are generated, and subjected to broadband ground motion synthetics from simulations of a wide range of magnitude-distance scenarios. Monte Carlo simulations are implemented to evaluate the uncertainty propagation from the soil parameters to the ground surface response, and the ground motion variability results for each site are presented as a function of the ground motion intensity (here represented by the rock-outcrop peak ground acceleration $\mathrm{PGA_{RO}}$) and frequency.

Advancing the state-of-the art, a fully nonlinear soil model in the site response simulations, realistic statistical descriptions of the soil properties, and conducted Monte Carlo simulations are simultaneously implemented for approximately 500 incident ground motion time-histories and three sites, to evaluate the intensity-frequency dependency of soil parameter uncertainty in ground motion variability. Results show strong dependency of the effects of nonlinear soil property uncertainties (G/G_{max}) to the seismic motion intensity, which is shown to be stronger for soft soil profiles. By contrast, ground motion variability associated with uncertainties in the velocity structure of soil profiles (V_S) is found to be less intensity-dependent, and is more pronounced for soil profiles with a strong impedance contrast in the near-surface governing the amplification potential of the site.

CHAPTER V

"NONLINEAR SITE EFFECTS" IN NONLINEAR STRUCTURAL PERFORMANCE PREDICTION

[1]

5.1 introduction

With the emerging trends of performance-based design engineering, nonlinear structural response analyses are increasingly involved in the aseismic design of structures and the development of design criteria. Since the design level ground motions are scarce, engineers often rely on the use of artificial time-histories, modified from real earthquake recordings to be compatible with regional hazard-consistent design spectra (Design Spectrum Compatible Acceleration Time History, DSCTH). Indeed, the so-called Uniform Hazard Spectrum (UHS) evaluated from Probabilistic Seismic Hazard Analyses (PSHA) of regional ground motion data is nowadays the most frequently employed target spectrum in seismic structural analysis. Nonetheless, as pointed out by Katsanos et al. (2010), there exist many studies (Reiter, 1990; Naeim and Lew, 1995; Bommer et al., 2000, e.g.) that question the validity of using the UHS as a single event target spectrum, arguing that it is in fact an envelope of spectra corresponding to different seismic sources. Therefore, use of UHS may result in design motions unrealistically corresponding to multiple earthquakes from multiple sources occurring simultaneously.

Alternatively, synthetic ground motions computed via stochastic or physics-based fault rupture simulations may be used in nonlinear structural performance estimations. Indeed, the recent advancements in the numerical representation of dynamic source rupture predictions as well as the development of 3D crustal velocity and fault system models for seismically active regions have led to broadband ground motion simulations of realistic

[1] This chapter is extracted and modified from a working paper submitted to "Earthquake Spectra"

seismic waveforms over the engineering application frequency range (<10Hz). To investigate the accuracy of structural response predictions obtained via synthetic ground motions, Bazzurro et al. (2004) used seven source simulation techniques to compute the structural response of inelastic Single Degree of Freedom (SDOF) oscillators, and statistically compared the results to the structural response predicted when using real accelerograms. They showed that the synthetic ground motions produce structural responses that are less variable and less severe than those caused by real records in the short period range, the range of wavelengths comparable to the thickness of near-surface soil layers that were not simulated by Bazzurro et al. (2004).

Indeed, the response of soils to strong earthquake loading has been shown to significantly affect the amplitude, frequency content and duration of seismic motions (Wiggins, 1964; Idriss and Seed, 1968; Borcherdt and Gibbs, 1976; Joyner et al., 1976; Berrill, 1977; Duke and Mal, 1978; Chin and Aki, 1991; Darragh and Shakal, 1991; Hartzell, 1992; Silva and Stark, 1992; Su et al., 1992, e.g.), and the consequent effects of site response on the performance of structures have been investigated in the past. More specifically, Whitman and Protonotarios (1977) studied the inelastic response of structures with different fundamental periods to site-modified ground motions. They found that the inelastic response spectra for site-modified motions did not show pronounced peaks at the fundamental period of the soil profile, and that the inelastic response had not affected significantly the details of the frequency content for given peak ground acceleration and velocity. They also suggested that one should be conservative in selecting design forces for stiff structures resting upon soft ground. O'Connor and Ellingwood (1992) compared the statistics of demand parameter obtained from ground motions generated using three alternative site-dependent stochastic models, i.e. the Modified Kanai-Tajimi model (Tajimi, 1960; Kanai, 1961; Paparizos, 1986), Boores spectral model (Boore, 1983) and the Auto-regressive Moving Average (ARMA model (Ellis and Cakmak, 1987)). They concluded that no stochastic model alone was sufficient to fully characterize the ground motion and reproduce the structural inelastic response, and that each model parameter affected differently the various response quantities. Miranda (1993) evaluated the strength reduction factor (R_y) demands of SDOF systems

for ground motions recorded on firm and soft sites. He observed that strength reduction factors of systems on soft soil sites with periods of vibration near the predominant period of the ground motion are typically much larger than the displacement ductility ratio. As a result, the response of those systems was shown to deviate from the equal displacement rule. This observation was confirmed by subsequent studies by the author (Miranda, 2000; Ruiz-García and Miranda, 2004), where it was shown that the inelastic deformation ratios of SDOF systems from motions recorded on soft sites are much lower that those obtained using motions recorded on firm sites, provided that the fundamental period of the SDOF oscillator is close the fundamental period of the soft site.

The above studies confirm that the response of soil layers does affect the inelastic response of structures, and intuitively, if the ground motion is strong enough to cause inelastic structural deformation, it should most probably also trigger nonlinear effects particularly at soft sites. The extent, however, to which soil nonlinearity affects the inelastic structural response, has not been quantitatively established, primarily due to lack of a statistically significant number of strong ground motion records on soft sites and the coarse discretization between soil and rock adopted in the above studies. For example, the average PGA of ground motions collected by Ruiz-García and Miranda (2004) is on the order of $0.03G$, which is not strong enough to cause nonlinear effects even for soft sites. As a result, limited guidance exists both in engineering practice and in the seismological literature regarding the models that should be employed for the prediction of the response in synthetic ground motion simulations intended for inelastic structural response analyses.

In this study, the effects of soil response on the inelastic structural performance prediction are quantified by combining downhole strong motion observations and broadband ground motion synthetics for characteristic soft site conditions in Southern California. More specifically, the variability in structural demand, caused by the soil model adopted for the site response predictions in the ground motion simulations, is investigated. By resorting to the synthetic motions, it is possible to subject the soil profiles to design level ground motions of different magnitude and distance combinations, and study the demand on buildings subjected to ground motions as a function of the site response characteristics. Overarching

goal of this study is the development of quantitative guidelines for the efficient integration of nonlinear site response models into large-scale end-to-end physics-based ground motion simulations intended for structural performance predictions.

The soil sites used in this study are the calibration sites compiled by Stewart and coworkers as part of the PEER 2G02 project Calibration Sites for Validation of Nonlinear Geotechnical Models (http://cee.ea.ucla.edu/faculty/CalibrationSites/Webpage/main.htm. Detailed velocity profiles down to a hundred meters depth were available for the majority of sites, along with the dynamic soil parameters expressed as modulus reduction and material damping curves. To investigate the role of the site response model in the evaluation structural response, four kinds of site response models are implemented and discussed in a section that follows. The effect of using different soil models for the structural performance assessment will be quantified as the bias and uncertainty in the inelastic deformation ratios of bilinear SDOF systems.

The site conditions and broadband ground motion synthetics are described in section 3.2 and methods of site response analysis used in this study are described in section 3.3

5.2 Nonlinear Soil Response to Strong Ground Motion

The nonlinear site response to strong ground motion are elaborated in section 3.4, and the relevant portions are summarized as following for the sake of completeness.

Ground motion synthetics computed on rock-outcrop were deconvolved to estimate the incident seismic motion at 100m depth, where nonlinear effects are not likely to manifest during strong motions for the soil conditions studied here. Successively, the estimated incident motions were propagated through the 24 soil profiles to the surface by means of the three site response models investigated. Weak ground motions (rock-outcrop PGA $< 1\text{m/sec}^2$), which are unlikely to cause yielding of medium soft to soft profiles and the overlying structures, were excluded from the ground and structural response analyses. Overall, 510 out of 6300 synthetic ground motions were selected for our simulations; Fig. 3.2(b) depicts the magnitude (M_w), PGA and distance (R)-to-fault distribution of these motions.

Next, the deviation between nonlinear and linear elastic ground surface predictions for all

profiles and all synthetic motions was evaluated. This measure is used to describe the extent of soil nonlinearity manifesting during strong ground motion. Note that the nonlinear model used here was benchmarked in Assimaki et al. (2008b) by comparison with downhole array recordings; thus, the deviation of linear site response from the 'true' nonlinear predictions is expected to increase as the intensity of nonlinear effects in the soil increases.

Denoting the spectral acceleration at period T_i of the linear site response prediction as $\mathrm{SA_i^{LIE}}$ and the spectral acceleration at period T_i of the nonlinear prediction as $\mathrm{SA_i^{MKZ}}$, the divergence between the responses is evaluated as:

$$e_{SA} = \mu(e_{SA_i}) = \mu\left(\log\left(\frac{\mathrm{SA_i^{LIE}}}{\mathrm{SA_i^{MKZ}}}\right)\right) \tag{5.1}$$

where the operator μ corresponds to the non-weighted average, and the subscript i refers to period . The averaged error is here evaluated for periods between 0.2 sec and 2.0 sec, a range that covers the dominant period of most common structures.

The error between linear and nonlinear predictions (e_{SA}^{LIE}) is expressed as a function of the ground motion intensity, frequency content and soil profile characteristics. For soil profiles with soft layers likely to respond nonlinearly during a strong event, the amplitude and frequency content of input motion describe whether the seismic waves will "see" the soft layers and whether they "carry" sufficient energy to impose large strains cause nonlinearity. The rock outcrop PGA ($\mathrm{PGA_{RO}}$) was used to describe the ground motion intensity, and a dimensionless index referred to as frequency index (FI) to quantify the similarity between the transfer function of the profile and the Fourier amplitude spectrum of the incident motion. Large FI means large amplification potential of the input motion as it propagates through the soil profile, and if the amplified motion is characterized by a high $\mathrm{PGA_{RO}}$, it will most likely trigger nonlinear soil effects. The Frequency Index (FI) is expressed as

$$\mathrm{FI} = \frac{2\sum_{\mathrm{i=1}}^{\mathrm{N}} \mathrm{ATF_i FAS_i}}{\sum_{\mathrm{i=1}}^{\mathrm{N}} \mathrm{ATF_i ATF_i} + \sum_{\mathrm{i=1}}^{\mathrm{N}} \mathrm{FAS_i FAS_i}} \tag{5.2}$$

where $\mathrm{ATF_i}$ and $\mathrm{FAS_i}$ are the amplitude of the elastic transfer function of the profile and the Fourier amplitude spectrum of incident motion at the i^{th} frequency point, normalized

by their respective peak value, and N is the total number of frequency points in the range of interest, namely 0Hz to twice the fundamental frequency of the site.

Fig. 3.4 shows the variation of e_{SA}^{LIE} as a function of FI and $\mathrm{PGA_{RO}}$ for three sites. As can be readily seen, the deviation between linear and nonlinear predictions, , increases with increasing ground motion intensity (i.e. $\mathrm{PGA_{RO}}$) and increasing frequency index (FI), and attains maximum values at the up-right corner of the contour plot. The $\mathrm{PGA_{RO}}$-FI regions of large values correspond to combinations of sites and incident ground motions with large sensitivity of the site response predictions on the selection of the soil model. In these cases, It is recommended that nonlinear analyses should be employed to ensure credibility of the site response analyses.

Fig. 3.4 also shows that the quantitative dependency of on $\mathrm{PGA_{RO}}$ and FI is site-specific. It is identified that the following empirical relation exists between e_{SA}^{LIE}, ground motion and soil profile parameters to describe the variability in absolute values as a function of the site characteristics:

$$e_{SA}^{LIE} = \alpha \cdot \frac{760}{V_{S30}} \cdot \mathrm{PGA_{RO}} + \beta \cdot Amp \cdot FI + \epsilon \tag{5.3}$$

where α and β are regression coefficients, Amp is the site amplification at the fundamental period of the soil site, and ϵ is the normally distributed residual of the regression. This equation can be used as a proxy to describe the extent of nonlinear soil effects expected during a given event at a given site, and the associated uncertainties as a function of the soil profile and the ground motion characteristics. Regression coefficients α and β were also estimated in chapter 3 for a limited number of sites, which along with an error threshold $e_{SA} \leq e_{SA}^{\max}$, can be used to quantitatively determine whether nonlinear simulations are required for site response predictions at a given site during a given event.

5.3 Uncertainty and Bias in Structural Response Predictions

Next, it is investigated how the modeling variability in site response analyses propagates to the prediction of inelastic structural response for a series of nonlinear SDOF oscillators. More specifically, the bias and uncertainty in structural response introduced by the soil

model are estimated, using the nonlinear site response analyses as reference. The inelastic deformation ratio (C) is used as an Engineering Demand Parameter (EDP) to measure the displacement demand, while its variability resulting from the selection of the soil model is mapped as a function of the site- an ground-motion characteristics described above, namely as a function of $\mathrm{PGA_{RO}}$ and FI.

5.3.1 Inelastic deformation ratio

The inelastic deformation ratio (C) is defined as the ratio of the peak deformation (u_m) of an inelastic oscillator to its corresponding linear (u_0) response (see Fig. 5.1). This ratio varies considerably as a function of period and approaches unity only in the displacement-sensitive spectral region of the oscillator response, which is the basis of the so-called equal deformation rule ($u_m/u_0 = 1$) (Veletsos et al., 1965).

When expressed as a function of the elastic vibration period T_n and the ductility factor μ, the inelastic deformation ratio (C) may be used to determine the inelastic deformation demand of a structure with given global ductility capacity; on the other hand, when expressed as a function of the elastic vibration period and the yield-strength reduction factor R_y (Eq. 5.4), it can be used to estimate the inelastic deformation of an existing structure with known lateral strength. Compared to the alternative indirect method of $R_y - \mu - T_n$ relations, this direct method can give relatively unbiased estimation of the peak deformation of an inelastic SDOF system. (Miranda, 2001; Chopra and Chintanapakdee, 2004).

A bilinear force-displacement response $f_s(u, \mathrm{sgn}\dot{u})$ schematically shown in Fig. 5.1 was selected to simulate the idealized inelastic structural response of a series of SDOF oscillators. As shown in Fig. 5.1, the elastic stiffness of the model is k and the post-yield stiffness is αk, where α is defined as the post-yield stiffness ratio. The yield strength of the oscillator is f_y and the yield deformation u_y. Within the linear elastic range namely $u = [0 - u_y]$ the system has a natural vibration period T_n and damping ratio ξ . The yield strength reduction factor of the structure (R_y) is defined as:

$$R_y = \frac{f_0}{f_y} = \frac{u_0}{u_y} \tag{5.4}$$

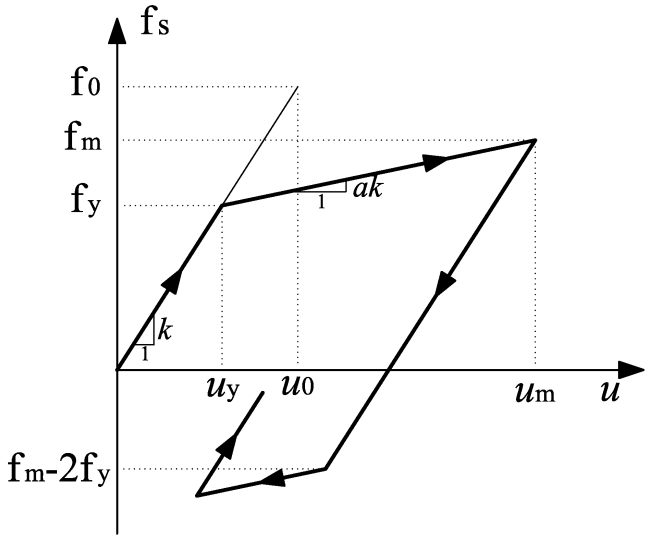

Figure 5.1: Bilinear force-deformation relationship of inelastic SDOF system and corresponding notation for elastic and post-yield characteristics (after Chopra and Chintanapakdee (2004))

where f_0 and u_0 are the minimum yield strength and yield deformation required for the structure to remain elastic during the ground motion, or the peak response values for the corresponding linear system. The peak force in the inelastic system is f_m(Fig. 5.1). The peak deformation of the bilinear system is denoted by u_m and the corresponding ductility ratio μ is defined as:

$$\mu = \frac{u_m}{u_y} \tag{5.5}$$

Finally, it can be shown that the inelastic deformation ratio (C) can be evaluated as:

$$C = \frac{u_m}{u_0} = \frac{\mu}{R_y} \tag{5.6}$$

When the equal displacement rule applies $C = 1$, or $\mu = R_y$. To ensure a uniform intermediate inelastic level in the nonlinear oscillators, The main focus is the constant yield strength reduction factor ($R_y = 4$) approach. The constant ductility ratio ($\mu = 4$) approach is also investigated, instead of keeping constant the yield strength (f_y) of the oscillator. Therefore, in order to have the same R_y factor for all our analyses, the oscillators f_y are

simply tuned according to the record's first mode spectral acceleration. The reason is that the highly variable intensity (PGA=0.1g–2.0g) of the ground motions will cause also high inelastic demands on the oscillator of constant yield strength, i.e. constant yield acceleration for structure with unit mass was fixed, which will totally overshadow the signature of site effects in the structural response.

5.3.2 Bias and Uncertainty in prediction of inelastic deformation ratio

Successively, the variability in inelastic deformation ratio (C) predictions, for each of the different site response methods for structures with different fundamental period T_n and yield strength f_y, is investigated. The results are differentiated using subscripts corresponding to abbreviations of the site response methods. Specifically, the C values corresponding to the empirical amplification model are denoted as $\mathrm{C_{EAF}}$; similarly, the C values corresponding to the linear visco-elastic models are denoted as $\mathrm{C_{LIE}}$; the C values of the equivalent linear models are denoted as $\mathrm{C_{EQL}}$; and the C values of the modified Kondner and Zelasko (MKZ) model as $\mathrm{C_{MKZ}}$.

In this section, for brevity only some representative results from three sites with NEHRP class C (site CLS), D (site G02), and E (site EME) are shown to illustrate our key observations. The statistical correlation analysis between bias in the prediction of the displacement demand, C and the site parameters using the results from all the sites will be shown at the end of the section.

Fig. 5.2 shows the C_{EAF}, C_{LIE}, C_{EQL} and C_{MKZ} for $R_y = 4$ as functions of the fundamental period (T_n) of the inelastic SDOF for the selected sites. The C values are averaged within five different $\mathrm{PGA_{RO}}$ bins shown in the legend to illustrate the PGA dependency. It can be readily seen that the C_{LIE} curves show no PGA dependency, i.e. the C_{LIE} curves from different $\mathrm{PGA_{RO}}$ groups almost coincide one another. The reason is that the site amplification of LIE model is independent of the intensity of the incident motion, and therefore it only uniformly alters the frequency content of the incident motion. Although the intensities of the ground responses are highly variable, their frequency contents are same, which results in intensity-independent C_{LIE} values for the constant R_y structure model.

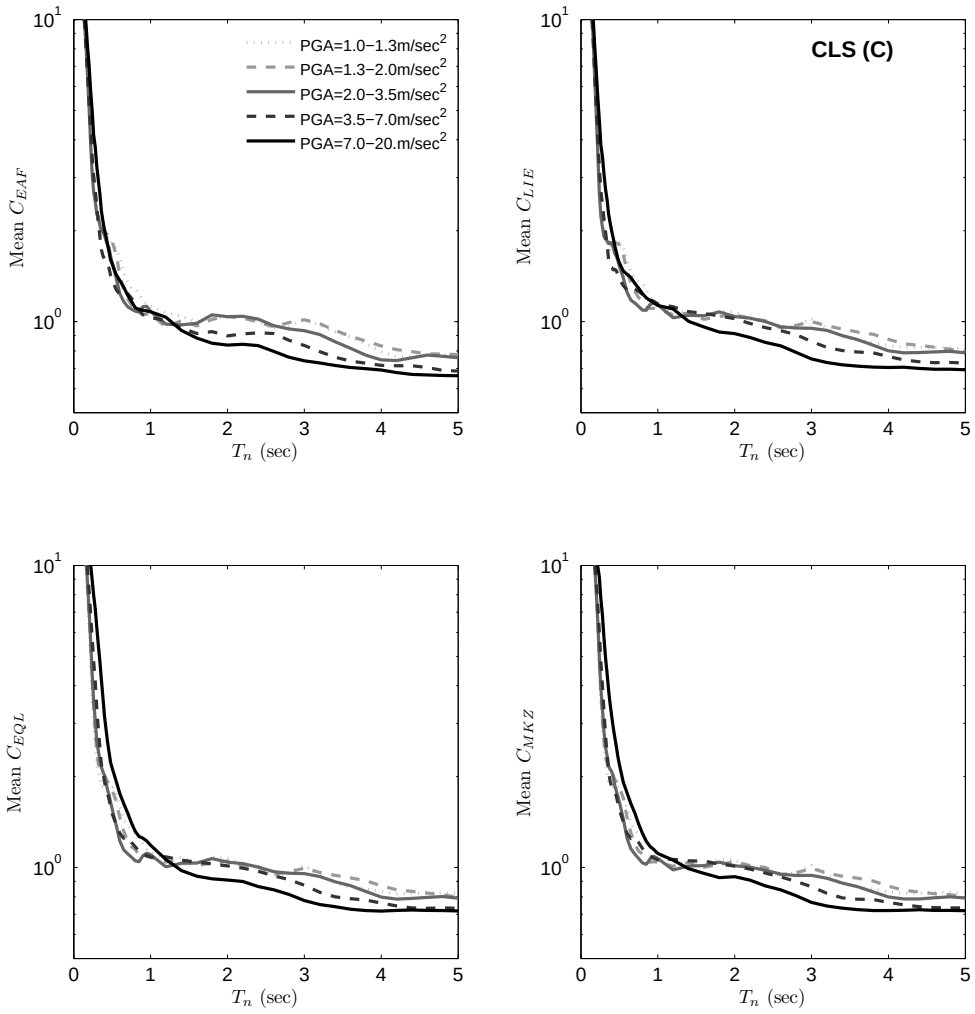

Figure 5.2: The mean inelastic deformation ratio (C) of bilinear SDOF structures with constant strength reduction factors ($R_y = 4$) (averaged within the PGA bins shown in the legend) evaluated using ground motions from different site response models as a function of the natural elastic vibration period of the bilinear SDOF (The site response models are differentiated by the subscript of C. EAF means Empirical Amplification Factor model; LIE means LInear visco-Elastic model; EQL means EQuivalent Linear model and MKZ means Modified Kondner-Zelasko model) (CLS Site) (To be continued)

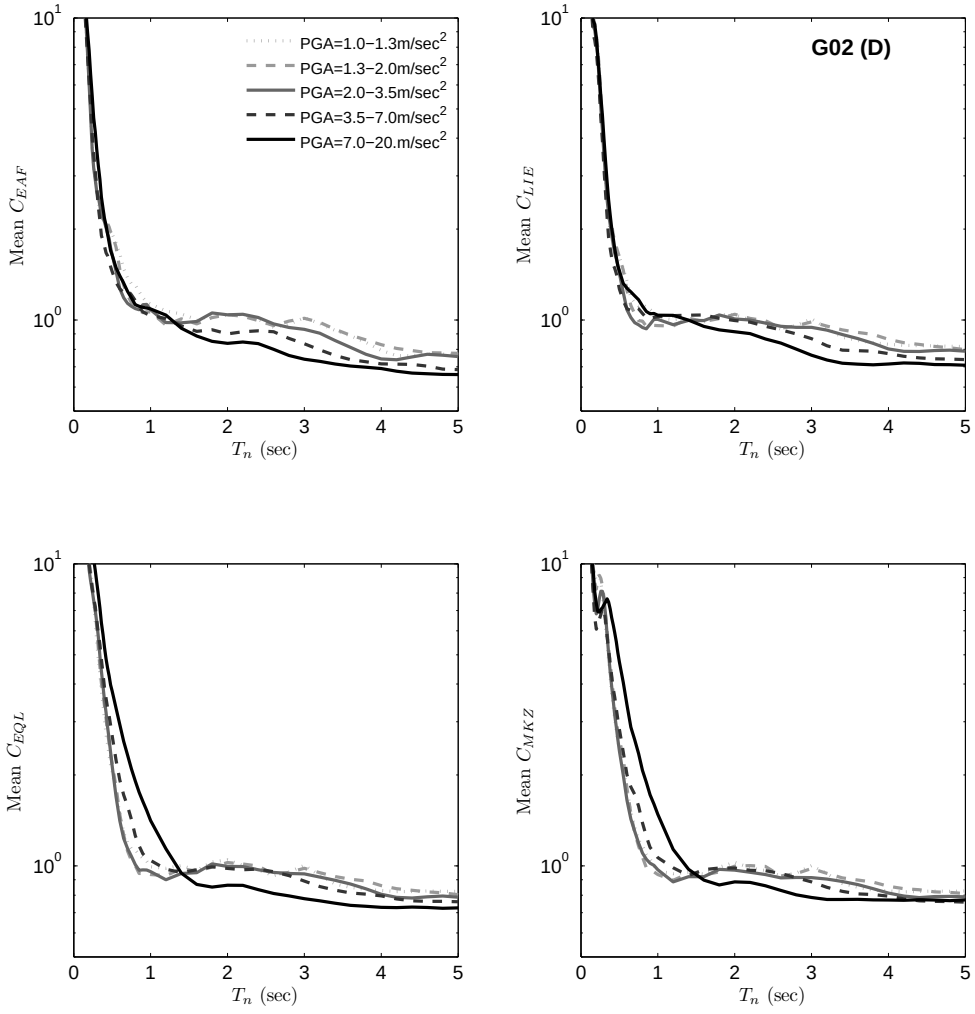

Figure 5.2: Continued (G02 Site)

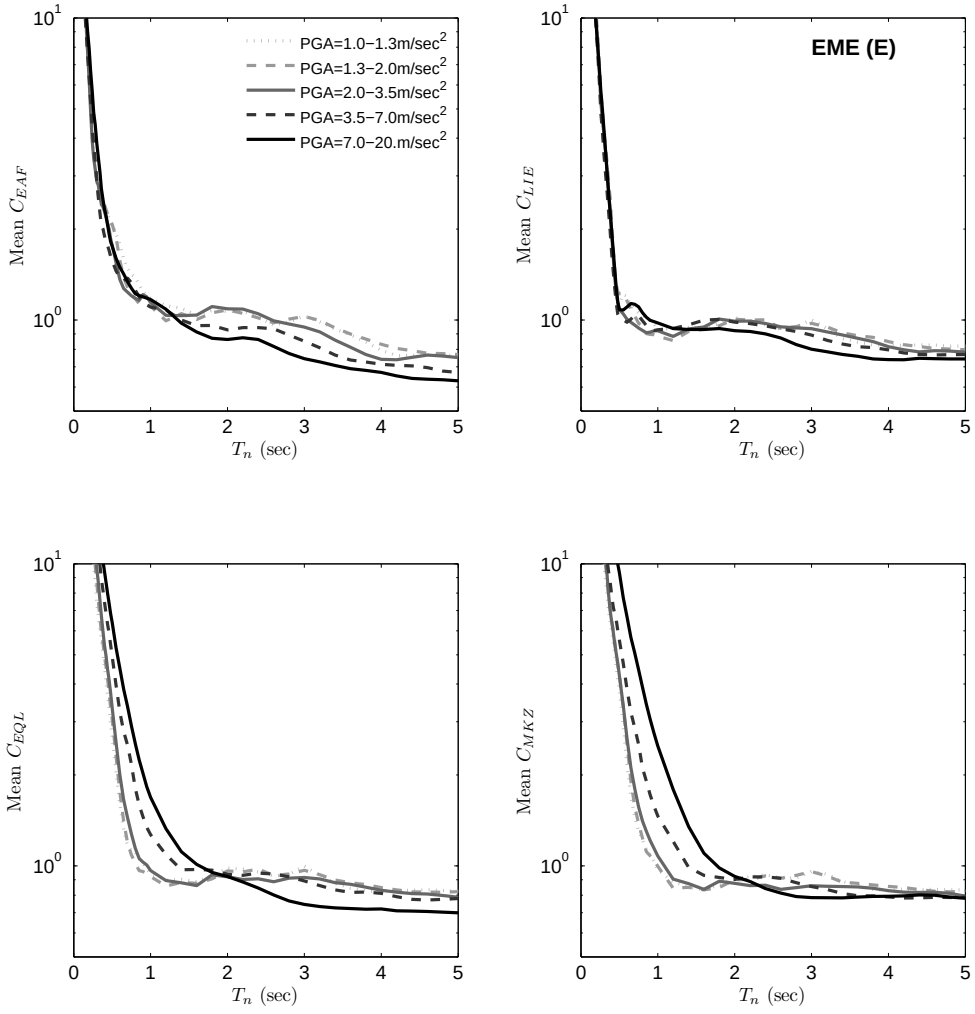

Figure 5.2: Continued (EME Site)

C_{EAF} curves show a slight PGA dependency and the overall shapes are similar to those of the C_{LIE} curves. The site amplification of EAF model is derived based on the mean spectral acceleration (SA) ordinates predicted by the NGA relations. The mean SA predictions can only reflect a blended average site response effect, which will result in a relatively uniform or smooth site amplification. Therefore, the performance of the EAF model is similar to that of the LIE model.

By contrast to C_{LIE} and C_{EAF}, C_{EQL} and C_{MKZ} show obvious PGA dependency, i.e. the C_{EQL} and C_{MKZ} curves from different $\mathrm{PGA_{RO}}$ groups deviate from one another, with C_{EQL} or C_{MKZ} associated with higher $\mathrm{PGA_{RO}}$ showing higher C values. Since the same constant yield strength reduction factor ($R_y = 4$) SDOF models are used to calculate the C_{EQL} and C_{MKZ} values, the only source of the $\mathrm{PGA_{RO}}$ dependency is the difference in the frequency content of the ground motions due to adoption of different site response models. Both the amplitude and frequency content of the input motion will be substantially modified as a result of the nonlinear site response when the intensity of the input motion is high enough, and this modification in the amplitude and the frequency content can be realistically approximated by EQL and MKZ models. Usually the higher the intensity of the incident motion, the larger the change in the frequency content of the ground response relative to the linear elastic response, which results in the deviation in the prediction of the inelastic deformation ratio C.

In order to have a quantitative description of the effect of nonlinear site response on the C prediction, the bias and uncertainty in predictions of C will be represented as the ratio of the mean C predictions from different models, which denoted by Q_{μ_C}, and the ratio between coefficient of variation (COV) of C predictions from different models, denoted as Q_{σ_C}. Considering that the MKZ model is the most realistic of the four, the quantities (i.e. mean and COV) associated with this model are always set as denominator when taking the ratio. For instance, the ratio between mean C predictions from LIE model and MKZ model can be expressed as $Q_{\mu_C} = \mu_{C_{LIE}}/\mu_{C_{MKZ}}$; and the ratio between the COV of C predictions from LIE model and MKZ model can expressed as $Q_{\sigma_C} = \sigma_{C_{LIE}}/\sigma_{C_{MKZ}}$. Therefore, the deviation of Q_{μ_C} or Q_{σ_C} from unity indicates deviation of the C prediction due to the

adoption of different site response methodologies and thus propagation of the sensitivity of the ground response assessment to the prediction of the structural inelastic performance.

Fig. 5.2 shows the Q_{μ_C} for $R_y = 4$ at selected sites as a function of the elastic vibration period (T_n) of the SDOF system, normalized by the fundamental period (T_g) of the site. The mean C values here are averaged within the ranges of $\mathrm{PGA_{RO}}$ indicated by the legend. As mentioned before, a constant R_y was here selected to illustrate results of our study, namely depict the propagation of ground motion modeling variability to the inelastic structural response prediction while keeping the inelastic structural characteristics invariable.

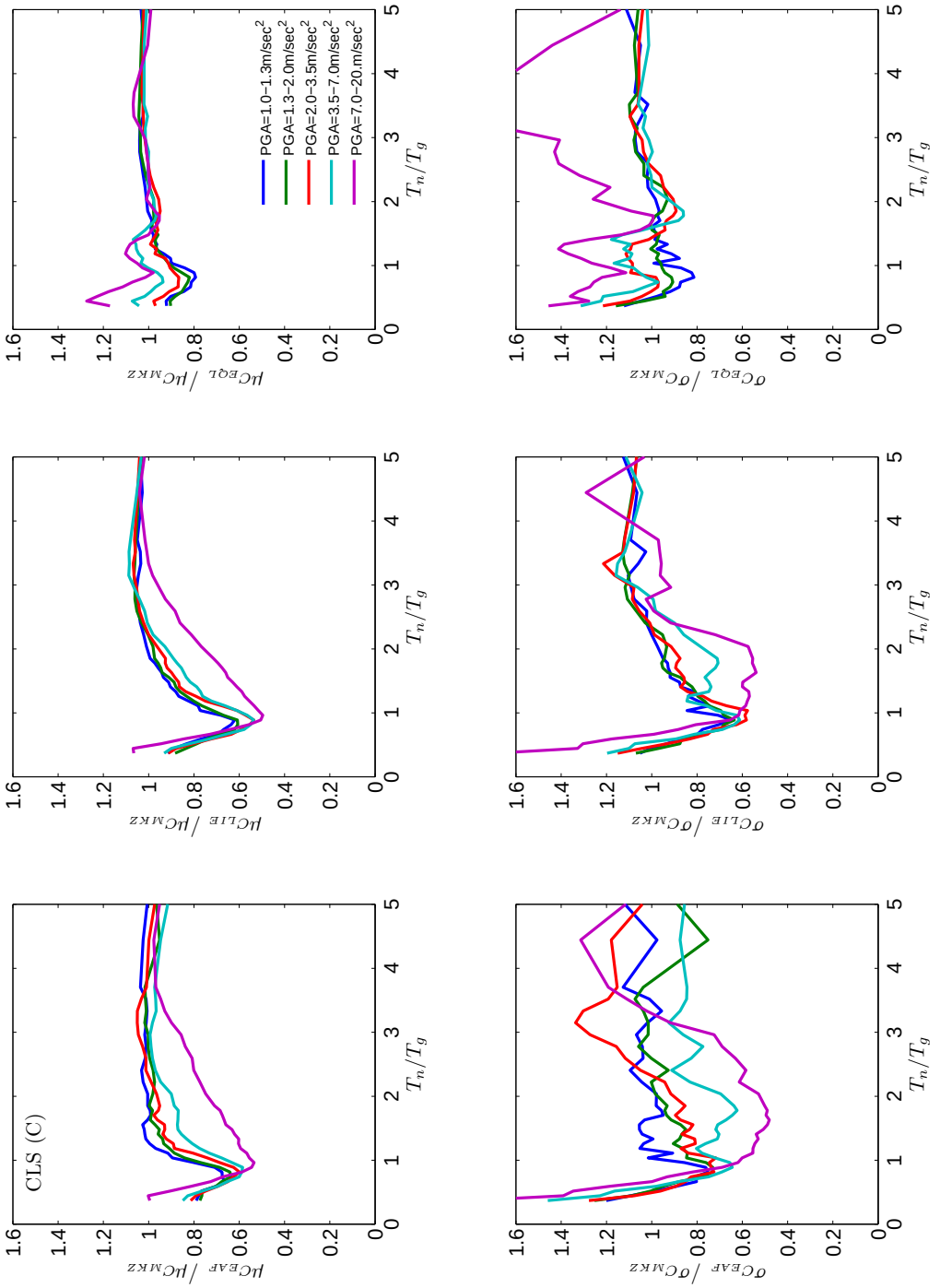

Figure 5.2: The ratio between mean inelastic deformation ratios of bilinear SDOF structures ($R_y = 4$)(counted within the PGA bins shown in the legend) evaluated using ground motions from different site response models (differentiated by the subscript of C) as a function of the elastic natural vibration period of the bilinear SDOF system normalized by the fundamental period of the site (CLS Site) (To be continued)

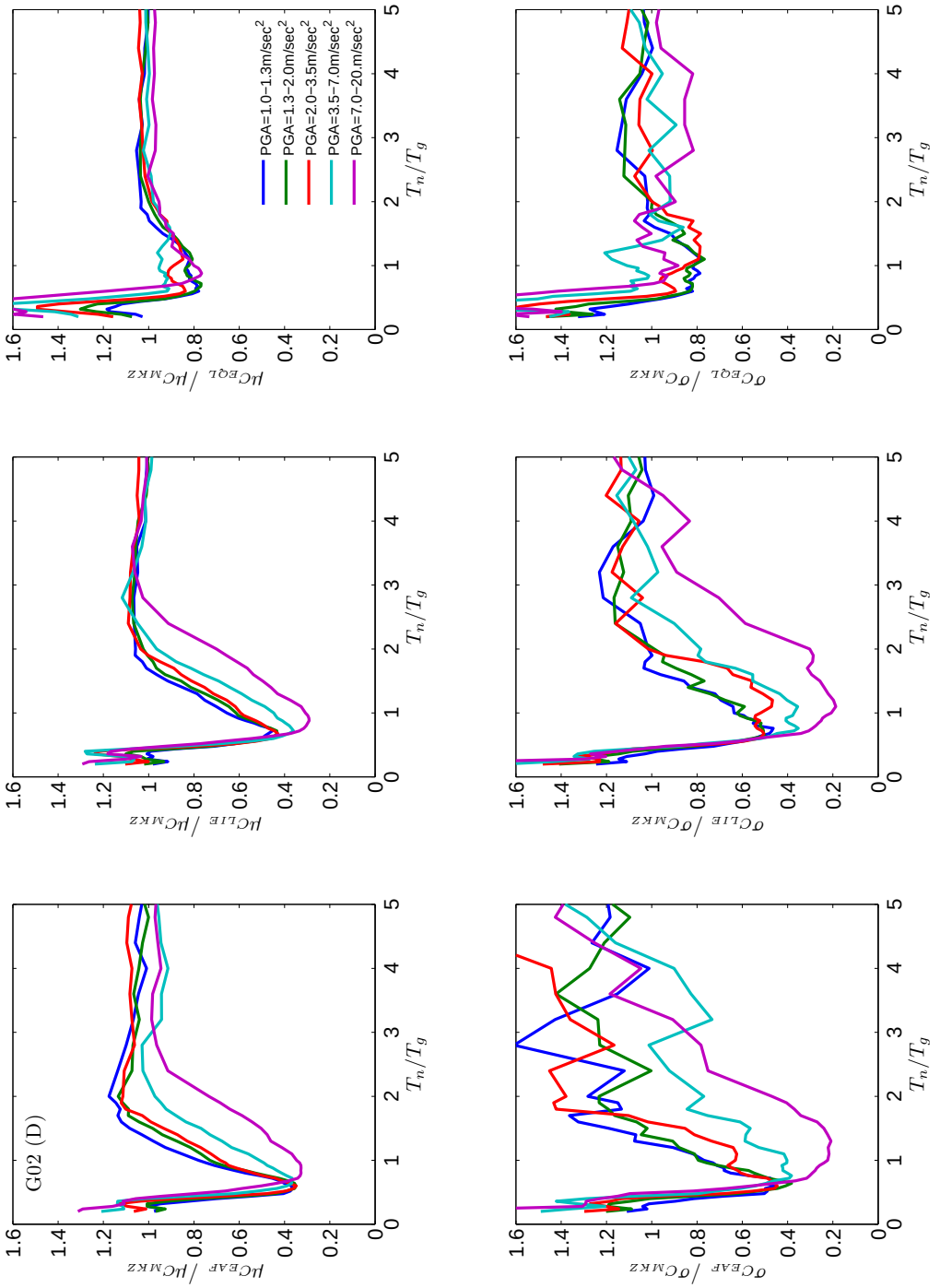

Figure 5.2: Continued (G02 Site)

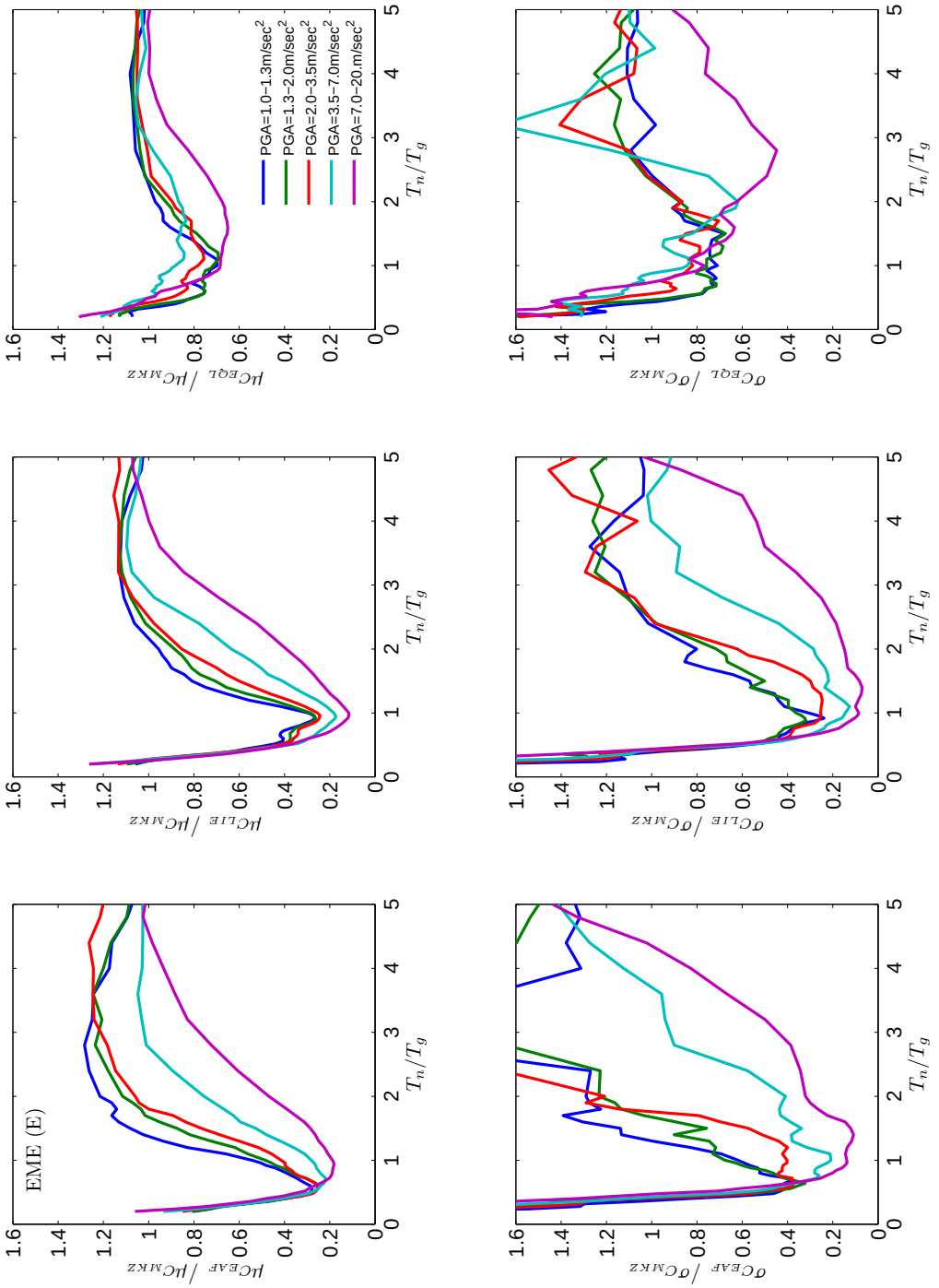

Figure 5.2: Continued (EME Site)

It can be seen from Fig. 5.2 that the LIE and EAF models give biased C predictions relative to the MKZ model for all three sites, and the bias reaches the peak value around the abscissa of unity (note that the lower the value of Q_{μ_C}, the higher bias), i.e. when the elastic vibration period of the SDOF system is close the to natural period of the site. Furthermore, the band width of the bias is proportional to the natural period of the site, i.e. is a function of the site stiffness. As expected, the performance of EAF model is very similar to the LIE model since both of them give the same bias value and bias range. The bias in C prediction caused by EQL model is much lower than that of EAF and LIE model and as expected, the stiffer the site, the better the performance of EQL model. This is because the strain level at a stiffer site is smaller for seismic excitations of the same intensity, and the smaller the strain level, the smaller the deviation between the EQL and MKZ model predictions.

The $\mathrm{PGA_{RO}}$ and site dependency of the bias can be clearly seen in Fig. 5.2. As can be inferred from previous observations, the higher $\mathrm{PGA_{RO}}$, the higher bias in the C prediction by the LIE and EAF models. Similarly, the softer the site, the higher the bias introduced in the C predictions by the LIE and EAF models. Since the $\mathrm{PGA_{RO}}$ values and the relative stiffness of the sites are directly associated with the extend of nonlinearity in the ground response, the high $\mathrm{PGA_{RO}}$ and site dependency of Q_{μ_C} lead to the conjecture that the bias in the C prediction is due to the inability of LIE and EAF models to capture the nonlinear effect in the ground response. For simplicity, only $Q_{\mu_C} = \mu C_{LIE}/\mu C_{MKZ}$ is taken as the quantitative measure of the bias in the prediction of the mean C demand.

For each site, the Q_{μ_C} value in each PGA bin at the period of highest bias is plotted as function of $\mathrm{PGA_{RO}}$ in Fig. 5.2. Clearly, different sites show different degree of PGA dependency. If the degree of dependency is measured using the linear regression slopes to the data of each Q_{μ_C} vs. PGA plot, and the absolute values of the slopes is named as proportion coefficients, it can be shown that there is some correlation between these proportion coefficients and the V_{S30} values of the sites, which illustrated in Fig. 5.3. It can be readily seen that the softer the site (i.e. lower V_{S30} value), the higher the PGA dependency of Q_{μ_C} value. This observation also implies that the nonlinear site effects

are most likely the origin of bias in the mean C estimation because softer sites are more susceptible to nonlinear deformations.

It should be noted here that although the trend in site dependency and PGA dependency of Q_{μ_C} is very clear when the C values are grouped (averaged) in PGA bins, the original Q_C values without averaging of C are highly scattered. Fig. 5.4 shows the minimum Q_C value for all the motions at selected sites. As can been observed in Fig. 5.4, the Q_C may reach very low value even at very low PGA.

Analogous to Fig. 5.2, the C values from different site response can be averaged within frequency index (FI) bins before taking the ratio, to show the FI dependency of inelastic response bias. Fig. 5.5 shows the Q_{μ_C} and Q_{σ_C} for $R_y = 4$ at selected sites as a function of the elastic vibration period (T_n) of the SDOF normalized by the fundamental period of the site (T_g); the mean C values here are averaged within the ranges of FI indicated by the legend. The trend of bias indicated by Q_{μ_C} and Q_{σ_C} is very similar to what shown in Fig. 5.2, except that the FI dependency of Q_{μ_C} and Q_{σ_C} is not as prominent as the PGA dependency. This observation is consistent with the fact that PGA dependency estimated for the site response prediction error by the alternative methods in chapter 2 is stronger than the FI dependency.

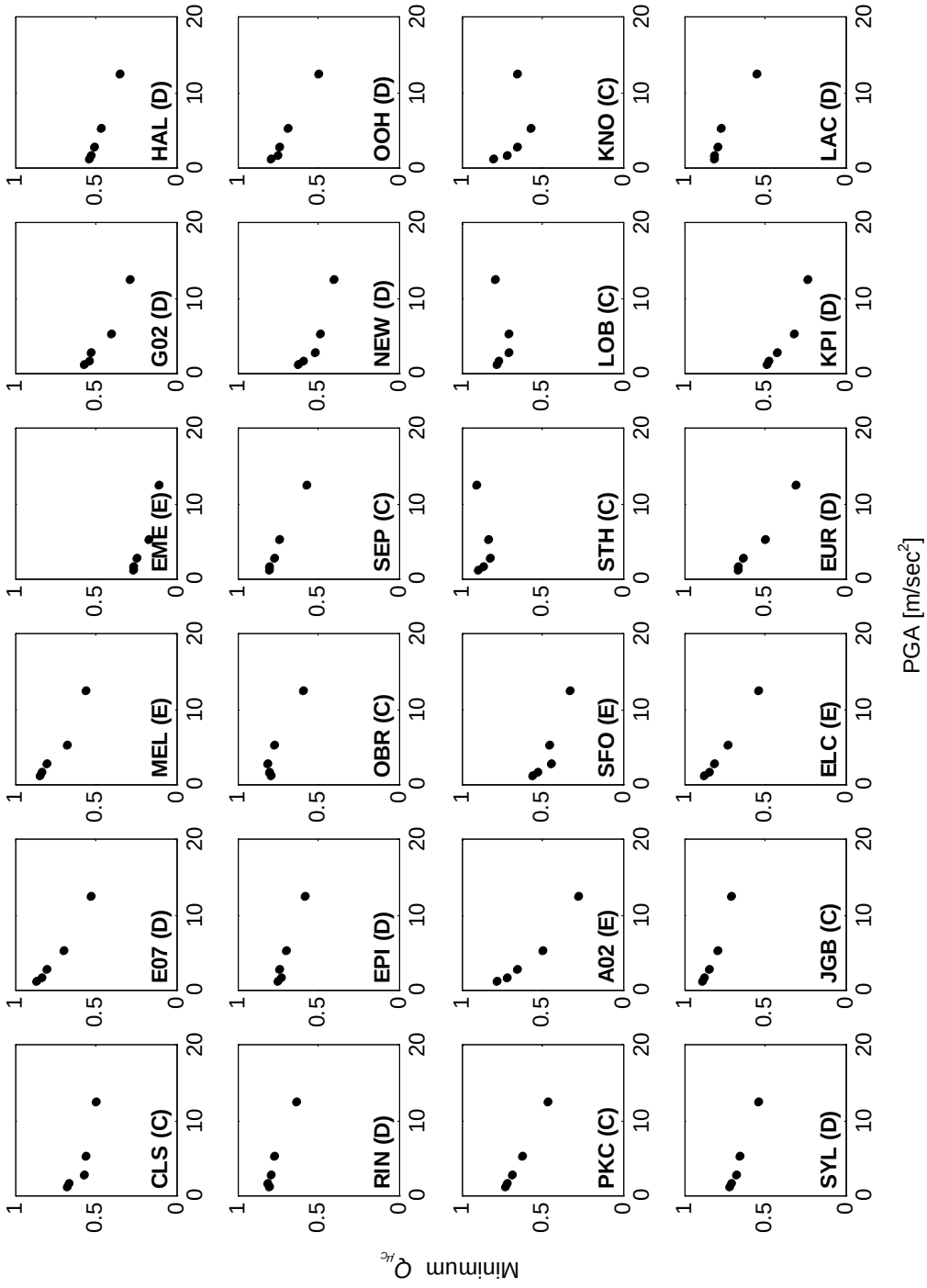

Figure 5.2: The correlation between Q value (evaluated at the period of highest bias) and PGA for each site ($R_y = 4$)

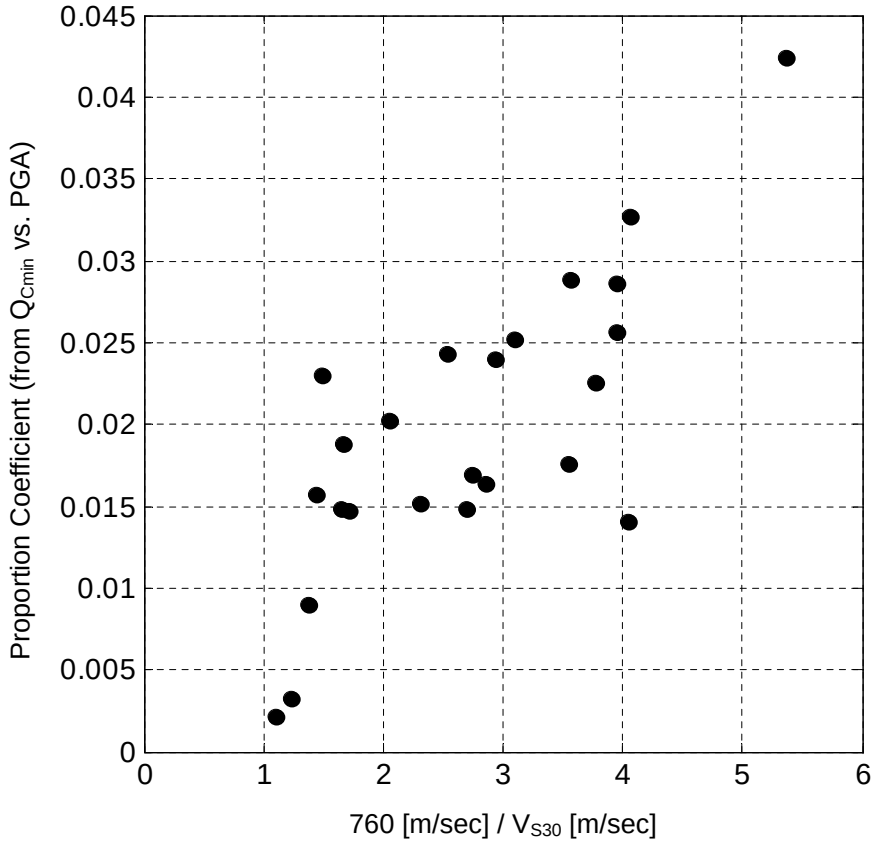

Figure 5.3: Correlation between the proportion coefficient (slope of Minimum Q vs. PGA) in Figure 5.2 and V_{S30} (R_y=4)

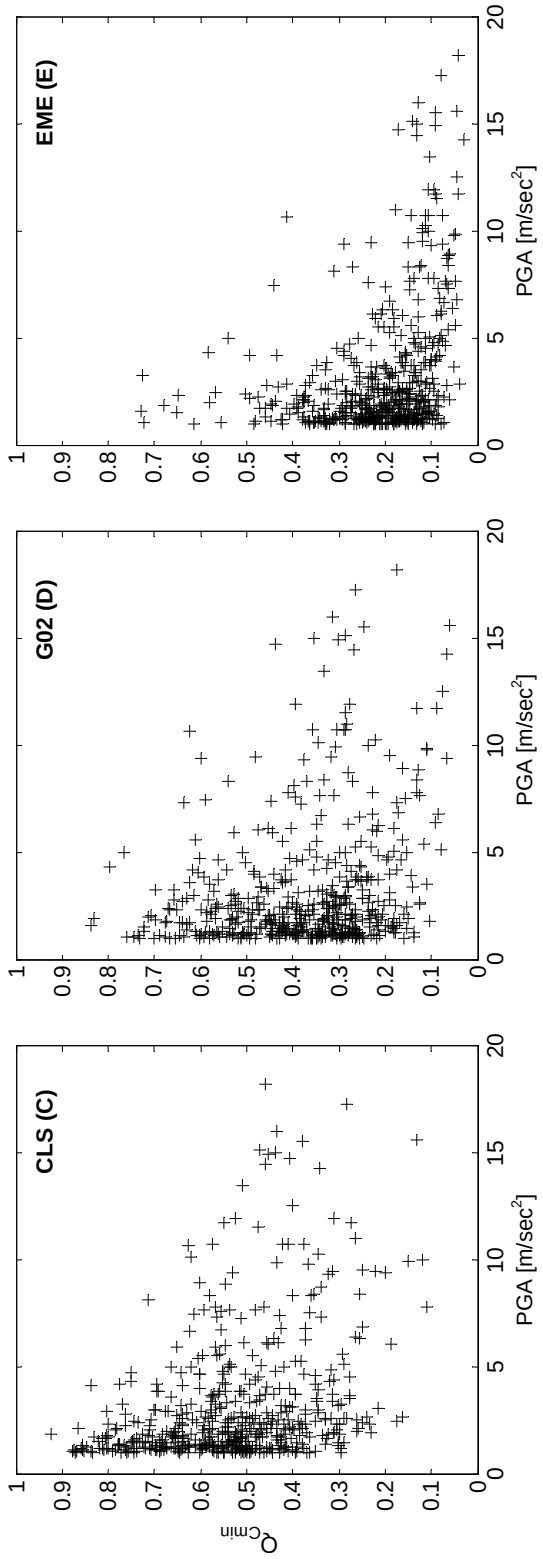

Figure 5.4: Minimum Q value versus PGA for selected sites (Ry=4). Scattering in data is much more pronounced than averaging Q within PGA bins as in Figure

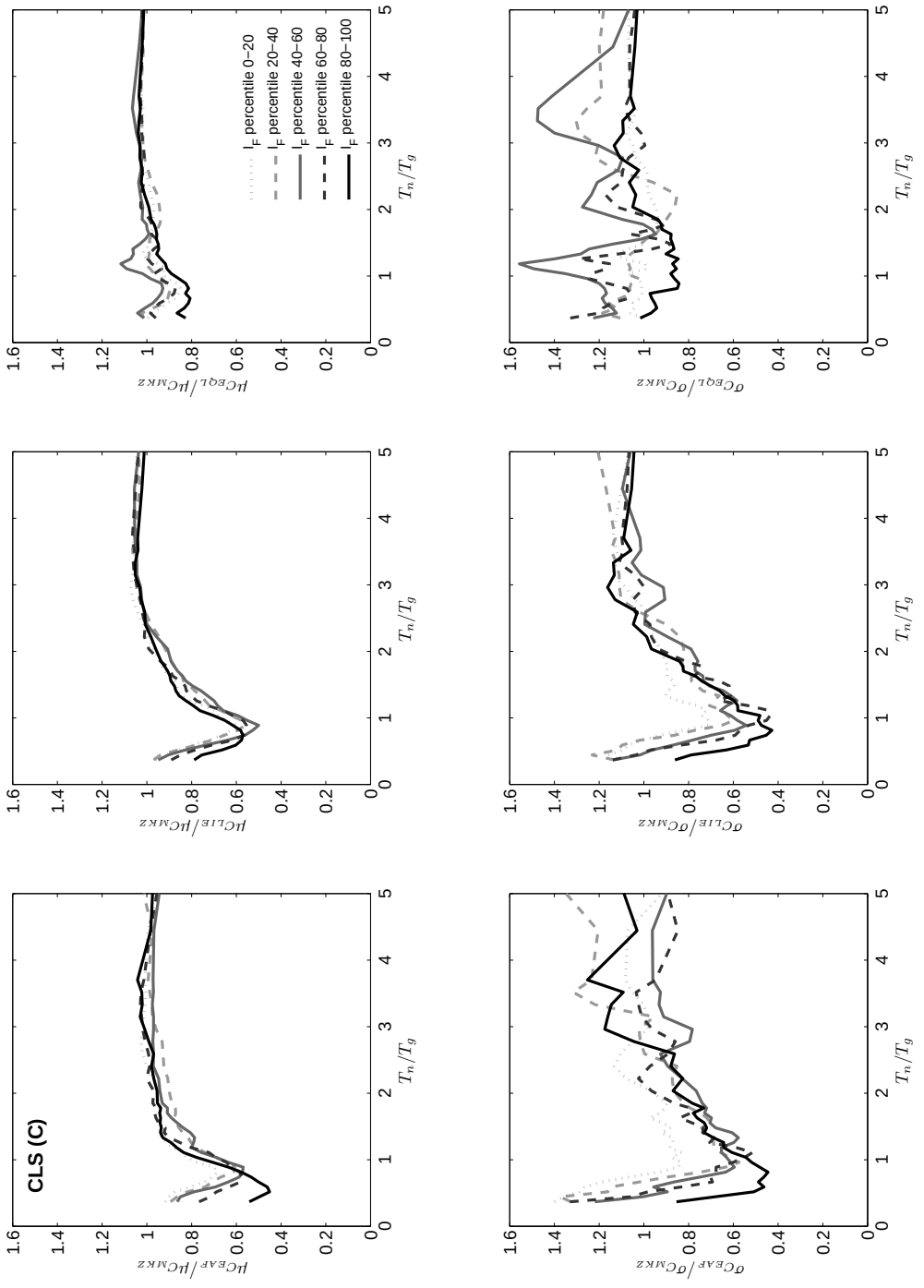

Figure 5.5: The ratio between mean inelastic deformation ratios of bilinear SDOF structures with constant strength reduction factors (R_y=4) (averaged within the FI bins shown in the legend) evaluated using ground motions from different site response models (differentiated by the subscript of C) as a function of the elastic natural vibration period of the bilinear SDOF system normalized by the fundamental period of the site (CLS Site) (To be continued)

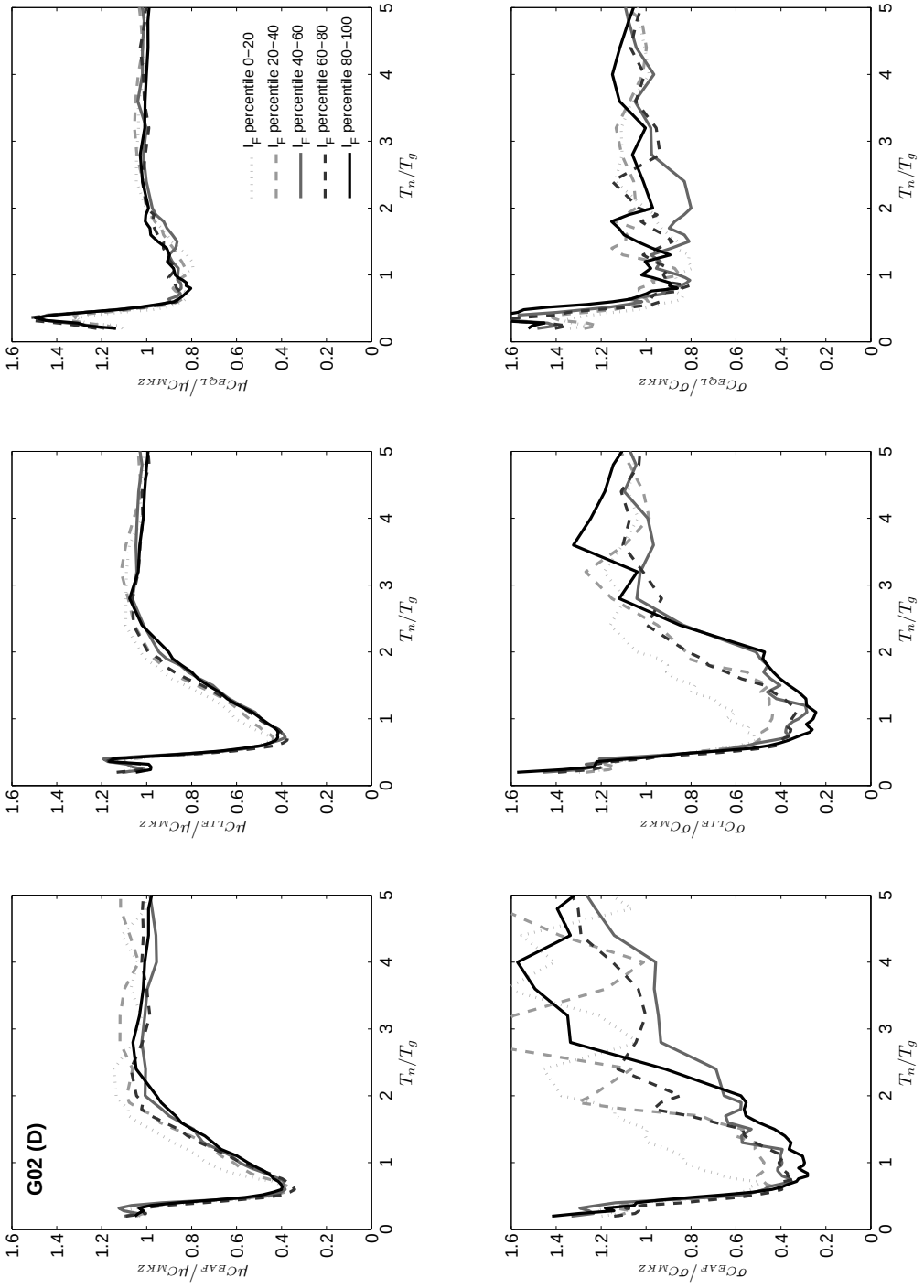

Figure 5.5: Continued (G02 Site)

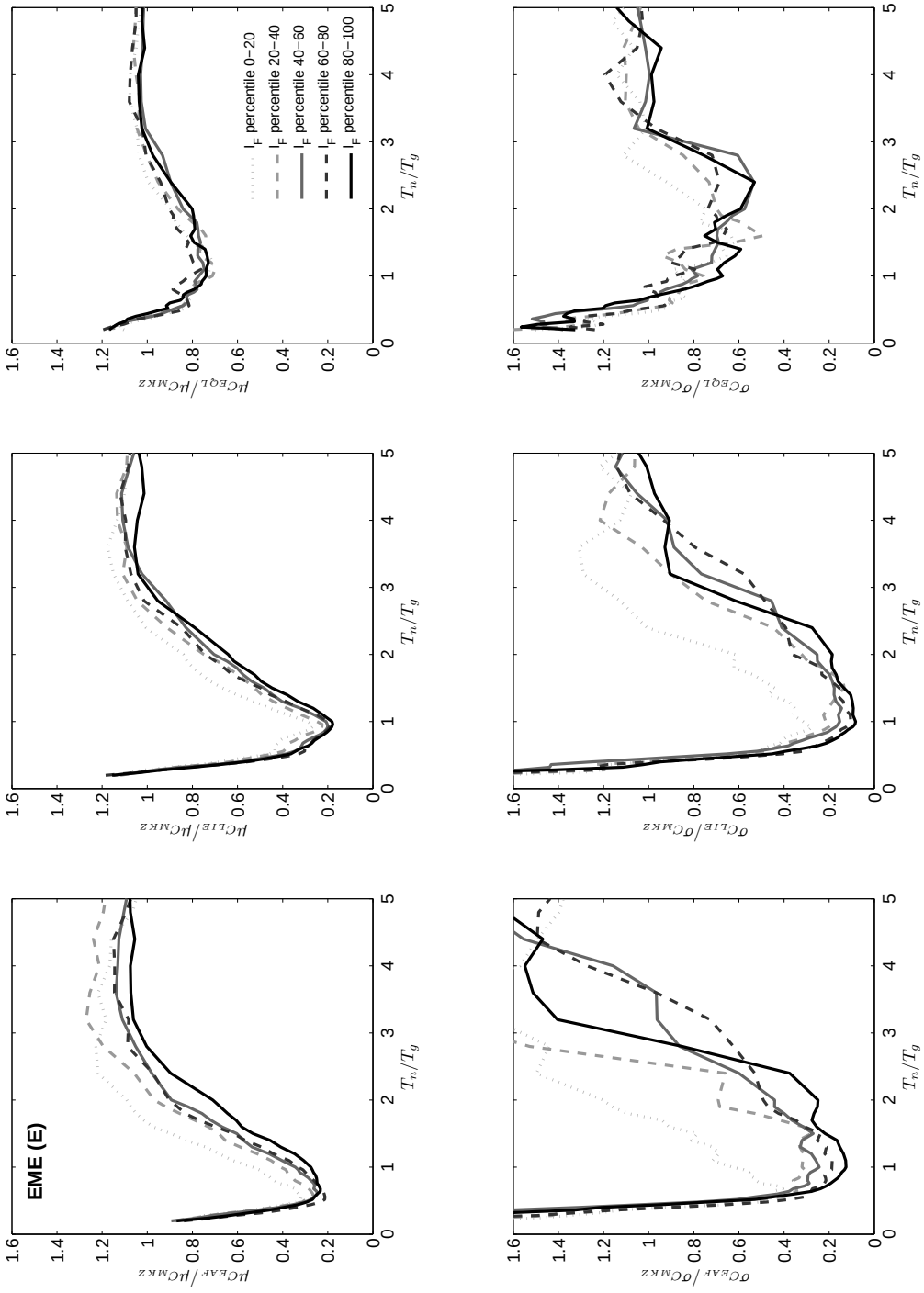

Figure 5.5: Continued (EME Site)

Similar to Fig. 5.2, the value in each FI bin at the period of highest bias can be plotted as function of FI for all the sites as shown in Fig. 5.5. It can be readily seen that some sites do show strong dependency of Q_{μ_C} on FI, while others do not. If the minimum Q value of each site in Fig. 5.5 is taken as a representative bias degree of the site, which is denoted as $Q_{C_{min}}$, it seems these $Q_{C_{min}}$ values have some correlation with the amplification amplitude at the fundamental frequency of the site, which shown in Fig. 5.6. Again, it can be shown in Fig. 5.7 that the individual minimum Q values without C averaging are actually very scattered and that very low Q may appear even in the low FI range.

It should be noted again that since constant R_y models are used to calculate the inelastic structure response, the bias in C prediction is purely caused by the differences in the frequency content of the ground motions for different site response models. Such differences in the frequency content maybe significant and cause large discrepancy the C prediction, even though the differences in amplitudes are very small as in the low PGA scenarios.

Analogous to Fig. 5.3 and Fig. 5.6, the correlation between and bias in C prediction for the constant ductility ratio case ($\mu = 4$) is presented in Fig. 5.8 and Fig. 5.9. The general trends are almost same as what shown in Fig. 5.3 and Fig. 5.6. The difference is that the bias in the constant ductility case is consistently less than in the case of constant strength reduction case. The reason is that the inelasticity levels in the bilinear SDOF structures in the constant $\mu = 4$ case are always lower than those in the constant $R_y = 4$ case and thus less inelastic deformations happen in the constant $\mu = 4$ case.

Finally, it should be noted that the bias trends in Fig. 5.2 and Fig. 5.5 are consistent with results published by Bazzurro et al. (2004), which were based on the comparison between the inelastic structural response obtained using synthetic and recorded ground motions. This consistency also implies that bias in the latter study may be caused by insufficient consideration of the nonlinear site effect in the synthetic ground motion predictions.

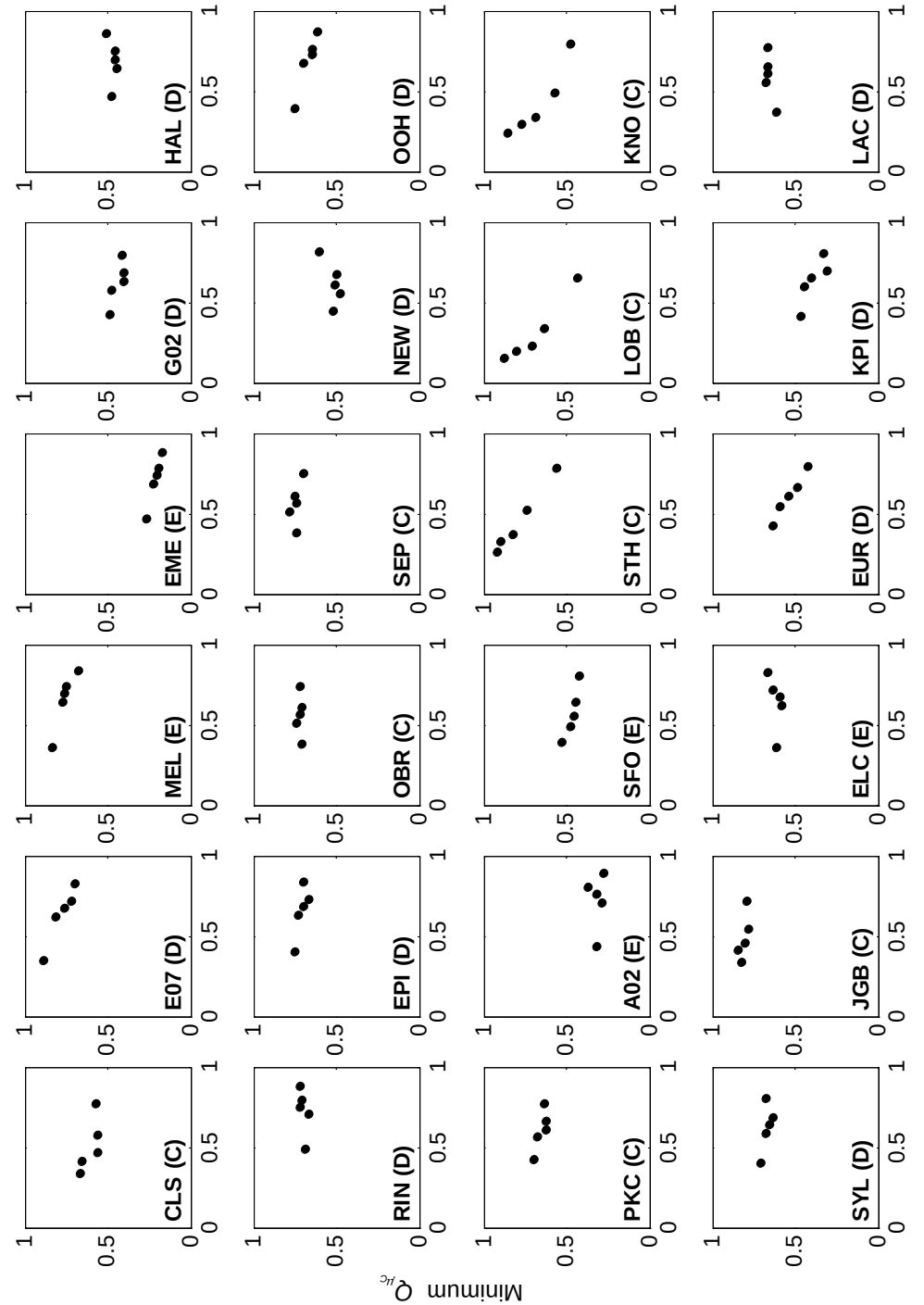

Figure 5.5: Correlation between minimum Q value (evaluated at the period of highest bias) and frequency index (FI) for each site (R_y=4)

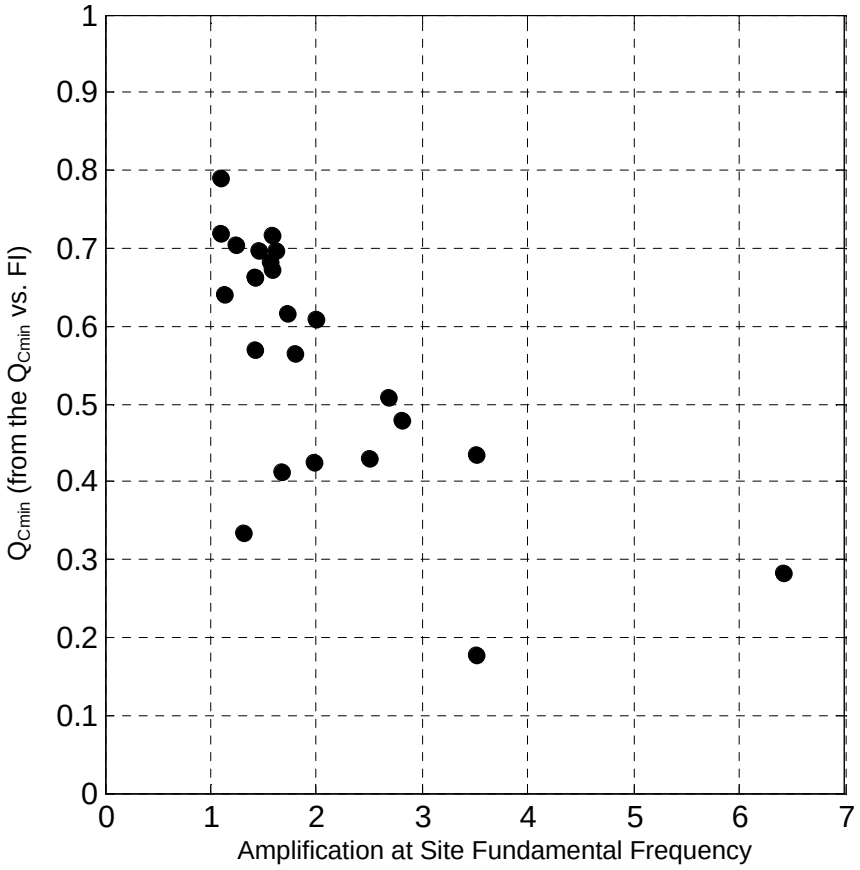

Figure 5.6: The correlation between the minimum Q in Figure 5.5 and the amplification at the fundamental frequency of the soil profile, evaluated from the linear elastic site response (Ry=4)

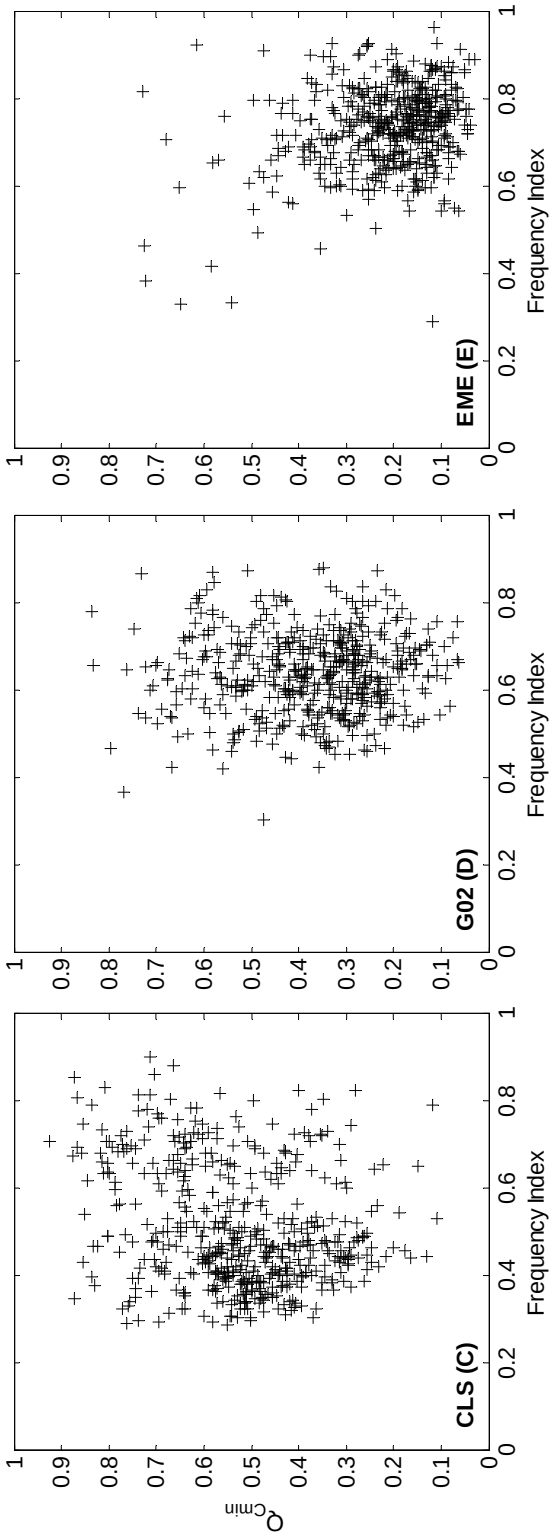

Figure 5.7: Minimum Q value versus FI for selected sites (R_y=4). Scattering in data is much more pronounced than averaging Q within FI bins as in Figure 5.5.

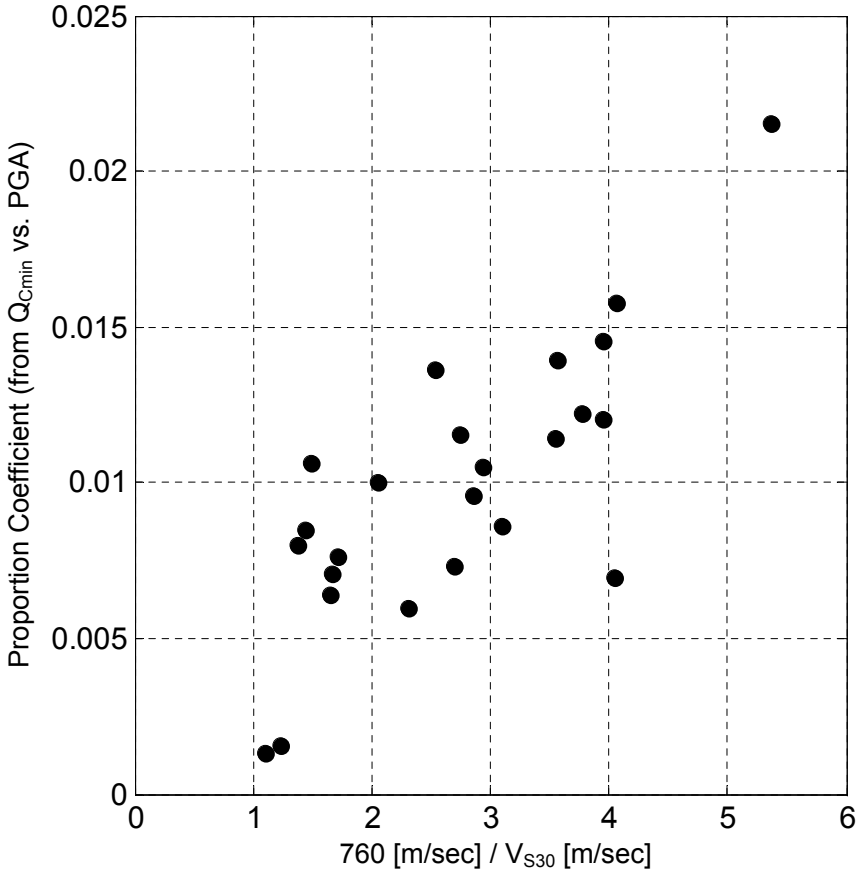

Figure 5.8: Correlation between the proportion coefficient (slope of Minimum Q vs. PGA) and V_{S30} for constant ductility demand (μ=4)

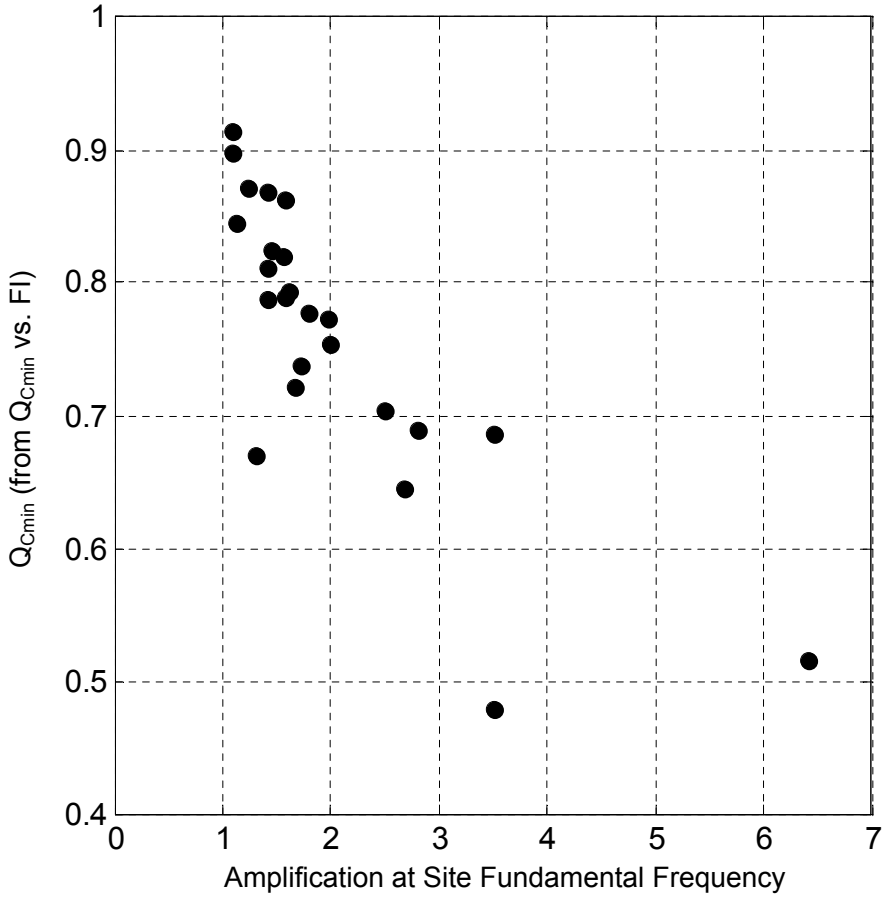

Figure 5.9: The correlation between the slope of minimum Q and the amplification at the fundamental frequency of the soil profile for constant ductility demand (μ=4)

5.4 Conclusion

The uncertainty in nonlinear structural response predictions, that results from site response models implemented in synthetic ground motion simulations, is investigated. Typical profiles in Southern California are studied, the errors between downhole observations and site response predictions are estimated in an intensity-frequency (PGA_{RO}-FI) domain. A consistent pattern of prediction error in ground response is observed, with high intensity-high frequency index regions reflecting large deviation between elastic and nonlinear predictions, independent of the soil profile characteristics. The quantitative relations between this prediction error and site-motion parameters are established, which enable C-given a profile and an incident ground motion– the estimation of mean and variance of expected site response prediction error relative to nonlinear time domain solutions

Next, the propagation of site response modeling uncertainty to the assessment of inelastic SDOF structural response revealed consistent bias and uncertainty by the linear site response model in the prediction of inelastic deformation. The results indicate that, for most of the sites with exception of the very stiff ones, the predicted inelastic deformation ratios using ground motions from visco-elastic site response models are consistently lower than those using ground motions from incremental nonlinear site response models around particular period range. The results also show that the former are less variable than the latter. These observations imply that the design based on inelastic SDOF analysis using the synthetic motions without considering nonlinear site effects may be on the unsafe part as a result of underestimation of the mean and uncertainty of deformation demand.

It was found that the mean bias in the inelastic deformation ratio (C) prediction has good correlation with some characteristics of input ground motions and site parameters. In general, the bias in C predictions increase with increasing ground motion intensity (PGA), decreasing V_{S30}, and increasing first mode amplification. Overall, the bias is reduced as more elaborate site response models are implemented.

This ground motion (PGA and FI) and site (V_{S30} and Amp) dependency of the mean bias in C predictions implies that the source of bias is most likely the inability of simplified models (linear viscoelastic, empirical amplification factors) to capture nonlinear site effects

and the corresponding altering of ground motion frequency content. This conjecture is also favorable to the establishment of a guideline for efficient integration of nonlinear site response models into end-to-end ground motion simulations.

CHAPTER VI

SUMMARY, CONCLUSIONS AND RECOMMENDATIONS

6.1 Summary and Conclusions

This study addresses some issues regarding the efficient integration of nonlinear site response models in end-to-end ground motion models. The motivation of the study is lack of quantitative guideline to determine (i) under what conditions are nonlinear models necessary; (ii) what is the adequate model complexity to ensure computationally-efficient simulations?; and (iii) What are the implications of nonlinear effect predictions in the estimation of structural performance measures?

The impediment of the study is the lack of statistically significant number of strong motion records at sites with both geotechnical information and downhole array observations. For this purpose, broadband ground motion synthetics are combined with sites with detailed geotechnical information to investigate the variability propagation from the seismic excitation to the inelastic structure response. Four critical site-motion parameters were identified and used to describe the site and ground motion characteristics governing the intensity of nonlinear effects, which are the peak ground acceleration PGA of rock outcrop motion, the Frequency Index (FI) of the motion, the V_{S30} of the site, and the first mode amplification (Amp) of the site.

In chapter 2, the site response models used in this study were validated against downhole array observations at three sites in LA basin.

In chapter 3, a quantitative measure of site nonlinearity susceptibility was proposed (e_{SA}), namely the ground response prediction error of linear response relative to that of the nonlinear model based on the comparison among ground response from different models. The empirical relation between e_{SA} and the site and ground motion parameters was developed, which allows the first order estimation of the error that would be introduced in ground motion predictions if nonlinear effects were to be ignored, and contributes towards

the efficient integration of nonlinear site response models in end-to-end ground motion simulations.

In chapter 4, The effects of soil parameter uncertainty were evaluated as a function of the seismic input intensity and frequency content. It was shown that the effects of nonlinear soil property uncertainties on the ground-motion variability strongly depend on the seismic motion intensity, and this dependency is more pronounced for soft soil profiles. By contrast, the effects of velocity profile uncertainties are less intensity dependent and more sensitive to the velocity impedance in the near surface that governs the maximum site amplification.

In chapter 5, a series of bilinear single degree of freedom oscillators were subjected to the ground motions computed using the alternative soil models, and the consequent variability in the structural response was evaluated. Results showed high bias and uncertainty of the inelastic structural displacement ratio predicted using the linear site response model for periods close to the fundamental period of the soil profile. The amount of bias and the period range where the structural performance uncertainty manifests are shown to be a function of both input motion and site parameters.

In conclusion, this work shows that the susceptibility of a site to nonlinear effects is a function of both the profile and the ground motion characteristics as opposed to the widely employed V_{S30} classification, quantifies the error introduced in ground motion predictions by ignoring nonlinear effects as a function of these parameters, categorizes the soil parameters governing the uncertainty in site response predictions as a function of site and ground motion, and illustrates the implications of nonlinear site response predictions in the inelastic structural design procedures.

6.2 Recommendations for Future Research

For each earthquake scenario, only one realization of the ground motion was generated. The variability of soil and ground motion parameters in this study was obtained using ground motions from all scenarios simulated, and as a result, this study describes the so-called inter-scenario variability of nonlinear site response. Therefore, multiple realizations of each individual scenario could be used to develop the intra-scenario variability of the quantities

under investigation.

As mentioned previously, although this study is specific to the site conditions and broad-band synthetics in southern California, the methodology used is in accordance to the principles of wave propagation theory. Therefore, extension of proposed research procedure to other site conditions and ground motion synthetics is possible.

The determination of some site motion parameters such as FI and Amp requires detailed velocity and damping profiles of the site under investigation. Unfortunately, this information may not be available for most of the sites, especially in large-scale ground motion simulations or in engineering practice. Therefore, simplified procedures are necessary to estimate these parameters using the minimal available information about the site. One possible proposal was to make use of the available spectral ratios of recorded acceleration histories to develop empirical site or motion parameters. Nonetheless, additional studies would be necessary to investigate the effectiveness of the proposed procedure.

In chapter 5, a highly simplified bilinear SDOF oscillator was used as the idealization of the structural model. It was shown that insufficient consideration of nonlinear site response will cause high bias in C prediction, and the degree of bias was shown to be well correlated with some of the site parameters. However, the effectiveness of this conclusion for more elaborated structural models and other performance demands is still under investigation. Further studies would be necessary to explore the implications of nonlinear site response predictions on more complex structural models.

Finally, this study is limited to one dimensional site response, while additional site effects, such as basin and topography effects or liquefaction have not been considered. These effects may be incorporated in a future phase of study.

REFERENCES

N. Abrahamson, G. Atkinson, D. Boore, Y. Bozorgnia, K. Campbell, B. Chiou, I. M. Idriss, W. Silva, and R. Youngs. Comparisons of the NGA ground-motion relations. *Earthquake Spectra*, 24(1):45–66, 2008.

N. A. Abrahamson and W. J. Silva. Summary of the Abrahamson & Silva NGA ground-motion relations. *Earthquake Spectra*, 24:7–97, 2008.

J. Aguirre and K. Irikura. Nonlinearity, liquefaction, and velocity variation of soft soil layers in Port Island, Kobe, during the Hyogo-ken Nanbu earthquake. *Bulletin of the Seismological Society of America*, 87(5):1244–1258, 1997.

D. G. Anderson. Laboratory testing of nonlinear soil properties: I & II. Technical report, CH2M HILL, 2003.

J. E. Andrade and R. I. Borja. Quantifying sensitivity of local site response models to statistical variations in soil properties. *Acta Geotechnica*, 1:3–14, 2006.

D. Assimaki and E. Kausel. An equivalent linear algorithm with frequency- and pressure-dependent moduli and damping for the seismic analysis of deep sites. *Soil Dynamics and Earthquake Engineering*, 22:959 – 965, 2002.

D. Assimaki and J. Steidl. Inverse analysis of weak and strong motion downhole array data from the Mw7.0 Sanriku-Minami earthquake. *Soil Dynamics and Earthquake Engineering*, 27:73–92, 2007.

D. Assimaki, A. Pecker, R. popescu, and J. Prevost. Effects of spatial variability of soil properties on surface ground motion. *Journal of Earthquake Engineering*, 7(Special Issue 1):1–44, 2003.

D. Assimaki, J. Steidl, and P.-C. Liu. Attenuation and velocity structure for site response analyses via downhole seismogram inversion. *Pure appl. geophys.*, 163:81–118, 2006.

D. Assimaki, W. Li, J. H. Steidl, and K. Tsuda. Site amplification and attenuation via downhole array seismogram inversion: A comparative study of the 2003 Miyagi-Oki aftershock sequence. *Bulletin of the Seismological Society of America*, 98(1):301–330, 2008a.

D. Assimaki, W. Li, J. M. Steidl, and J. Schmedes. Quantifying nonlinearity susceptibility via site response modeling uncertainty at three sites in the Los Angeles basin. *Bulletin of the Seismological Society of America*, 98(5):2364–2390, 2008b.

H. Bao, J. Bielak, O. Ghattas, L. F. Kallivokas, D. R. OHallaron, J. R. Shewchuk, and J. Xu. Large-scale simulation of elastic wave propagation in heterogeneous media on parallel computers. *Comput. Methods Appl. Mech. Eng.*, 152:85–102, 1998.

J. P. Bardet and T. Tobita. NERA A computer program for nonlinear earthquake site response analyses of layered soil deposits. Technical report, University of Southern California, 2001.

J. P. Bardet, K. Ichii, and C. H. Lin. EERA a computer program for equivalent-linear earthquake site response analyses of layered soil deposits. Technical report, University of Southern California, 2000.

J. P. Bardet, T. Tobita, K. Ichii, and A. Rogers. Site response analysis at the vertical arrays of the cerritos college police station and san bernardino main fire station. Technical report, University of Southern California, 2001.

M. B. Baturay and J. P. Stewart. Uncertainty and bias in ground-motion estimates from ground response analyses. *Bulletin of the Seismological Society of America*, 93(5):2025–2042, 2003.

P. Bazzurro and C. A. Cornell. Ground-motion amplification in nonlinear soil sites with uncertain properties. *Bulletin of the Seismological Society of America*, 94(6):2090 – 2109, 2004.

P. Bazzurro, B. Sjoberg, and N. Luco. Post-elastic response of structures to synthetic ground motions. Technical report, AIR Worldwide Co., 2004.

J. R. Benjamin and C. A. Cornell. *Probability, statistics, and decision for civil engineers.* McGraw-Hill, 1970.

I. A. Beresnev and G. M. Atkinson. Modeling finite-fault radiation from the ω_n spectrum. *Bulletin of the Seismological Society of America*, 87:67–84, 1997.

I. A. Beresnev and G. M. Atkinson. FINSIM - a FORTRAN program for simulating stochastic acceleration time histories from finite faults. *Seism. Res. Lett.*, 69:27–32, 1998. Synthetic motion for structure response.

I. A. Beresnev, G. M. Atkinson, P. A. Johnson, and E. H. Field. Stochastic finite-fault modeling of ground motions from the 1994 Northridge, California, earthquake. II. widespread nonlinear response at soil sites. *Bulletin of the Seismological Society of America*, 88(6): 1402–1410, 1998.

J. Berrill. Site effects during the San Fernando, California, earthquake. In *Proceedings of the Sixth World Conf. on Earthquake Engineering*, pages 432–438, India, 1977.

J. Bommer, S. Scott, and S. Sarma. Hazard-consistent earthquake scenarios. *Soil Dynamics and Earthquake Engineering*, 19:219–231, 2000.

D. M. Boore. Stochastic simulation of high-frequency ground motions based on seismological models of the radiated spectra. *Bull. seism. soc. Am.*, 73:1865–1894, 1983.

D. M. Boore and G. M. Atkinson. Ground-motion prediction equations for the average horizontal component of PGA, PGV, and 5%-damped PSA at spectral periods between 0.01 s and 10.0 s. *Earthquake Spectra*, 24(1):99–138, 2008.

D. M. Boore and W. B. Joyner. Site amplification for generic rock sites. *Bull. Seismol. Soc. Am.*, 87:237–341, 1997.

R. D. Borcherdt. Effects of local geology on ground motion near San Francisco Bay. *Bull. Seismol. Soc. Am.*, 60:29–61, 1970.

R. D. Borcherdt and J. F. Gibbs. Effects of local geological conditions in the San Francisco Bay region on ground motions and the intensities of the 1906 earthquake. *Bulletin of the Seismological Society of America*, 66(2):467–500, 1976.

R. I. Borja, C.-H. Lin, K. M. Sama, and G. M. Masada. Modelling non-linear ground response of non-liquefiable soils. *Earthquake Engineering & Structural Dynamics*, 29: 63–83, 2000.

BSSC. NEHRP recommended provisions for seismic regulations for new buildings and other structures (FEMA 450). Technical report, prepared by the Building Seismic Safety Council for the Federal Emergency Management Agency, Washington, D.C., 2003.

K. W. Campbell and Y. Bozorgnia. NGA ground motion model for the geometric mean horizontal component of PGA, PGV, PGD and 5% damped linear elastic response spectra for periods ranging from 0.01 to 10 s. *Earthquake Spectra*, 24:139–171, 2008.

J. M. Carcione, D. Kosloff, and R. Kosloff. Wave propagation in a linear viscoacoustic medium. *Geophys. J. R. Astr. Soc.*, 93:393407, 1988.

B.-H. Chin and K. Aki. Simultaneous study of the source, path, and site effects on strong ground motion during the 1989 Loma Prieta earthquake: a preliminary result on pervasive nonlinear site effects. *Bulletin of the Seismological Society of America*, 81(5):1859–1884, 1991.

B. S. J. Chiou and R. R. Youngs. Chiou-youngs NGA ground motion relations for the geometric mean horizontal component of peak and spectral ground motion parameters. *Earthquake Spectra*, 24:173–215, 2008.

A. K. Chopra. *Dynamics of Structures: Theory and Applications to Earthquake Engineering (2nd Edition)*. Prentice Hall, 2000.

A. K. Chopra and C. Chintanapakdee. Inelastic deformation ratios for design and evaluation of structures: Single-degree-of-freedom bilinear systems. *Journal of Structural Engineering*, 130(9):1309–1319, 2004.

C. Cramer. Comparing weak- and strong-motion spectral ratios at the Turkey Flat site effects test area, Parkfield, California: Possible nonlinear soil behavior. In *Proceedings Geotechnical Earthquake Engineering and Soil Dynamics IV, ASCE*, Sacramento, CA, 2008. Turkey Flat Parkfield earthquake.

C. H. Cramer. Site-specific seismic-hazard analysis that is completely probabilistic. *Bulletin of the Seismological Society of America*, 93(4):1841–1846, 2003.

C. H. Cramer. Quantifying the uncertainty in site amplification modeling and its effects on site-specific seismic-hazard estimation in the upper Mississippi Embayment and adjacent areas. *Bulletin of the Seismological Society of America*, 96(6):2008–2020, 2006.

C. H. Cramer, J. S. Gomberg, E. S. Schweig, B. A. Waldron, and K. Tucker. The Memphis, Shelby County, Tennessee, seismic hazard maps. Technical report, U.S. Geological Survey Open-File Report 04-1294, 2004.

M. B. Darendeli. *Development of a new family of normalized modulus reduction and material damping curves*. PhD thesis, University of Texas at Austin, 2001.

R. B. Darragh and A. F. Shakal. The site response of two rock and soil station pairs to strong and weak ground motion. *Bulletin of the Seismological Society of America*, 81(5): 1885–1899, 1991.

S. M. Day and J. R. Minster. Numerical simulation of attenuated wavefields using a Pade approximant method. *Geophys. J. R. Astr. Soc.*, 78:105–118, 1984.

S. Dham and R. Ghanem. Stochastic finite element analysis for multiphase flow in heterogeneous porous media. In P. D. Spanos, editor, *Computational Stochastic Mechanics*, pages 429–434. Rotterdam: Balkema, 1995.

R. Dobry, R. D. Borcherdt, C. B. Crouse, I. M. Idriss, W. B. Joyner, G. R. Martin, M. S. Power, E. E. Rime, and R. B. Seed. New site coefficients and site classification system used in recent building seismic code provisions. *Earthquake Spectra,*, 16(1):41, 2000.

D. S. Dreger and A. Kaverina. Seismic remote sensing for the earthquake source process and near-source strong shaking: a case study of the october 16, 1999 Hector Mine earthquake. *Geophys. Res. Lett.*, 27:1941–1944, 2000.

V. P. Drnevich, J. R. H. Jr, and F. E. R. Jr. Large amplitude vibration effects on the shear modulus of sand. Technical report, University of Michigan Report to Waterways Experiment Station, Corps of Engineers, U.S. Army, 1966.

C. Duke and A. Mal. Site and source effects on earthquake ground motion. Technical report, University of California, Los Angeles, 1978.

A. Elgamal, Z. Yang, and J. Lu. Cyclic1D: A computer program for seismic ground response. Technical report, University of California, San Diego, La Jolla, CA., 2006.

A. W. Elgamal, M. Zeghal, H. Tang, and J. Stepp. Lotung downhole array. I: Evaluation of site synamic properties. *Journal of Geotechnical Engineering*, 121(4):350–362, 1995.

G. W. Ellis and A. S. Cakmak. Modeling earthquake ground motions in seismically active regions using parametric time series methods. Technical report, Technical Report NCEER-87-0014, Nationa Center for Earthquake Engineering Research, 1987.

H. Emmerich and M. Korn. Incorporation of attenuation into time-domain computations of seismic wave fields. *Geophysics*, 52(9):1252–1264, 1987.

G. A. Fenton. *Simulation and Analysis of Random Fields*. PhD thesis, Princeton University, 1990.

G. A. Fenton and D. V. Griffiths. Stochastics of free surface flow through stochastic earth dam. *J. Geotech. Engrg.*, 122(6):427–436, 1996.

G. A. Fenton and D. V. Griffiths. Bearing capacity of spatially random c-ϕ soils. In *Proc. 10th Int. Conf. Computer Meth. Adv. Geomech.*, pages 1411–1415, Tucson, AZ, 2001.

E. H. Field and K. H. Jacob. Monte-carlo simulation of the theoretical site response variability at Turkey Flat, California, given the uncertainty in the geotechnically derived input parameters. *Earthquake Spectra*, 9(4):669–701, 1993.

E. H. Field, P. A. Johnson, I. A. Beresnev, and Y. Zeng. Nonlinear ground-motion amplification by sediments during the 1994 Northridge earthquake. *Nature*, 390(11):599–602, 1997.

E. H. Field, Y. Zeng, P. A. Johnson, and I. A. Beresnev. Nonlinear sediment response during the 1994 Northridge earthquake: Observations and finite source simulations. *Journal of Geophysical Research*, 103(B11):26869–26883, 1998.

D. V. Griffiths and G. A. Fenton. Seepage beneath water retaining structures founded on spatially random soil. *Geotechnique*, 43(4):577–587, 1993.

M. Guatteri, P. Mai, G. Beroza, and J. Boatwright. Strong ground-motion prediction from stochastic-dynamic source models. *Bulletin of the Seismological Society of America*, 93: 301–313, 2003.

H. Haddadi, A. Shakal, and C. Real. The Turkey Flat blind prediction experiment for the September 28, 2004 Parkfield earthquake: Comparison with other Turkey Flat recordings,. In *Proceedings Geotechnical Earthquake Engineering and Soil Dynamics IV, ASCE*, Sacramento, California, 2008. Turkey Flat Parkfield earthquake.

B. O. Hardin and V. P. Drnevich. Shear modulus and damping in soils: Design equations and curves. *J. Soil Mech. Found. Div., ASCE,*, 98:667–692, 1972a.

B. O. Hardin and V. P. Drnevich. Shear modulus and damping in soils: measurement and parameter effects. *J. Soil Mech. Found. Div., ASCE,*, 98:603–624, 1972b.

S. Hartzell. Site response estimation from earthquake data. *Bulletin of the Seismological Society of America*, 82(6):2308–2327, 1992.

S. Hartzell, L. F. Bonilla, and R. A. Williams. Prediction of nonlinear soil effects. *Bulletin of the Seismological Society of America*, 94(5):1609–1629, 2004.

Y. Hashash, D. Groholski, C. Phillips, and D. Park. DEEPSOIL V3.5beta user manual and tutorial. Technical report, University of Ilinois at Urbana-Champaign, 2008a.

Y. M. Hashash and D. Park. Viscous damping formulation and high frequency motion propagation in non-linear site response analysis. *Soil Dynamics and Earthquake Engineering*, 22:611–624, 2002.

Y. M. Hashash, C.-C. Tsai, C. Phillips, and D. Park. Soil-column depth-dependent seismic site coefficients and hazard maps for the upper Mississippi Embayment. *Bulletin of the Seismological Society of America,*, 98(4):2004–2021, 2008b.

C. R. Houck, J. A. Joines, and M. G. Kay. Comparison of genetic algorithms, random restart and two-opt switching for solving large location-allocation problems. *J Comput. Oper. Res.*, 23(6):587–596, 1996.

L. Hutchings. Kinematic earthquake models and synthesized ground motion using empirical green's functions. *Bulletin of the Seismological Society of America*, 84(4):1028–1050, 1994.

H. H. M. Hwang and C. S. Lee. Parametric study of site response analysis. *Soil Dynamics and Earthquake Engineering*, 10(6):282–290, 1991. Only three realizations for each parameter.

S. Iai, T. Morita, T. Kameoka, Y. Matsunaga, and K. Abiko. Response of a dense sand deposit during 1993 KushiroOki earthquake. *Soils Found.*, 30:115–131, 1995.

I. Idriss and H. Seed. Seismic response of horizontal soil layers. *J. Soil Mech. and Found. Div., ASCE*, 94(4):1003–1031, 1968.

I. M. Idriss and J. I. Sun. SHAKE91: Users manual. Technical report, Center for Geotechnical Modeling, Department of Civil and Environmental Engineering, University of California, Davis, 1992.

W. D. Iwan. On a class of models for the yielding behavior of continuous and composite systems. *Journal of Applied Mechanics*, 34(3):612–617, 1967.

W. B. Joyner, E. Warrick, Richard, and I. Adolph A. Oliver. Analysis of seismograms from a downhole array in sediments near San Francisco Bay. *Bulletin of the Seismological Society of America*, 66(3):937–958, 1976.

K. Kanai. An empirical formula for the spectrum of strong earthquake motions. *Bull. earthquake res. inst.*, 39:85–95, 1961.

E. I. Katsanos, A. G. Sextos, and G. D. Manolis. Selection of earthquake ground motion records: A state-of-the-art review from a structural engineering perspective. *Soil Dynamics and Earthquake Engineering*, 30(4):157 – 169, 2010.

M. D. Kohler, H. Magistrale, and R. W. Clayton. Mantle heterogeneities and the SCEC reference three-dimensional seismic velocity model version 3. *Bulletin of the Seismological Society of America*, 93(2):757–774, 2003.

A. R. Kottke and E. M. Rathje. Technical manual for strata. Technical report, Pacific Earthquake Engineering Research Center, 2009.

Kramer. *Geotechnical Earthquake Engineering*. Prentice-Hall, Upper Saddle River, NJ, 1996.

A. O. L. Kwok, J. P. Stewart, Y. M. A. Hashash, N. Matasovic, R. Pyke, Z. Wang, and Z. Yang. Use of exact solutions of wave propagation problems to guide implementation of nonlinear seismic ground response analysis procedures. *Journal of Geotechnical and Geoenvironmental Engineering*, 133(11):1385–1398, 2007.

A. O. L. Kwok, J. P. Stewart, and Y. M. A. Hashash. Nonlinear ground-response analysis of Turkey Flat shallow stiff-soil site to strong ground motion. *Bulletin of the Seismological Society of America*, 98(1):331–343, 2008. Turkey Flat Parkfield earthquake.

W. Li and D. Assimaki. Site- and motion-dependent parametric uncertainty of site-response analyses in earthquake simulations. *Bulletin of the Seismological Society of America*, 100: 995–1009, 2010.

X. Li, Z. Wang, and C. Shen. SUMDES a nonlinear procedure for response analysis of horizontally-layered sites subjected to multi-directional earthquake loading. Technical report, University of California, Davis, 1992.

P. Liu and R. J. Archuleta. Efficient modeling of Q for 3D numerical simulation of wave propagation. *Bulletin of the Seismological Society of America*, 96(4A):1352–1358, 2006.

P. Liu, R. J. Archuleta, and S. H. Hartzell. Prediction of broadband ground-motion time histories: Hybrid low/high-frequency method with correlated random source parameters. *Bulletin of the Seismological Society of America*, 96:2118–2130, 2006.

S. Ma and P. Liu. Modeling of the perfectly matched layer absorbing boundaries and intrinsic attenuation in explicit finite-element methods. *Bulletin of the Seismological Society of America*, 96(5):1779–1794, 2006.

H. Magistrale, S. Day, R. W. Clayton, and R. Graves. The SCEC southern california reference three-dimensional seismic velocity model version 2. *Bulletin of the Seismological Society of America*, 90(6B):S65–S76, 2000.

N. Matasović and G. A. Ordonez. D-MOD2000 a computer program package for seismic response analysis of horizontally layered soil deposits, earthfill dams and solid waste landfills, user's manual. Technical report, GeoMotions, LLC, 2007.

N. Matasović and M. Vucetic. Cyclic characterization of liquefiable sands. *Journal of Geotechnical Engineering*, 119(11):1805–1822, 1993.

E. Miranda. Site-dependent strength-reduction factors. *Journal of Structure Engineering*, 119(12):3503–3519, 1993.

E. Miranda. Inelastic displacement ratios for structures on firm sites. *Journal of Structural Engineering*, 126(10):1150–1159, 2000.

E. Miranda. Estimation of inelastic deformation demands of SDOF systems. *Journal of Structural Engineering*, 127(9):1005–1012, 2001.

G. Muravskii. On description of hysteretic behavior of materials. *International Journal of Solids and Structures*, 42:2625–2644, 2005.

F. Naeim and M. Lew. On the use of design spectrum compatible time histories. *Earthquake Spectra*, 11:111–127, 1995.

A. Nobahar and R. Popescu. Spatial variability of soil properties - effects on foundation design. In *Proc. 53rd Canadian Geotechnical Conference*, volume 2, pages 1139–1144, Montreal, Quebec, 2000.

A. Nour, A. Slimani, N. Laouami, and H. Afra. Finite element model for the probabilistic seismic response of heterogeneous soil profile. *Soil Dynamics and Earthquake Engineering*, 23:331–348, 2003.

J. M. O'Connor and B. R. Ellingwood. Site-dependent models of earthquake ground motion. *Earthquake Engineering and Structural Dynamics*, 21:573–589, 1992.

D. D. Oglesby and S. M. Day. Stochastic faulting stress: implications from fault dynamics and ground motion. *Bulletin of the Seismological Society of America*, 92:3006–3021, 2002.

K. Ohtomo and M. Shinozuka. Two-dimensional spatial severity of liquefaction. In *Proc. 8th Japan Earthquake Engineering Symposium*, Tokyo, 1990.

G. M. Paice, D. V. Griffiths, and G. A. Fenton. Finite element modeling of settlements on spatially random soil. *J. Geotech. Engrg.*, 122(9):777–779, 1996.

L. G. Paparizos. Some observations on the random response of hysterestic systems. Technical report, Report No. EERL86-02, The California Institute of Technology, 1986.

D. Park and Y. M. Hashash. Soil damping formulation in nonlinear time domain site response analysis. *Journal of Earthquake Engineering*, 8(2):249–274, 2004.

D. Park and Y. M. Hashash. Evaluation of seismic site factors in the Mississippi Embayment. I. estimation of dynamic properties. *Soil Dynamics and Earthquake Engineering*, 25:133–144, 2005a.

D. Park and Y. M. Hashash. Evaluation of seismic site factors in the Mississippi Embayment. II. probabilistic seismic hazard analysis with nonlinear site effects. *Soil Dynamics and Earthquake Engineering*, 25:145 – 156, 2005b.

S. Parolai, D. Bindi, M. Baumbach, H. Grosser, C. Milkereit, S. Karakisa, and S. Zunbul. Comparison of different site response estimation techniques using aftershocks of the 1999 izmit earthquake. *Bulletin of the Seismological Society of America,*, 94(3):1096–1108, 2004.

V. Pavlov. A convenient technique for calculating synthetic seismograms in a layered half-space. In *Proceedings of the 4th International Conference "Problems of Geocosmos"*, pages 320–323, St. Petersburg, 2002.

K.-K. Phoon and F. H. Kulhawy. Characterization of geotechnical variability. *Canadian Geotechnical Journal*, 36:612–624, 1999.

R. Popescu. *Stochastic variability of soil properties: data analysis, digital simulation, effects on system behavior*. PhD thesis, Princeton University, 1995.

R. Popescu, J. H. Prevost, and E. H. Vanmarcke. Numerical simulations of soil liquefaction using stochastic input parameters. In *Proc. 3rd International Conference on Recent Advances in Geotechnical Earthquake Engineering and Soil Dynamics*, St. Louis, MO, 1997.

R. Pyke. Nonlinear soil model for irregular cyclic loading. *Journal of the Geotechnical Engineering Division*, 105:715–726, 1979.

R. Pyke. TESS: a computer program for nonlinear ground response analyses. Technical report, TAGA Engineering Systems and Software, Lafayette, CA, 1992.

M. Rahman and C. Yeh. Variability of seismic response of soils using stochastic finite element method. *Soil Dynamics and Earthquake Engineering*, 18:229–245, 1999.

C. Real, A. Shakal, and B. Tucker. Overview of the Turkey Flat ground motion prediction experiment. In *Proceedings of SMIP06 Seminar on Utilization of Strong-Motion Data, September 28, 2006*, pages 117–136, Oakland, California, 2006. Turkey Flat Parkfield earthquake.

C. Real, A. Shakal, and B. Tucker. The Turkey Flat blind prediction experiment for the September 28, 2004 Parkfield earthquake: General overview and models tested. In *Proceedings Geotechnical Earthquake Engineering and Soil Dynamics IV, ASCE*, Sacramento, California, 2008. Turkey Flat Parkfield earthquake.

L. Reiter. *Earthquake hazard analysis – issues and insights*. Columbia University Press, New York, 1990.

C. J. Roblee, W. J. Silva, G. R. Toro, and N. A. Abrahamson. Variability in site-specific seismic ground motion design predictions. In C. D. Shakelford and P. P. Nelson, editors, *ASCE Geotech Special Publication No. 58, Uncertainty in the Geologic Environment: from theory to practice*, volume 2, 1996.

V. H. S. Rodriguez and S. Midorikawa. Applicability of the h/v spectral ratio of microtremors in assessing site effects on seismic motion. *Earthquake Engineering & Structural Dynamics*, 31(2):261–279, 2002. 10.1002/eqe.108.

J. Ruiz-García and E. Miranda. Inelastic displacement ratios for design of structures on soft soils sites. *Journal of Structural Engineering*, 130(12):2051–2061, 2004.

K. Sato, T. Kokusho, M. Matsumoto, and E. Yamada. Nonlinear seismic response and soil property during strong motion. *Soils and Foundations*, Special Issue on Geotechnical Aspects of the January 17, 1995, HyogokenNambu Earthquakes:41–52, 1996.

T. Satoh, H. Kawase, and T. Sato. Evaluation of local site effects and their removal from borehole records observed in the Sendai region, Japan. *Bulletin of the Seismological Society of America*, 85:1770–1789, 1995.

T. Satoh, M. Fushimi, and Y. Tatsumi. Inversion of strain-dependent nonlinear characteristics of soils using weak and strong motions observed by borehole sites in Japan. *Bulletin of the Seismological Society of America*, 91(2):365–380, 2001.

P. B. Schnabel, J. Lysmer, and H. B. Seed. SHAKE: A computer program for earthquake response analysis of horizontally layered sites. Technical report, Earthquake Engineering Research Center, University of California, 1972.

H. B. Seed and I. M. Idriss. Soil moduli and damping factors for dynamic response analyses,. Technical report, Earthquake Engineering Research Center, University of California,, 1970.

H. B. Seed, R. T. Wong, I. M. Idriss, and K. Tokimatsu. Moduli and damping factors for dynamic analyses of cohesionless soils. Technical report, Earthquake Engineering Research Center , University of California, Berkeley, 1984.

A. Shakal, H. Haddadi, V. Grazier, K. Lin, and M. Huang. Some key features of the strong motion data from the M6.0 Parkfield, California, earthquake of 28 September 2004. *Bulletin of the Seismological Society of America*, 96(4B):90–118, 2006a. Turkey Flat Parkfield earthquake.

A. Shakal, H. Haddadi, and C. Real. Recorded data and preliminary review of predictions in the Turkey Flat blind prediction experiment for the September 28, 2004 Parkfield earthquake. In *Proceedings of SMIP06 Seminar on Utilization of Strong-Motion Data, September 28, 2006*, pages 137–152, Oakland, California, 2006b. Turkey Flat Parkfield earthquake.

W. J. Silva and C. L. Stark. Source, path, and site ground motion model for the 1989 M 6.9 Loma Prieta earthquake. Technical report, Calif. Div. Mines Geol. Final ept., 1992.

W. J. Silva, R. Darragh, C. Stark, I. Wong, J. C. Stepp, J. Schneider, and S.-J. Chiou. A methodology to estimate design response spectra in the near-source region of large earthquakes using the band-limited-white-noise ground motion model. In *Proceedings of the Fourth U.S. Conf. on Earthquake Engineering*, pages 487–494, Palm Springs, California, 1990. Synthetic motion for structure response.

P. Somerville, R. Graves, and C. Saikia. Characterization of ground motions during the Northridge earthquake of January 17, 1994. Technical report, Program to Reduce the Earthquake Hazards of Steel Moment Frame Buildings, SAC Report 95-03., 1995.

P. Somerville, C. Saikia, D. Wald, and R. Graves. Implications of the Northridge earthquake for strong ground motions from thrust faults. *Bulletin of the Seismological Society of America*, 86:S115–S125, 1996.

J. Steidl, A. Tumarkin, and R. Archuleta. What is a reference site? *Bulletin of the Seismological Society of America*, 86:1733–1748, 1996.

J. Stewart and A. Kwok. Nonlinear seismic response analysis: code usage protocols and verification against vertical array data. In *Proceedings Geotechnical Earthquake Engineering and Soil Dynamics IV, ASCE*, Sacramento, California, 2008.

J. P. Stewart, A. O.-L. Kwok, Y. M. Hashash, N. Matasovic, R. Pyke, Z. Wang, and Z. Yang. Benchmarking of nonlinear geotechnical ground response analysis procedures. Technical report, Pacific Earthquake Engineering Research Center, 2008.

F. Su, K. Aki, T. Teng, S. Koyanagi, and M. Mayeda. The relation between site-amplification factor and surficial geology in central California. *Bulletin of the Seismological Society of America*, 82:580–602, 1992.

F. Su, J. G. Anderson, and Y. Zeng. Study of weak and strong ground motion including nonlinearity from the Northridge, California, earthquake sequence. *Bulletin of the Seismological Society of America*, 88(6):1411–1425, 1998.

S. Suzuki and K. Asano. Dynamic amplification functions of the surface layer considering the variation of soil parameters. In *Proceedings of 10th World Conference of Earthquake Engineering*. Rotterdam: Balkema, 1992.

K. Tajimi. A statistical method of determining the maximum response of a building structure during an earthquake. In *Proc 2nd world conf. earthquake eng. Tokyo and Kyoto, Japan*, 1960.

N. Theodulidis, P.-Y. Bard, R. Archuleta, and M. Bouchon. Horizontal-to-vertical spectral ratio and geological conditions: The case of garner valley downhole array in southern california. *BULLETIN OF THE SEISMOLOGICAL SOCIETY OF AMERICA*, 86(2): 306–319, 1996.

L. Tian and L. Jie. Influence of random mchanical parameter on earthquake response analysis of site. In *Earthquake Engineering, Tenth World Conference*, 1992.

G. R. Toro. Probabilistic model of soil-profile variability. Technical report, Electric Power Research Institute, 1993.

G. R. Toro and W. J. Silva. Scenario earthquakes for Saint Louis, MO, and Memphis, TN, and seismic hazard maps for the central United States region including the effect of site conditions. Technical report, Risk Engineering, Inc., 2001.

D. Ural. *Effects of spatial variability of soil properties on liquefaction*. PhD thesis, Princeton University, 1995.

A. Veletsos, N. Newmark, and C. Chepalati. Deformation spectra for elastic and elastoplastic systems subjected to ground shock and earthquake motion. In *Proc. 3rd World Conf. on Earthquake Engineering, Vol. II*, pages 663–682, Wellington, New Zealand, 1965.

M. Walling, W. Silva, and N. Abrahamson. Nonlinear site amplification factors for constraining the NGA models. *Earthquake Spectra*, 24(1):243–255, 2008.

S. Wang and H. Hao. Effects of random variations of soil properties on site amplification of seismic ground motions. *Soil Dynamics and Earthquake Engineering*, 22:551–564, 2002.

K.-L. Wen, I. A. Beresnev, and Y. T. Yeh. Nonlineafr soil amplification inferred from downhole strong seismic motion data. *Geophysical Research Letters*, 21:2625–2628, 1994.

R. V. Whitman and J. N. Protonotarios. Inelastic response to site-modified ground motions. *Journal of the Geotechnical Engineering Division*, 103:1037–1053, 1977.

J. Wiggins. Effects of site conditions on earthquake intensity. *J. Structural Div., ASCE*, 90 (2):279–313, 1964.

Z. Wu and G. Han. Stochastic seismic response analysis for soil layers with random dynamic parameters. In *Tenth World Conference on Earthquake Engineering*, Madrid, Spain, 1992. Rotterdam: Balkema.

Z. Yang, A. Elgamal, and E. Parra. Computational model for cyclic mobility and associated shear deformation. *Journal of Geotechnical and Geoenvironmental Engineering*, 129(12): 1119–1127, 2003.

M. Zeghal and A. W. Elgamal. Analysis of site liquefaction using earthquake records. *J. Geotech. Eng.*, 120:996–1017, 1994.

Y. Zeng, J. G. Anderson, and G. Yu. A composite source model for computing realistic synthetic strong ground motions. *Geophysical Research Letters*, 21(8):725–728, 1994.

J. X. Zhao, K. Irikura, J. Zhang, Y. Fukushima, P. G. Somerville, A. Asano, Y. Ohno, T. Oouchi, T. Takahashi, and H. Ogawa. An empirical site-classification method for strong-motion stations in japan using h/v response spectral ratio. *Bulletin of the Seismological Society of America*, 96(3):914–925, 2006.

VITA

Wei Li was born on January 5, 1974 in Taian City, People's Republic of China. He earned a B.S. degree in Civil Engineering from Shandong Polytechnic University in 1996, and a M.S degree in Civil Engineering from Hohai Unversity in 1999. He worked as a Geotechnical Engineer in Tianjin Port Engineering Institute from 1999 to 2004. He had been a Graduate Research Assistant in the University of Akron from 2004 to 2005. He started his doctoral studies at the Georgia Institute of Technology in the Spring of 2006. His main research topic during his doctoral studies was Geotechnical Earthquake Engineering, particularly in the nonlinear site response analysis.